

University of Louisville

## ThinkIR: The University of Louisville's Institutional Repository

---

Electronic Theses and Dissertations

---

12-2014

# Signaling mechanisms in regenerative myogenesis.

Sajedah M. Hindi 1986-  
*University of Louisville*

Follow this and additional works at: <https://ir.library.louisville.edu/etd>



Part of the [Nervous System Commons](#)

---

### Recommended Citation

Hindi, Sajedah M. 1986-, "Signaling mechanisms in regenerative myogenesis." (2014). *Electronic Theses and Dissertations*. Paper 1740.  
<https://doi.org/10.18297/etd/1740>

This Doctoral Dissertation is brought to you for free and open access by ThinkIR: The University of Louisville's Institutional Repository. It has been accepted for inclusion in Electronic Theses and Dissertations by an authorized administrator of ThinkIR: The University of Louisville's Institutional Repository. This title appears here courtesy of the author, who has retained all other copyrights. For more information, please contact [thinkir@louisville.edu](mailto:thinkir@louisville.edu).

# SIGNALING MECHANISMS IN REGENERATIVE MYOGENESIS

By

Sajedah M. Hindi, M.S.

A dissertation submitted to the Faculty of School of Medicine of the University of Louisville  
in Partial Fulfillment of the Requirements for the Degree of

Doctor of Philosophy

Department of Anatomical Sciences and Neurobiology,  
University of Louisville  
Louisville, Kentucky

December 2014



# SIGNALING MECHANISMS IN REGENERATIVE MYOGENESIS

By

Sajedah M. Hindi, M.S.

A Dissertation Approved on

November 25, 2014

By the following Dissertation Committee:

---

Ashok Kumar, PhD.  
Dissertation Director

---

Robert P. Friedland, M.D.

---

Robert F. Lundy, PhD.

---

J. Patrick Moore, Ph.D.

---

Jeffrey C. Petruska, Ph.D.



*To my parents*

*Mrs. Fatima J. Romman-Hindi and Dr. Mahmoud Y Hindi*

*for their support and unconditional love*

## ACKNOWLEDGMENTS

Above all I thank God, the most gracious and most merciful of all

Thank you to my committee members; Dr. Robert Friedland, Dr. Robert Lundy, Dr. Patrick Moore, Dr. Jeffery Petruska, and previously Dr. Theo Hagg, Thank you for your support and critical advice!

I thank Dr. William Guido, Dr. Suresh Tyagi, Dr. Guillermo Rougier, Dr. Shihuan Kuang and once more Dr. Robert Lundy and Dr. Theo Hagg for the impactful recommendation letters for the NRSA and John M. Hunchens prize.

My lab members, currently and previously; Samara Carvalho, Kyle Bohnert, Dr. Shuichi Sato, Dr. Marjan Tajrishi, Dr. Guangyan Xiong, Dr. Yuji Ogura, Dr. Jonghyun Shin, Dr. Pradyut Paul, Dr. Saurabh Dahiya, Dr. Vivek Mishra, Dr. Shephali Bhatnagar, Dr. Sanjay Gupta, and Dr. Hong Li. Thank you for creating a great working environment.

Thank you for the love and warmth of ASNB office staff; Ms. Donna Bottorff, Ms. Dana Thomas, Ms. Barbara Hughes, Ms. Chris Ekstrom, and Ms. Camilla Harden.

Pradeepa Poudyal, my buddy, Thank you!

Thank You to the Kumar family: Savita Kumar, Aman Mann and the one and only, Eira Mann!

My awesome family: My parents Mahmoud and Fatima Hindi, My siblings: Musa, Samiha, Yousef, Lubna, Mohammad, and Balsam; and my four legged siblings: Mia, Dabdoob, Fried Chicken, and M&Ms, I thank you every day.....I'll tell you more later;)

And last but most definite certainly not least, Dr. Ashok Kumar, my mentor, Thank You for being!

ABSTRACT

SIGNALING MECHANISMS IN REGENERATIVE MYOGENESIS

Sajedah M. Hindi

November 25, 2014

Skeletal muscle constitutes a highly plastic and malleable tissue that rapidly and profoundly adapts to various environmental and physiological stimuli. This response takes place by means of regulated signaling transduction which elicits changes in gene expression, biochemical, and metabolic properties. Adult muscle is composed by alignment of multi-nucleated, post mitotic muscle fibers formed during embryonic and neonatal development. Residing in the niche of mature muscle fibers is a small population of undifferentiated muscle progenitors termed satellite cells. Satellite cells are muscle stem cells that carry out regenerative response in adult myofibers. Coordinated signaling emitting from terminally differentiated muscle fibers and un-differentiated muscle progenitors sustains muscle homeostasis. De-regulation in the components of this synchronized signaling machinery manifests in deleterious disease states and myopathies.

The main focus of my research has been towards understanding the role of the adaptor protein, tumor necrosis factor-associated factor 6 (TRAF6) in regulation of regenerative myogenesis. Utilizing the Cre-loxP system, we generated TRAF6 muscle-specific knock-out mice: TRAF6<sup>mk0</sup>, and TRAF6 satellite cell-specific knock-out mice:

TRAF6<sup>scko</sup>. Our findings displayed distinct roles of TRAF6 in differentiated myofibers vs. satellite cells. Deletion of TRAF6 under the control of muscle creatine kinase (MCK) promoter (differentiated muscle) led to improvement in muscle regeneration in wild-type (WT) mice following induced muscle injury. This improvement was brought about by prevalence of an anti-inflammatory environment characterized by reduced signaling from inflammatory pathways such as NF- $\kappa$ B and a domination of pro-regeneration M2c over pro-inflammatory M1 macrophages. Regenerating muscle of TRAF6<sup>mk0</sup> mice also displayed a higher up-regulation in Notch signaling family proteins and target genes which in turn enhanced the activation of satellite cells leading to accelerated regeneration. Similar results were also observed upon deletion of TRAF6 in differentiated muscle of mdx mice (model for Duchenne muscular dystrophy). However, mdx;TRAF6<sup>mk0</sup> muscle later displayed exacerbated signs of myopathy possibly due to diminished autophagy which has been associated with progressive myopathy in mdx mice.

Employing the same models of muscle injury, our analysis revealed an absolute requirement of TRAF6 in satellite cell function during regenerative myogenesis. Contrary to its role in differentiated muscle, injured muscle of TRAF6<sup>scko</sup> mice displayed impaired regeneration due to a cell-autonomous defect in TRAF6-deficient satellite cells. Deletion of TRAF6 in satellite cells dramatically repressed the levels of Pax7 resulting in precocious differentiation and progressive depletion of the satellite cell reservoir. Myopathy was further exaggerated in dystrophic muscle of mdx;TRAF6<sup>scko</sup> due to satellite cell dysfunction. Our results further demonstrate that TRAF6 regulates proliferation and self-renewal of satellite cells through activation of mitogen-activated protein kinases (MAPKs) such as ERK1/2 and

JNK and through modulating the levels of muscle specific microRNA's: miR-1, miR-206, and mir-133a.

The findings of this work highlight the importance of implementing a holistic approach upon development of target-based therapies. Oversight of the fundamental roles of targeted molecules has been associated with virulent outcomes. Developing a universal understanding of the various implications of individual molecules maximizes therapeutic potential.

## TABLE OF CONTENTS

	PAGE
DEDICATIONS.....	iii
ACKNOWLEDGEMENTS.....	iv
ABSTRACT.....	vi
LIST OF FIGURES .....	ixiii
CHAPTERS	
CHAPTER 1 .....	1
1.1 SKELETAL MUSCLE REGENERATION.....	1
1.2 MUSCULAR DYSTROPHY.....	2
1.3 TRAF6 SIGNALING.....	4
1.4 TRAF6 SIGNALING IN SKELETAL MUSCLE ATROPHY.....	5
1.5 ROLE OF TRAF6 IN DIFFERENTIATED MYOFIBERS VS. MUSCLE PROGENITOR CELLS DURING REGENERATIVE MYOGENESIS .....	8
CHAPTER 2 .....	11
2.1 INTRODUCTION.....	11
2.2 MATERIALS AND METHODS .....	15
2.3 RESULTS.....	19
2.3.1 TARGETED DELETION OF TRAF6 IMPROVES MYOFIBER REGENERATION IN RESPONSE TO INJURY .....	20
2.3.2 OVEREXPRESSION OF TRAF6 WORSENS MYOFIBER REGENERATION UPON INJURY .....	21
2.3.3 DEPLETION OF TRAF6 IMPROVES FORMATION OF NEW MYOFIBERS IN RESPONSE TO INJURY .....	22

2.3.4 INHIBITION OF TRAF6 PROMOTES SATELLITE CELLS ACTIVATION IN INJURED MYOFIBERS IN VIVO .....	23
2.3.5 ABLATION OF TRAF6 PROMOTES ACTIVATION AND SELF-RENEWAL OF SATELLITE CELLS IN SINGLE MYOFIBER CULTURES .....	24
2.3.6 TRAF6 INHIBITS NOTCH SIGNALING IN REGENERATING MYOFIBER .....	25
2.3.7 INHIBITION OF NOTCH SIGNALING BLUNTS THE PROLIFERATION AND SELF-RENEWAL OF SATELLITE CELLS IN MYOFIBER CULTURES OF TRAF6 <sup>MKO</sup> MICE .....	26
2.4 DISCUSSION .....	27
CHAPTER 3 .....	46
3.1 INTRODUCTION.....	46
3.2 MATERIALS AND METHODS .....	49
3.3 RESULTS.....	55
3.3.1 TRAF6 LEVELS ARE INCREASED IN SKELETAL MUSCLE OF MDX MICE .....	55
3.3.2 TARGETED DELETION OF TRAF6 IMPROVES MUSCLE STRENGTH IN 7-WEEK OLD MDX MICE .....	56
3.3.3 DEPLETION OF TRAF6 IMPROVES MUSCLE HISTOPATHOLOGY IN YOUNG MDX MICE .....	57
3.3.4 INHIBITION OF TRAF6 REDUCES MACROPHAGE ACCUMULATION, NF $\kappa$ B ACTIVATION, AND EXPRESSION OF INFLAMMATORY CYTOKINES IN DYSTROPHIC MUSCLE OF YOUNG MDX MICE .....	58
3.3.5 DEPLETION OF TRAF6 IMPROVES MYOFIBER REGENERATION IN 7-WEEK OLD MDX MICE.....	59
3.3.6 INHIBITION OF TRAF6 EXAGGERATES MYOPATHY IN 9-MONTH OLD MDX MICE.....	60
3.3.7 IMUSCLE-SPECIFIC DEPLETION OF TRAF6 INCREASES FIBROSIS IN 9-MONTH OLD MDX MICE .....	61
3.3.8 INHIBITION OF TRAF6 REDUCES MARKERS OF AUTOPHAGY IN DYSTROPHIC MUSCLE OF MDX MICE .....	61
3.3.9 INHIBITION OF TRAF6 REDUCES THE ACTIVATION OF AKT IN DYSTROPHIC MUSCLE OF MDX MICE .....	63
3.4 DISCUSSION .....	63
CHAPTER 4 .....	88



4.1 INTRODUCTION.....	88
4.2 MATERIALS AND METHODS .....	92
4.3 RESULTS.....	97
4.3.1 ABLATION OF TRAF6 IN SATELLITE CELLS IMPAIRS REGENERATION OF INJURED MYOFIBERS IN ADULT MICE .....	97
4.3.2 ABLATION OF TRAF6 IN SATELLITE CELLS IMPAIRS MYOFIBER FORMATION UPON INJURY .....	99
4.3.3 TRAF6 IS REQUIRED FOR MAINTENANCE OF SATELLITE CELLS POOL IN SKELETAL MUSCLE .....	99
4.3.4 ABLATION OF TRAF6 INHIBITS SATELLITE CELL SELF-RENEWAL AND CAUSES PREMATURE DIFFERENTIATION .....	102
4.3.5 TRAF6 MEDIATES PROLIFERATION AND GENE EXPRESSION OF PAX7 IN SATELLITE CELLS .....	104
4.3.6 TRAF6 REGULATES THE EXPRESSION OF PAX7 IN SATELLITE CELLS THROUGH ACTIVATION OF ERKS AND JNK .....	105
4.3.7 ABLATION OF TRAF6 AUGMENTS THE LEVELS OF MUSCLE-SPECIFIC MICRORNAs (MYOMIRS) IN SATELLITE CELLS .....	108
4.3.8 DELETION OF TRAF6 IN SATELLITE CELLS EXACERBATES MYOPATHY IN MDX MICE .....	108
4.4 DISCUSSION .....	110
 CHAPTER 5 .....	 137
CONCLUSIONS AND FUTURE WORK	
5.1 REVIEW OF DISSERTATION .....	137
5.2 CONTRIBUTION OF DISSERTATION AND FUTURE IMPLEMENTATIONS..	140
5.3 LIMITATIONS OF FUTURE IMPLICATIONS.....	141
 REFERENCES .....	 143
 APPENDICES.....	 168
APPENDIX 1.....	168
APPENDIX 2.....	169

CURRICULUM VITAE..... 172

## LIST OF FIGURES

FIGURE	PAGE
FIGURE 1.1 .....	9
FIGURE 1.2 .....	10
FIGURE 2.1 .....	34
FIGURE 2.2 .....	35
FIGURE 2.3 .....	36
FIGURE 2.4 .....	37
FIGURE 2.5 .....	38
FIGURE 2.6 .....	40
FIGURE 2.7 .....	42
FIGURE 2.8 .....	44
FIGURE 3.1 .....	70
FIGURE 3.2 .....	72
FIGURE 3.3 .....	73
FIGURE 3.4 .....	75
FIGURE 3.5 .....	77
FIGURE 3.6 .....	78
FIGURE 3.7 .....	80
FIGURE 3.8 .....	82
FIGURE 3.9 .....	84
FIGURE 3.10 .....	85
FIGURE 3.11 .....	87
FIGURE 4.1 .....	115
FIGURE 4.2 .....	116
FIGURE 4.3 .....	118
FIGURE 4.4 .....	120
FIGURE 4.5 .....	122
FIGURE 4.6 .....	124

FIGURE 4.7 .....	126
FIGURE 4.8 .....	127
FIGURE 4.9 .....	129
FIGURE 4.10 .....	130
FIGURE 4.11 .....	132
FIGURE 4.12 .....	134
FIGURE 4.13 .....	135

## CHAPTER 1

### GENERAL INTRODUCTION

**1.1 Skeletal muscle regeneration.** Skeletal muscle constitutes the most abundant tissue in the mammalian organ system. The genesis of muscle transpires through a series of molecular events that follow precise temporal and spatial regulation (1, 2). During embryogenesis, proliferating mesodermal myoblasts are directed to align at juxtapose of one another. Molecular and mechanical cues provoke rearrangement of actin cytoskeleton at contact sites allowing for membrane-membrane fusion and myofiber formation. In resolution of embryonic development, a fraction of undifferentiated muscle precursor cells exit the cell cycle and inhabit the muscle niche in a sub-mitotic and -metabolic state. Characterized as “satellite” by their sublaminar localization and intimate association with the myomembrane, satellite cells compose the major adult stem cell population of skeletal muscle. At neonatal age, satellite cells compromise 30% of myonuclei in mouse skeletal muscle. However, this percentage sharply declines to reach 4% at adulthood and 2% in aging mice (1-4). High adaptability of skeletal muscle is owed in large to the remarkable regenerative capacity of satellite cells. When activated by stimuli such as muscle injury or exercise, satellite cells begin to proliferate and commit to a myoblast cell fate, characterized by the expression of certain myogenic regulatory factors (MRFs) and lineage markers, such as Myf5, MyoD and  $\alpha$ 7-integrin, and in resolution, exit the cell cycle to either terminally

differentiate and fuse to form nascent myotubes or self-renew and return back to quiescence to replenish the satellite cell pool to participate in next rounds of regeneration. Impairment in the process of myogenesis contributes significantly to loss of skeletal muscle mass in many disease conditions. A better understanding of the process of skeletal muscle regeneration is required not only to improve muscle repair but also to develop better stem-cell based therapies for treatment of genetic muscular diseases (1-4).

**1.2 Muscular dystrophy.** Muscular dystrophy comprises a group of genetic diseases that cause progressive degeneration of skeletal muscle fibers resulting in severe pain, disability, and eventually death (5). The primary cause for various forms of muscular dystrophies is the mutations in individual genes that encode a wide variety of proteins, including extracellular matrix (ECM) proteins, transmembrane and membrane-associated proteins, cytoplasmic enzymes, and nuclear matrix proteins (6, 7). However, the most severe forms of muscular dystrophies occur due to mutations in the components of the dystrophin-glycoprotein complex (DGC), a molecular scaffold which is localized to sarcolemma and provides mechanical stability to striated muscle. For example, mutations in dystrophin or any of the sarcoglycans leads to destabilization of sarcolemma (i.e. muscle membrane) and a dystrophic phenotype.

Duchenne muscular dystrophy (DMD) is one of the most prevalent forms of muscular dystrophies that results from total or partial deficiency of functional dystrophin protein (**Figure 1.1**). Dystrophin is a critical component of DGC, which links the cytoskeleton of the muscle fibers to the ECM (8). Dystrophin has also been suggested as an important cytolinker that stabilizes cells by linking actin filaments, intermediate filaments,

and microtubules to transmembrane complexes (9). In the absence of dystrophin, the DGC is functionally impaired and the mechanical stress associated with muscle contraction leads to sarcolemmal damage and fiber necrosis (10, 11). While mechanical injury and sarcolemmal defects are important triggering mechanisms promoting dystrophic phenotype, neither fully explains the onset of DMD or its progression. Studies in animal models and humans have shown that partial or complete loss of DGC proteins results in the activation of several pathological cascades which aggravate disease progression (10, 12-15).

Besides acting as a molecular scaffold serving mechanical function, DGC also has an important signaling role in striated muscle. Loss of dystrophin in skeletal muscle leads to aberrant activation of a number of signaling pathways such as nuclear factor- $\kappa$ B (NF- $\kappa$ B), phosphatidylinositol 3-kinase (PI3K)/Akt, and mitogen-activated protein kinases (MAPKs) (16-21). Intriguingly, many signaling pathways that have been found to be involved in pathogenesis of muscular dystrophy are activated before the onset of fiber necrosis signifying that loss of functional DGC is sufficient to disrupt physiological signaling in striated muscle (17). Furthermore, abnormal myogenic signaling has also been reported in other forms of muscular dystrophies that result from loss of nuclear membrane protein (e.g. lamins A/C, Emerin) or cytoplasmic enzymes (e.g. calpain-3) suggesting that signaling defects is a common pathological mechanism in all types of muscular dystrophies (17). Because activation of different signaling cascades results in altered gene expression, aberrant myogenic signaling could be critical for the onset and perpetuation of pathology in muscular dystrophy.

Although the long term studies covering the entire life-span of the animals are yet to be performed, several studies have shown that the inhibition of MAPK or NF- $\kappa$ B signaling

pathways using molecular and pharmacological approaches improves muscle pathology in animal models of DMD (16-18, 20, 21). However, given the progressive degenerative nature of DMD and the convoluted involvement of many secondary processes, developing a pan therapeutic strategy that proves beneficial during the course of the disease has been challenging. Indeed, recent studies have provided evidence that combinatorial approaches which involve simultaneous intonation of multiple pathological pathways would be more effective therapies for DMD (17, 22-24). While it is clear that pathogenesis of muscular dystrophy involves aberrant activation of multiple signaling pathways, it remains unknown whether they are activated through upstream activation of a common signaling network or they are independently regulated.

**1.3 TRAF6 signaling.** TRAF family is a group of seven adaptor proteins (TRAF1-TRAF7) that link a wide variety of cell surface receptors to the intracellular signaling proteins (25). TRAF6 has several distinct features that are not shared by other members of the family (26, 27). TRAF6 (along with TRAF2) is an important E3 ubiquitin ligase. The N-terminal RING domain of TRAF6 is required for its ability to transmit signal, by functioning as an E3 ubiquitin ligase, which together with the ubiquitin conjugating enzyme complex Ubc13/Uev1A catalyzes the synthesis of a unique polyubiquitin chain linked through lysine-63 (K63) residue in ubiquitin (28, 29). This unique ubiquitin modification does not target TRAF6 for degradation, but rather the auto-ubiquitination of TRAF6 serves as a scaffold to recruit molecules essential for downstream activation of various signaling pathways (**Figure 1.2**) (30-34). Studies in the recent past have established that TRAF6 is central to the activation of many signaling pathways including NF- $\kappa$ B, MAPK, and PI3K/Akt in response to cytokines and microbial products (29, 33-36). Of note is the discovery that among all



known TRAFs, only TRAF6 interacts with scaffold protein p62/Sequestosome1 which is involved in regulation of autophagy and TRAFficking of ubiquitinated (Ub K48-linked) proteins to the proteasome (37-40). More recently, it has been found that TRAF6 promotes the Lys-63-linked ubiquitination of Beclin1, which is critical for the induction of autophagy, in response to Toll-like receptor 4 (TLR4) signaling. While the role of TRAFs in tissue destruction and cell death in several other diseases has been studied, how TRAFs regulates muscle regeneration in normal and diseased muscle and the role of TRAF6 in myogenesis was not previously studied. My dissertation is focused to understanding the role of TRAF6 in regenerative myogenesis.

**1.4 TRAF6 signaling in skeletal muscle atrophy.** Skeletal muscle atrophy has been explored extensively over the last decade. Many of these studies were aimed to unearth the mechanisms that orchestrate catabolic changes in an atrophic program. Expression and activation of E3 ubiquitin ligases, MuRF1, and Atrogin-1, has been suggested to be at the distal end of several catabolic pathways and biochemical changes observed in atrophying skeletal muscle. TRAF6, being a different type of E3 ubiquitin-ligase, may not be directly involved in targeting myofibrillar proteins for degradation, however, it can potentially be an upstream regulator for the activation of signaling cascades that eventually lead to loss of muscle proteins in conditions of atrophy. Our group has done the pioneer work towards understanding the role of TRAF6 in skeletal muscle atrophy. We have reported that TRAF6 is the only TRAF that is regulated through myogenic differentiation (41, 42). The levels of TRAF6 are also significantly induced in skeletal muscle in response to denervation, tumor-induction, or diabetes onset (41). More recent findings in our laboratory have suggested that

the levels and autoubiquitination of TRAF6 are also increased in skeletal muscle of mice in response to fasting (43).

A previous graduate student (Dr. Pradyut K. Paul) in our laboratory evaluated the role of TRAF6 in skeletal muscle atrophy using muscle-specific TRAF6-knockout (TRAF6<sup>mk0</sup>) mice. While previous studies have shown that TRAF6-null mice show significant abnormalities and are perinatally lethal (44, 45), there was no overt phenotype upon depletion of TRAF6 only in skeletal muscle of mice (41). Remarkably, the hallmark signatures of atrophy such as loss of skeletal muscle mass, specific muscle proteins, fiber cross section area, and contractile force production were significantly rescued in TRAF6<sup>mk0</sup> mice compared to littermate control mice in two distinct models of atrophy: denervation and cancer cachexia (41). Skeletal muscle of TRAF6<sup>mk0</sup> mice also demonstrated reduced activation of UPS and expression of MuRF1 and MAFBx compared to control TRAF6<sup>ff</sup> mice in atrophic conditions [16]. The reduced expression of MuRF1 and MAFBx could be a result of inhibition of catabolic pathways and transcription as muscle specific ablation of TRAF6 was sufficient to inhibit the activation of NF-κB, AMPK, JNK, and p38 MAPK pathways [16]. It is already known that TRAF6 interacts with p62/SQSTM1-LC3 and Beclin-1 which are markers of autophagy (46). Recapitulating this in skeletal muscle, we observed not only a significant reduction in the expression of components of ALS but also reduced autophagosome formation and mitochondrial degradation [16].

Extending this quest further, our laboratory has investigated the role of TRAF6 in starvation-induced skeletal muscle atrophy. Surprisingly, it was observed that TRAF6 regulates different atrophic programs by employing distinct mechanisms. In addition to UPS and ALS, nutrient deprivation also induced the expression and activation of several

components of endoplasmic reticulum (ER) stress and unfolded protein response (UPR) (43). There was no previous evidence that TRAF6 has any interaction with components of UPR. We have shown that both TRAF6<sup>mk0</sup> mice and TRAF6-deficient mouse embryonic fibroblasts (MEFs) exhibit significantly reduced activation of ER-stress and UPR markers in response to starvation (43).

It is notable that while depletion of TRAF6 significantly inhibits muscle atrophy and activation of catabolic pathways in response to both cancer cachexia and denervation, the effect is more pronounced in cancer cachexia (41). Better rescuing effect of inhibition of TRAF6 in cancer cachexia model could be attributed to the fact that muscle wasting in tumor-bearing subjects involves systemic inflammation evident by increased levels of catabolic cytokines and fibrosis (47). A plethora of literature exists suggesting that several proinflammatory cytokines and tumor-derived factors require TRAF6 for downstream activation of NF- $\kappa$ B and MAPK signaling pathways which are also known to mediate skeletal muscle atrophy (27, 48, 49). By contrast, inflammatory response is not very common in denervated skeletal muscle though TWEAK cytokine has now been found to be an important mediator of muscle loss under conditions of denervation (50, 51). However, the denervation-induced muscle loss was also not completely blunted in TWEAK-KO mice (50) suggesting that muscle atrophy in response to denervation involves some other unidentified factor(s) that function independent of TRAF6.

Earlier research has established diversified regulatory roles of TRAF6 in several systems. Findings from our group extended this further to skeletal muscle atrophy and adds novel information by demonstrating that TRAF6 augments skeletal muscle atrophy through activation of several distinct mechanisms (41). Although this information underlines a new

potential of TRAF6 as a therapeutic target, the regulation of TRAF6 itself is not yet fully delineated. Future research will unveil the mechanisms leading to increased expression of TRAF6 in atrophying muscle and how TRAF6 mediates muscle atrophy in response to diverse stimuli.

**1.5 Role of TRAF6 in differentiated myofibers vs. muscle progenitor cells during regenerative myogenesis.** TRAF6 is highly expressed in proliferating myoblast and skeletal muscle of neonatal mice, however, its expression is sharply reduced upon terminal differentiation of myotubes and completion of development in skeletal muscle (41). Interestingly, the expression of TRAF6 re-emerges in adult skeletal muscle in response to catabolic stimuli and muscle injury. Regulated expression of TRAF6 during myogenesis and re-expression in response to triggering stimuli implies a complex role of TRAF6 in regulating myogenesis. Experiments conducted throughout this study aim at dissecting the functional outcome of TRAF6 signaling at various stages of regenerative myogenesis and a disease model.

FIGURE 1.1

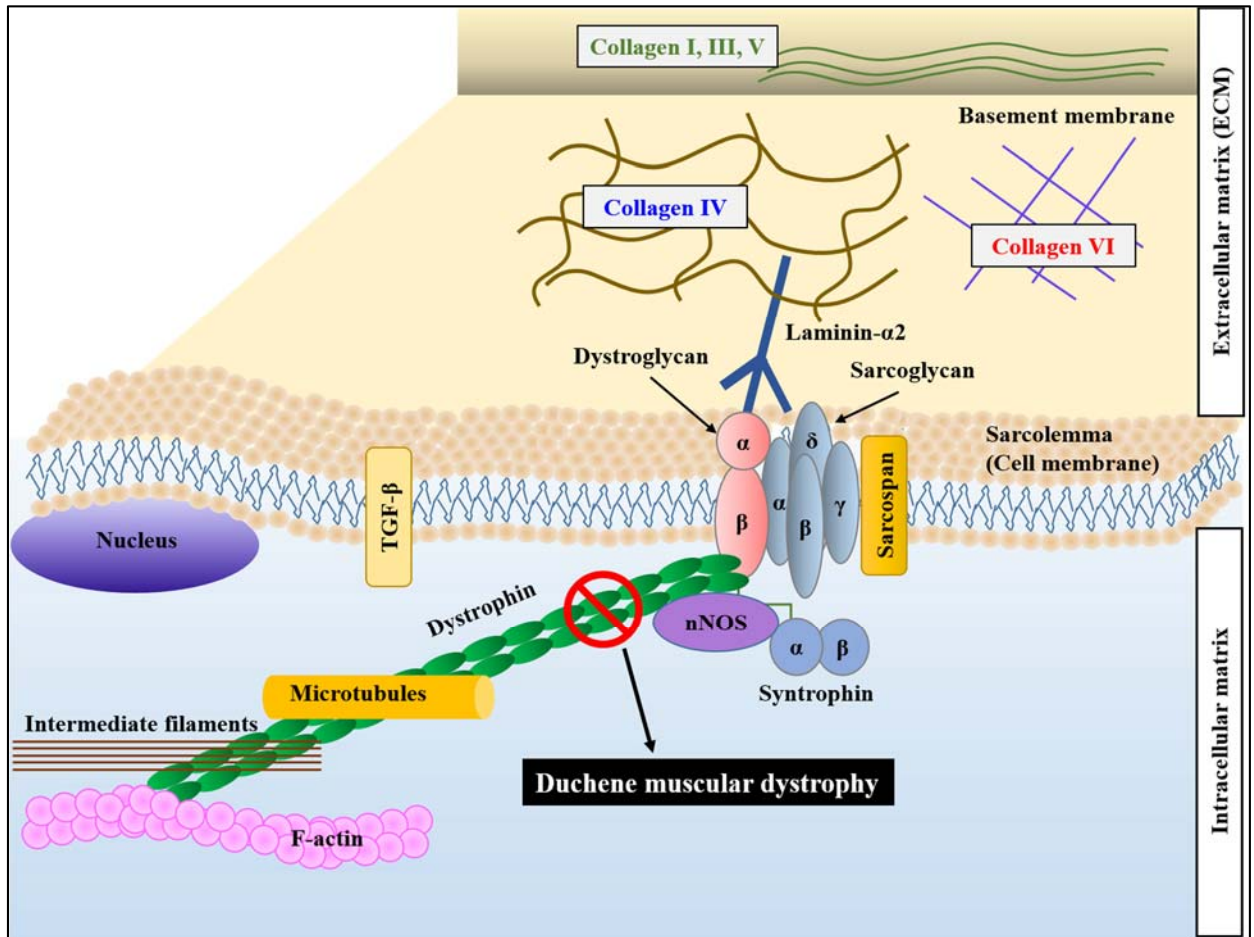
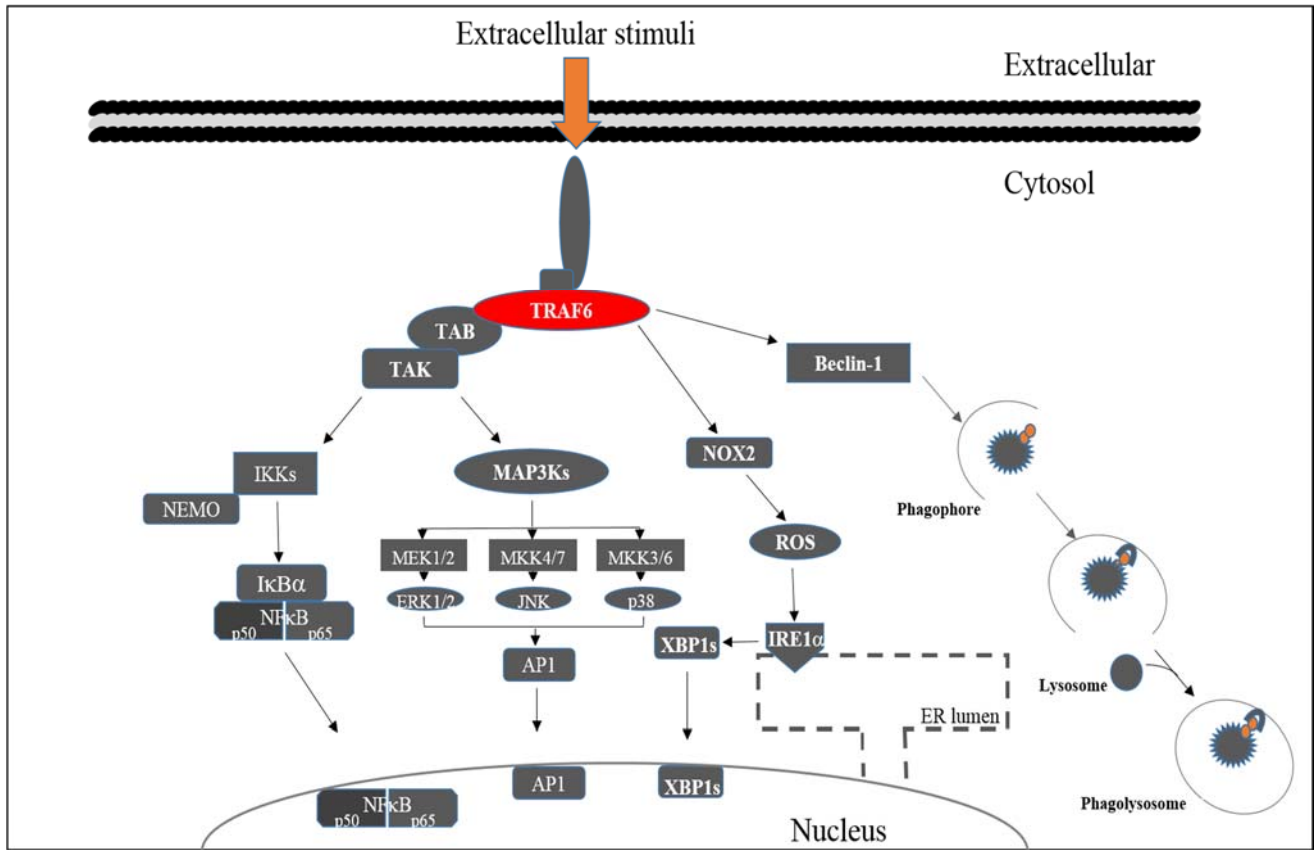


FIGURE 1.1. Genetic basis of Duchenne muscular dystrophy

**FIGURE 1.2**



**FIGURE 1.2. TRAF6-mediated regulation of signaling pathways**

## CHAPTER 2

# RECIPROCAL INTERACTION BETWEEN TRAF6 AND NOTCH SIGNALING REGULATES ADULT MYOFIBER REGENERATION UPON INJURY

### 2.1 INTRODUCTION

Skeletal muscle regeneration following injury is facilitated by a population of undifferentiated muscle precursor cells, commonly referred to as satellite cells (3). Satellite cells reside between the plasma membrane and basal lamina in a relatively quiescent state and with diminished metabolic activity (1, 52). Quiescent satellite cells express cell surface markers such as CD34, M-cadherin and Pax7 (53). When activated by stimuli such as muscle injury or exercise, satellite cells begin to proliferate and commit to a myoblast cell fate, characterized by the expression of certain myogenic regulatory factors (MRFs) and lineage markers, such as Myf5, MyoD and  $\alpha 7$  integrin, and in resolution exit the cell cycle to either terminally differentiate and fuse to form nascent myotubes or self-renew and return back to quiescence to replenish the satellite cell pool to participate in next rounds of regeneration (1).

Myofiber regeneration is dynamically regulated by signals released from both the damaged/regenerating muscle as well as other cell types either resident in the muscle or recruited to assist in clearing the damaged myofibers (3, 54, 55). Although considerable progress has now been made to understanding the mechanisms of muscle regeneration, the

proximal signaling events leading to the activation of various signal pathways in regenerating myofibers remain poorly understood. Tumor necrosis factor (TNF) receptor-associated factors (TRAFs) are a family of conserved adaptor proteins which act as signaling intermediates for TNF receptor superfamily members and several other receptor-mediated events leading to context-dependent activation of nuclear factor-kappa B (NF- $\kappa$ B), phosphatidylinositol 3-kinase (PI3K)/Akt, and MAPK (27, 48). Distinct from other TRAFs, TRAF2 and TRAF6 are also E3 ubiquitin ligases which promote Lys63-linked poly-ubiquitination of target proteins (33). TRAF6 is unique because it is the only TRAF that mediates toll-like receptor (TLR)/interleukin-1 receptor (IL-1R) superfamily signaling (27). Interestingly, the expression of TRAF6 (but not other TRAFs) is highly regulated in C2C12 myoblasts. Proliferating myoblasts and skeletal muscle of neonatal mice express high levels of TRAF6. However, the expression of TRAF6 is considerably reduced upon their differentiation into myotubes (41). Importantly, the levels of TRAF6 are increased in differentiated myofibers in response to catabolic stimuli and TRAF6 mediates skeletal muscle wasting in multiple catabolic conditions (41, 43). However, the role of TRAF6 in satellite cell activation and adult myofiber regeneration remains completely unknown.

Notch is a key signaling pathway involved in embryonic myogenesis and in regulating events that lead to regeneration of adult skeletal muscle (56, 57). Notch signaling is initiated when a Notch ligand such as Jagged1, Jagged2, Delta-like 1 (DLL1), DLL3 or DLL4 binds to a transmembrane cell surface Notch receptor (Notch1-4) on the neighboring cell (58). These ligand-receptor interactions lead to proteolytic cleavage of the Notch receptors via the  $\gamma$ -secretase complex, releasing the Notch intracellular domain (NICD), which translocates to the nucleus and binds the transcriptional repressor, RBP-J $\kappa$ , converting



it into an activator and inducing the expression of downstream target genes (58, 59). Some of the most well-defined RBP-J $\kappa$ -dependent, Notch target genes include specific members of the Hes/Hey family of basic helix-loop-helix transcription factors: Hes1, Hes5, Hes7, Hey1, Hey2 and HeyL which encode basic helix-loop-helix (bHLH) transcriptional repressors that specifically bind to E-box (CANNTG) DNA sequences (60, 61) and mediate much of Notch function (62). In addition, Notch-regulated ankyrin repeat protein (Nrarp) has also been shown to be a target of Notch signaling (63).

Notch regulates proliferation and commitment of activated satellite cells to myogenic lineage. Activation of Notch signaling is a prerequisite for the expansion of postnatal satellite cells and to prevent the premature differentiation of myogenic precursors in injured myofibers (3, 57, 64-69). Age-associated decline in satellite cells proliferative capacity is attributed, at least in part, to the insufficient up-regulation of Notch ligand DLL and hence reduced activation of Notch leading to impaired muscle regeneration (65). The critical role of Notch in muscle regeneration has been validated by the findings that the forced activation of Notch restored the regenerative potential of aged skeletal muscle (65), an outcome recapitulated by exposure of aged regenerating muscle to serum from young animals (70). Notch signaling is also essential for asymmetric satellite cell division and for progression of cultured myoblasts through cell cycle (64, 67, 71). Recently, it has been shown that basal level of Notch activity is required for maintenance of satellite cells in undifferentiated state (72-74). Furthermore, Notch3 is highly expressed in a subpopulation of quiescent satellite cells (64, 75) indicating that Notch signaling may underlie the heterogeneity of satellite cells.

In contrast to Notch, the activation of nuclear factor-kappa B (NF- $\kappa$ B) signaling pathway has been found to inhibit the differentiation of cultured myoblasts (76, 77) and attenuates the regeneration of adult myofibers upon injury (78). Activation of NF- $\kappa$ B causes the expression of a number of proinflammatory molecules such as TNF- $\alpha$  and IL-1 $\beta$  which function by directly inhibiting differentiation of muscle progenitor cells (77). Cross-talk between NF- $\kappa$ B and Notch pathways has been implicated in regulating multiple cellular events such as proliferation, differentiation, and apoptosis. Previous studies have shown that NICD can modulate NF- $\kappa$ B-regulated promoters both positively, by sequestering RBPJ $\kappa$  (79, 80) or negatively, by interacting with the p50 subunit of NF- $\kappa$ B (80). It has been suggested that NICD functions as I $\kappa$ B-like molecule and regulates NF- $\kappa$ B-mediated gene expression through a direct interaction with the p50 subunit of NF- $\kappa$ B (80). This interaction prevents binding of NF- $\kappa$ B to DNA to regulate NF- $\kappa$ B-dependent gene expression (80). However, such interplay between Notch and NF- $\kappa$ B has not been yet characterized in the settings of skeletal muscle regeneration. It is also unclear whether there is a common denominator that controls the activation of these two signaling pathways in regenerating myofibers.

Using skeletal muscle-specific TRAF6-knockout mice, in the present study, we have investigated the role and the mechanisms by which TRAF6 regulates regeneration of adult skeletal muscle. Our study provides initial evidence that the ablation of TRAF6 dramatically improves myofiber regeneration upon injury. Inhibition of TRAF6 augments the expression of Notch ligands in injured myofibers leading to the activation of satellite cells in a Notch-dependent manner. Moreover, inhibition of TRAF6 attenuates activation of NF- $\kappa$ B and expression of inflammatory cytokines in injured skeletal muscle.

## 2.2 MATERIALS AND METHODS

**Animals.** Generation of transgenic floxed TRAF6 (TRAF6<sup>fl</sup>) and muscle specific knock-out for TRAF6 (TRAF6<sup>mkO</sup>) mice have been described previously (41, 81). All mice were in the C57BL6 background and their genotype was determined by PCR from tail DNA. At the age of 8 weeks, 100  $\mu$ l of 10  $\mu$ M cardiotoxin (Sigma Chemical Co.) dissolved in phosphate-buffered saline (PBS) was injected into the TA muscle to induce necrotic injury. At various time points, TA muscle was collected from euthanized mice for biochemical and histology studies. All experimental protocols with mice were approved by the Institutional Animal Care and Use Committee at University of Louisville.

**Histology and Morphometric Analysis.** Hind limb muscle from mice were isolated and frozen in isopentane cooled in liquid nitrogen and sectioned in a microtome cryostat. For the assessment of tissue morphology or visualization of fibrosis, 10- $\mu$ m-thick transverse sections of muscles were stained respectively with the Hematoxylin and Eosin (H&E) and examined under Nikon Eclipse TE 2000-U microscope (Nikon). Fiber cross-sectional area was analyzed in H&E-stained TA muscle sections using Nikon NIS Elements BR 3.00 software (Nikon). For each muscle, the distribution of fiber cross-sectional area (CSA) was calculated by analyzing 200 to 250 myofibers as described (41). The extent of fibrosis in transverse cryosections of TA muscle determined using Masson's Trichrome staining kit following a protocol suggested by the manufacturer (Richard-Allan Scientific).

**Electroporation of plasmid DNA in TA muscle:** The injection of plasmid DNA into TA muscle of mice and electroporation were performed according to a protocol as described (41, 50). In brief, pcDNA3 and pcDNA3-TRAF6 plasmids were amplified using an endotoxin-free kit (QIAGEN) and suspended in sterile saline solution. Mice were anesthetized, and a small portion of TA muscle of both hind limbs was surgically exposed and injected with 30  $\mu$ l of 0.5 U/ $\mu$ l hyaluronidase (EMD Biosciences). After 2 h, plasmid DNA (50  $\mu$ g in 25  $\mu$ l saline) was injected in TA muscle using 26 gauge needle, and 1 min later a pair of platinum plate electrodes was placed against the closely shaved skin on either side of the small surgical incision, and electric pulses were delivered. Four 20-ms square-wave pulses of 1-Hz frequency at 75V/cm were generated using a stimulator (Model S88; Grass Technologies) and delivered to the muscle. The polarity was then reversed, and a further three pulses were delivered to the muscle. After electroporation, the wound was closed with surgical clips, and mice were returned to their cages and fed a standard diet.

**Indirect Immunofluorescence:** For immunohistochemistry study, TA muscle section sections or paraformaldehyde-fixed cultured myotubes were blocked in 1% bovine serum albumin in PBS for 1h, and incubated with anti-Pax7 (1:20, Developmental Studies Hybridoma Bank, University of Iowa, Iowa City, IA), anti-E-MyHC (1:50, Developmental Studies Hybridoma Bank, University of Iowa, Iowa City, IA), anti-MF20 (1:250, Developmental Studies Hybridoma Bank, University of Iowa, Iowa City, IA) or anti-Jagged2 (1:100, SantaCruz Biotechnology) in blocking solution at 4°C overnight under humidified conditions. The sections were washed briefly with PBS before incubation with Alexa Fluor® 488 or 594-conjugated secondary antibody (1:3000, Invitrogen) for 1h at

room temperature and then washed 3 times for 30 minutes with PBS. The slides were mounted using fluorescence medium (Vector Laboratories) and visualized at room temperature on Nikon Eclipse TE 2000-U microscope (Nikon), a digital camera (Nikon Digital Sight DS-Fi1), and Nikon NIS Elements BR 3.00 software (Nikon). Image levels were equally adjusted using Adobe Photoshop CS2 software (Adobe).

**Isolation, Culture, and Staining of Single Myofibers.** Single myofibers were isolated from the extensor digitorum longus (EDL) muscles after digestion with collagenase A (Sigma) and trituration as previously described. Suspended fibers were cultured in 60-mm horse serum-coated plates in Dulbecco's modified Eagle's medium supplemented with 10% fetal bovine serum (FBS; Invitrogen), 2% chicken embryo extract (Accurate Chemical, Westbury, NY), and 1% penicillin-streptomycin for 3 days. Freshly isolated fibers and cultured fibers were then fixed in 4% PFA and stained for Pax7, MyoD, Ki67, or Jagged2 as described (82). To study the role of Notch signaling, myofibers were treated with 10 $\mu$ M DAPT after 24h of establishing cultures.

**Western Blot.** Quantitative estimation of specific protein was performed by Western blot using a method as described (41, 50). TA muscle were washed with PBS and homogenized in lysis buffer [50 mM Tris-Cl (pH 8.0), 200 mM NaCl, 50 mM NaF, 1 mM dithiotheritol (DTT), 1 mM sodium orthovanadate, 0.3% IGEPAL, and protease inhibitors].

Approximately, 100  $\mu$ g protein was resolved on each lane on 8-10 % SDS-PAGE, electrotransferred onto nitrocellulose membrane and probed using anti-MF20 or anti-E-MyHC (1:100, Developmental Studies Hybridoma Bank), anti-TRAF6(1:1000, Millipore),

anti-phospho-Akt (1:1000, Cell Signaling, Inc), anti-total Akt (1:1000, Cell Signaling, Inc), anti-phospho p38 (1:1000, Cell Signaling, Inc), anti-total p38 (1:1000, Cell Signaling, Inc.), and anti- $\alpha$ -tubulin (1:2000, Cell Signaling, Inc.) and detected by chemiluminescence.

**Fluorescence Activated Cell Sorting (FACS).** Activated satellite cells and M1 and M2c macrophages were analyzed by FACS as described (64, 83). Approximately  $2 \times 10^6$  cells were incubated in DMEM (supplemented with 2% FBS and 25 mM 4-(2-hydroxyethyl)-1-piperazineethanesulfonic acid) and dead cells (positive for Propidium iodide staining) which were around ~1% were excluded from all FACS analysis. For satellite cell quantification from heterogeneous cell population, cells were immunostained with antibodies against, CD45, CD31, CD56/Sca-1, and Ter-119 for negative selection (all PE conjugated, eBiosciences), and with  $\alpha 7\beta 1$ -integrin (MBL International) for positive selection. A tandem conjugate of R-PE (Alexa 647, Molecular Probes) was used as a secondary antibody against  $\alpha 7\beta 1$ -integrin. Macrophages were quantified from heterogeneous cell population by selection of F4/80<sup>+</sup> (PerCP Cy5.5-conjugated, eBiosciences) cells against negative selection by CD56/Sca-1, CD140a and Ter-119 (all PE-conjugated, eBiosciences). From F4/80<sup>+</sup> cells, CD11c<sup>+</sup> (APC-conjugated, eBiosciences) M1 and CD206<sup>+</sup> (FITC-conjugated, Biolegend) M2c macrophages were isolated. FACS analysis was performed on a C6 Accuri cytometer equipped with three lasers. The output data was processed and plots were prepared using FCS Express 4 RUO software (De Novo Software).

**Electrophoretic Mobility Shift Assay (EMSA).** DNA-binding of NF- $\kappa$ B was measured by performing EMSA as previously detailed (41). In brief, 20  $\mu$ g of nuclear extracts prepared

from control or CTX-injected TA muscle were incubated with 16 fmol of  $^{32}\text{P}$  end-labeled NF- $\kappa\text{B}$  consensus oligonucleotide (Promega) at 37 °C for 30 min, and the DNA-protein complex was resolved on a 7.5% native polyacrylamide gel. The radioactive bands from the dried gel were visualized and quantified by PhosphorImager (GE Health Care) using ImageQuant TL software.

**RNA Isolation and Quantitative Real-time PCR (QRT-PCR).** RNA isolation and QRT-PCR were performed using a method as previously described (41). The sequence of the primers is described in Table 2.1.

**Statistical Analyses.** Results are expressed as mean  $\pm$  standard deviation (SD). Statistical analyses used Student's *t*-test to compare quantitative data populations with normal distribution and equal variance. A value of  $P < 0.05$  was considered statistically significant unless otherwise specified.

## **2.3 RESULTS**

(**Note:** Some of the experiment on this part of the project were done by a previous graduate student, Pradyut K Paul as a part of his dissertation. I carried on with the project and performed a vast number of experiments to complete this study. I have not included any of his data in this chapter but referred to our joint first author publication for the results exclusively performed by Pradyut K. Paul (84)).

### **2.3.1 Targeted deletion of TRAF6 improves myofiber regeneration in response to**

**injury.** An acute injury to skeletal muscle is followed by a well-orchestrated series of events which facilitate rapid repair and regeneration of injured muscle (1, 4). We first investigated how the expression of TRAF6 is affected in skeletal muscle in response to injury. Wild-type mice were given intramuscular injection of saline alone or cardiotoxin (CTX) in the tibial anterior (TA) muscle. Western blot analysis showed that the levels of TRAF6 protein dramatically increased in CTX-injected TA muscle at 5d post injury (Figure 1A). The increased levels of TRAF6 protein was potentially due to its increased transcription because mRNA levels of TRAF6 were also found to be significantly increased in CTX-injected TA muscle compared to contralateral muscle injected with saline alone (please refer to (84)).

We next sought to determine the role of TRAF6 in skeletal muscle regeneration. To specifically delete TRAF6 in differentiated myofibers, floxed TRAF6 (TRAF6<sup>f/f</sup>) mice were crossed with muscle creatine kinase (MCK)-Cre mice to obtain muscle-specific TRAF6-knockout (henceforth TRAF6<sup>mk0</sup>) mice as previously detailed (41). The levels of TRAF6 protein (but not other TRAFs) are considerably reduced specifically in skeletal muscle of TRAF6<sup>mk0</sup> mice compared to littermate TRAF6<sup>f/f</sup> mice (41). Satellite cells prepared from TRAF6<sup>f/f</sup> and TRAF6<sup>mk0</sup> mice showed no difference in the protein levels of TRAF6 (**Figure 2.1**) suggesting that TRAF6 protein is reduced in differentiated myofibers but not in muscle progenitor cells of TRAF6<sup>mk0</sup> mice. TA muscle of 8-week old TRAF6<sup>mk0</sup> and its littermate TRAF6<sup>f/f</sup> mice were given intramuscular injection of saline alone or with CTX followed by isolation of the TA muscle at different time points and processing for Hematoxylin and Eosin (H&E) staining. Intramuscular injection of CTX caused equal necrosis in TA muscle of both TRAF6<sup>f/f</sup> and TRAF6<sup>mk0</sup> mice examined at 2d post CTX injection (data not shown).



Interestingly, regeneration of TA muscle was dramatically improved in TRAF6<sup>mk0</sup> mice compared to TRAF6<sup>f/f</sup> littermates (**Figure 2.2**). TA muscle of TRAF6<sup>mk0</sup> contained majority of newly formed centronucleated fibers (CNF) and reduced cellular infiltrate at 5d post CTX injection. Improved regeneration in TRAF6<sup>mk0</sup> mice was also evident at 10d and 21d after CTX injection (**Figure 2.2**). Morphometric analyses of CTX-injected TA muscle sections showed about 36% improvement in average fiber cross-sectional area (CSA) in TRAF6<sup>mk0</sup> mice compared to TRAF6<sup>f/f</sup> littermates. Moreover, the number of fibers containing two or more centrally located nuclei was significantly higher in TRAF6<sup>mk0</sup> mice compared to TRAF6<sup>f/f</sup> after 5d of CTX injection further suggesting accelerated regeneration of injured myofibers in TRAF6<sup>mk0</sup> mice (please refer to (84)).

**2.3.2 Overexpression of TRAF6 worsens myofibers regeneration upon injury.** We next studied the effects of overexpression of TRAF6 protein on adult myofiber regeneration. Left-side TA muscle of C57BL6 mice was electroporated with vector (pcDNA3) alone whereas right-side with plasmid encoding wild-type TRAF6 cDNA. Protein levels of TRAF6 were higher in TA muscle transfected with TRAF6 cDNA compared to that transfected with pcDNA3 alone (**Figure 2.1B**). However, there was no overt phenotype in TRAF6-transfected TA muscle compared to those transfected with vector alone in unchallenged conditions, studied 7d post electroporation (**Figure 2.1C**). Next, TA muscle was injected with CTX followed by analysis of muscle regeneration at 5d and 7d by H&E staining. Interestingly, overexpressing of TRAF6 inhibited the regeneration of TA muscle (**Figure 2.3**). The TRAF6 cDNA-transfected TA muscle contained considerably increased amount of cellular infiltrate (darkly stained nuclei of inflammatory cells) both at 5d and 7d

after CTX injection (**Figure 2.3**). In addition, the number of regenerating myofibers and the fiber cross-sectional area were noticeably reduced in TRAF6-transfected myofibers (**Figure 2.3**). These results indicate that TRAF6 inhibits the regeneration of adult myofiber upon injury.

### **2.3.3 Depletion of TRAF6 improves formation of new myofibers in response to injury.**

A shift from degenerative to regenerative stage is followed by transition of myogenic cells through expression of specific transcription factors and related genes. This pattern also mimics the embryonic development of skeletal muscle (1). CTX injection in mouse skeletal muscle stimulates the expression of MyoD in satellite cells by 2d. Thereafter, a decline in MyoD expression and an increase in myogenin expression occur by 3d post-injury followed by a consequential and persistent elevation of embryonic form of myosin heavy chain (eMyHC) (85, 86). Furthermore, as a regenerating muscle progresses towards normal architecture, embryonic isoform of MyHC is replaced by adult isoform. To investigate whether depletion of TRAF6 causes any change in the temporal expression pattern of these markers, we further examined CTX-injected TA muscle of TRAF6<sup>fl/fl</sup> and TRAF6<sup>mk0</sup> mice. Immunostaining revealed more uniform and abundant expression of eMyHC in TA muscle of TRAF6<sup>mk0</sup> compared to TRAF6<sup>fl/fl</sup> mice at 5d after CTX injection (**Figure 2.4A**). Western blot analysis showed that TRAF6 levels were reduced in uninjured TA muscle of TRAF6<sup>mk0</sup> mice compared to TRAF6<sup>fl/fl</sup> mice. Furthermore, TRAF6 levels in CTX-injected TA muscle of TRAF6<sup>mk0</sup> mice was ~50% less compared to corresponding TRAF6<sup>fl/fl</sup> mice (**Figure 2.4B**) suggesting that infiltrating cells and myofibers contribute almost equally to the increased levels of TRAF6 in CTX-injected TA muscle.

IGF-1 is a major growth factor which induces skeletal muscle regeneration through augmenting the proliferation and differentiation of myogenic cells. We next investigated whether signaling through TRAF6 also affects the expression of IGF-1 in injured skeletal muscle. As shown in **Figure 2.4C**, transcript levels of IGF-1 were significantly higher in CTX-injected TA muscle of TRAF6<sup>mko</sup> compared to TRAF6<sup>f/f</sup> mice (**Figure 2.4C**). Moreover, increased mRNA levels of myogenin in CTX-injected TA muscle of TRAF6<sup>mko</sup> mice affirmed enhanced muscle regeneration in these mice compared to TRAF6<sup>f/f</sup> mice at 6d post CTX-mediated injury (**Figure 2.4C**). Collectively, these results suggest that depletion of TRAF6 in adult myofibers accelerates muscle regenerative program upon injury.

**2.3. 4 Inhibition of TRAF6 promotes satellite cells activation in injured myofibers *in vivo*:** Muscle injury is followed by the activation of satellite cells which is prerequisite for induction of efficient regeneration program in injured muscle (1, 4). We next investigated whether TRAF6-mediated signaling affects the activation of satellite cells in injured myofibers. Pax7 is a marker of both quiescent and activated satellite cells (64, 87). We first performed immunostaining for Pax7 to evaluate the number of satellite cells in TA muscle of TRAF6<sup>f/f</sup> and TRAF6<sup>mko</sup> mice. There was no noticeable difference in the number of Pax7<sup>+</sup> cells between uninjured TA muscle of TRAF6<sup>f/f</sup> and TRAF6<sup>mko</sup> mice. However, the number of Pax7<sup>+</sup> cells per unit area was considerably higher in TA muscle of TRAF6<sup>mko</sup> compared to TRAF6<sup>f/f</sup> mice at 5d post CTX injection (**Figures 2.5A, 2.5B**).

A unique combination of cell surface markers (CD45<sup>-</sup>, CD31<sup>-</sup>, Ter119<sup>-</sup>, Sca-1<sup>-</sup>,  $\alpha$ 7- $\beta$ 1 integrin<sup>+</sup>) identify satellite cells in adult mouse skeletal muscle and allow their direct quantification by fluorescence-activated cell sorting (FACS) technique (88). To further

evaluate whether signaling through TRAF6 affects the activation of satellite cells in injured muscles, we also performed FACS analysis. There was no difference in the number of satellite cells in uninjured TA muscle of TRAF6<sup>fl/fl</sup> and TRAF6<sup>mkko</sup> mice. However, intramuscular injection of CTX significantly increased the number of satellite cells in TA muscle of both TRAF6<sup>fl/fl</sup> and TRAF6<sup>mkko</sup> mice measured at 5d (**Figures 2.5C and 2.5D**). Furthermore, the number of satellite cells was significantly higher in CTX-injected TA muscle of TRAF6<sup>mkko</sup> mice compared to littermate TRAF6<sup>fl/fl</sup> (~7.5% in TRAF6<sup>fl/fl</sup> vs. ~13% in TRAF6<sup>mkko</sup>) mice (**Figures 2.5C and 2.5D**).

### **2.3.5 Ablation of TRAF6 promotes activation and self-renewal of satellite cells in single**

**myofiber cultures.** Suspension culture of myofiber explants represents an ex-vivo model that mimics muscle injury *in vivo* with respect to satellite cell activation, proliferation, and differentiation (57, 64, 87). Upon isolation, each myofiber is associated with a fixed number of (Pax7<sup>+</sup>/MyoD<sup>-</sup>) satellite cells resting in quiescence. At around 24h in culture, satellite cells undergo their first round of cell division, through up regulating MyoD (Pax7<sup>+</sup>/MyoD<sup>+</sup>) and proliferating to form cell aggregates. Cells then either terminally differentiate (Pax7<sup>-</sup>/MyoD<sup>+</sup>) or self-renew (Pax7<sup>+</sup>/MyoD<sup>-</sup>) (64). Consistent with our *in vivo* results, immunostaining of freshly isolated myofibers from EDL muscle of TRAF6<sup>mkko</sup> and their littermates TRAF6<sup>fl/fl</sup> revealed comparable numbers of (Pax7<sup>+</sup>/MyoD<sup>-</sup>) cells and negligible levels of MyoD expression (data not shown). After 72h in suspension culture, a dramatic increase was observed in the number of Pax7<sup>+</sup>/MyoD<sup>-</sup> as well as Pax7<sup>+</sup>/MyoD<sup>+</sup> cells in TRAF6<sup>mkko</sup> compared to TRAF6<sup>fl/fl</sup> (**Figures 2.6A-E**) accompanied by an upregulation of cells expressing the proliferation marker Ki67. Moreover, the number of cells per cellular

aggregate was also increased, characterized by an upregulation of Pax7<sup>+</sup>/MyoD<sup>-</sup> cells (**Figures 2.6D-I**). Further analysis of clusters on myofibers in suspension cultures showed that while there was a significant increase in proportion of Pax7<sup>+</sup>/MyoD<sup>-</sup> cells (**Figure 2.6F**), there was no significant difference in the distribution of Pax7<sup>+</sup>/MyoD<sup>+</sup> cells (**Figure 2.6G**) in cellular aggregates of TRAF6<sup>f/f</sup> and TRAF6<sup>mko</sup> myofibers suggesting that while ablation of TRAF6 increases the proliferation and self-renewal, it also favors restoration of satellite cell pool by significant margin.

**2.3.6 TRAF6 inhibits Notch signaling in regenerating myofibers.** Notch signaling is an important regulator of cell proliferation, cell fate determination, and in asymmetric cell division during embryogenesis. Moreover, the role of Notch signaling in orchestrating satellite cell activation in regenerative adult muscle is well documented (56). To determine whether the accelerated regenerative phenomenon observed in TRAF6 ablated skeletal muscle is brought about through a Notch-dependent manner, transcript levels of a set of Notch target genes were analyzed using QRT-PCR technique. A significant increase in mRNA level of Hes1, Hes6, Hey1, HeyL and Nrarp was observed in CTX-injected TA muscle of TRAF6<sup>mko</sup> muscle compared to TRAF6<sup>f/f</sup> mice (**Figure 2.7A**). Additionally, transcript levels of Notch3 receptor (**Figure 2.7B**) and Notch ligands DLL1, DLL2, Jagged1, and Jagged2 (**Figure 2.7C**) were unregulated in CTX-injected TA muscle of TRAF6<sup>mko</sup> mice compared to TRAF6<sup>f/f</sup> mice. Western blot analysis also showed that the protein levels of Jagged2 were ~2.2 fold and DLL1 ~1.7 fold higher in regenerating TA muscle of TRAF6<sup>mko</sup> mice compared to TRAF6<sup>f/f</sup> mice (**Figure 2.7D**). Notch signaling involves the interaction between two neighbor cells, one expressing Notch ligand and other

expressing Notch receptors (56, 57). Since in our model, we depleted TRAF6 specifically in differentiated myofibers, by performing immunostaining, we tested the hypothesis that inhibition of TRAF6 increases the expression of Notch ligands in regenerating myofibers. As shown in Figure 5E, Jagged2 protein co-localized with eMyHC in CTX-injected TA muscle of both TRAF6<sup>f/f</sup> and TRAF6<sup>mk0</sup> mice. Furthermore, the expression of Jagged2 was higher around injured/regenerating myofibers of TRAF6<sup>mk0</sup> compared to TRAF6<sup>f/f</sup> mice (**Figure 2.7E**). Similar, immunostaining analysis revealed that Jagged2 was expressed in myofibers in suspension cultures and the level of expression was increased in cultured myofibers from TRAF6<sup>mk0</sup> mice compared to TRAF6<sup>f/f</sup> mice (**Figure 2.7F**).

We also studied the activation of Notch signaling pathway in satellite cells of TRAF6<sup>f/f</sup> and TRAF6<sup>mk0</sup> mice. TA muscle of TRAF6<sup>f/f</sup> and TRAF6<sup>mk0</sup> mice were given intramuscular injection of CTX for 5d and satellite cells were isolated using fluorescence-activated cell sorting (FACS) method followed by QRT-PCR assay to study the expression levels of Notch target genes. Interestingly, the mRNA levels of Hes6, HeyL, and Nrarp were found to be significantly higher in satellite cells from TRAF6<sup>mk0</sup> mice compared to TRAF6<sup>f/f</sup> mice (**Figure 2.7G**) indicating higher activation of Notch signaling pathway in satellite cells of injured myofibers of TRAF6<sup>mk0</sup> mice.

**2.3.7 Inhibition of Notch signaling blunts the proliferation and self-renewal of satellite cells in myofiber cultures of TRAF6<sup>f/f</sup> and TRAF6<sup>mk0</sup> mice.** Although the role of Notch signaling in satellite cell activation and self-renewal and muscle regeneration has been established using both genetic mouse models and pharmacological inhibitors (3, 57, 64-69), we further investigated whether the higher levels of activation of Notch pathway is

responsible for the increased proliferation of satellite cells in myofibers of TRAF6<sup>mk0</sup> mice. Previous studies have shown that  $\gamma$ -secretase inhibitor DAPT (N-[2S-(3,5-difluorophenyl)acetyl]-L-alanyl-2-phenyl-1,1-dimethylethyl ester-glycine) efficiently inhibits the activation of Notch signaling in various cell types including satellite cells (64, 66). DAPT function by inhibiting the cleavage of Notch intracellular domain (NICD) from transmembrane domain of Notch receptor and hence block the downstream Notch signaling. Single myofibers were prepared from TA muscle of TRAF6<sup>f/f</sup> and TRAF6<sup>mk0</sup> mice and treated with DAPT followed by immunostaining for Pax7, MyoD, and/or Ki67. Nuclei were identified by co-staining with DAPI. Consistent with published reports, DAPT reduced the number of clusters, average number of satellite cells per cluster, and the number of Ki67<sup>+</sup> cells in myofibers of both TRAF6<sup>f/f</sup> and TRAF6<sup>mk0</sup> mice (**Figure 2.8**). Interestingly, treatment with DAPT completely blunted the increased proliferative response of satellite cells observed in cultured myofibers of TRAF6<sup>mk0</sup> mice. Similarly, the proportion of Pax7<sup>+</sup>/MyoD<sup>-</sup> and Pax7<sup>+</sup>/MyoD<sup>+</sup> cells was also dramatically reduced upon treatment with DAPT (**Figure 2.8**). Collectively, these results demonstrate that depletion of TRAF6 in differentiated myofibers induces satellite cell proliferation and self-renewal through Notch signaling pathway.

## 2.4 DISCUSSION

Skeletal muscle regeneration involves activation of a complex array of signaling proteins not only in satellite cells and myoblasts but also in regenerating myofibers. However, except NF- $\kappa$ B where its targeted inhibition in adult/differentiated myofibers improved regeneration (78), majority of the studies have been performed employing myoblast- or satellite cell-

specific knockout mice or global knockout mouse models which made no distinction between signals originating in muscle progenitor cells and injured myofibers. Moreover, the initial events which govern the activation of downstream signaling pathways in regenerating myofibers remain poorly understood. In the present study, we provide genetic evidence that signaling through TRAF6 negatively regulate adult myofiber regeneration. We have also uncovered a previously unrecognized link between TRAF6, Notch signaling, and skeletal muscle regeneration. Our results demonstrate that the inhibition of TRAF6 up-regulates the expression of Notch ligands leading to enhanced Notch driven activation of satellite cells. Studies from our lab has also shown that blocking TRAF6 in differentiated myofibers inhibits the activation of NF- $\kappa$ B and increases levels of promyogenic M2c macrophages in regenerating skeletal muscle potentially through a cross-talk with Notch pathway (84).

Following muscle injury, quiescent satellite cells present in basal lamina get activated, which proliferate and finally fuse with injured myofibers leading to regeneration and repair (1, 52). Notch signaling is critical not only for the activation of satellite cells but also for their terminal differentiation into myofibers and to maintaining the satellite cell pool (3, 57, 64-69). We found that the depletion of TRAF6 specifically in differentiated myofibers significantly increases the number of satellite cells upon injury leading to rapid and faster restoration of muscle architecture. Similarly, satellite cells associated with cultured TRAF6<sup>mko</sup> myofibers displayed increased proliferative potential accompanied by up-regulation of Pax7<sup>+</sup>/MyoD<sup>-</sup> and Pax7<sup>+</sup>/MyoD<sup>+</sup> satellite cells (**Figure 2.6**). Transcriptional analysis of injured myofibers from TRAF6<sup>mko</sup> compared to their TRAF6<sup>f/f</sup> littermates denoted an augmentation of Notch signaling cascade evident by enhanced levels of Notch ligands (DLL1, DLL2, Jagged1, and Jagged2), Notch3 receptor, and a subset of Notch



target genes (Hes1, Hes6, Hey1, HeyL and Nrarp). This suggests that the inhibition of TRAF6 leads to the production of certain factors from regenerating myofibers and/or create a muscle microenvironment which augments Notch signaling resulting in the activation of resident satellite cells. Alternatively, the increased expression of Notch ligands on injured myofibers itself could be sufficient to activate Notch signaling in satellite cells residing on these myofibers. This later possibility is strongly supported by our results demonstrating that the expression of Jagged2 was noticeably higher in the periphery of regenerating myofibers of TRAF6<sup>mk0</sup> mice (**Figure 2.7**). Furthermore, freshly isolated satellite cells from CTX-injected TA muscle of TRAF6<sup>mk0</sup> mice showed increased mRNA levels of Notch target genes suggesting increased Notch signaling in satellite cells (**Figure 2.7**). Although the current study identifies TRAF6 signaling as being a negative regulator for the expression of Notch ligands on injured myofibers, one can next enquire as to the mechanism by which TRAF6 suppresses the expression of Notch ligands. This is an area of interest for future investigation.

Several molecules such as IGF-1, fibroblast growth factor, and hepatocyte growth factor have now been identified which affect the proliferation and/or differentiation of muscle progenitor cells (1, 52). Among them, IGF-1 is a well-known growth factor which stimulates both the proliferation and differentiation of muscle progenitor cells *in vivo* and *in vitro* (89). It has also been reported that muscle-specific overexpression of IGF-1 augments regeneration of myofibers in response to injury (90). Interestingly, the expression of IGF-1 was significantly higher in injured myofibers of TRAF6<sup>mk0</sup> mice compared to TRAF6<sup>f/f</sup> (**Figure 2.4C**) suggesting that the improved muscle regeneration in TRAF6<sup>mk0</sup> mice could also be a result of increased production of IGF-1.

NF- $\kappa$ B is one of the important signaling pathways activated through TRAF6-dependent mechanisms in response to various cytokines, growth factors, and recruitment of toll-like receptors (27, 91). NF- $\kappa$ B activation can occur *via* either the canonical or alternative pathway (92). In absence of activating stimuli, NF- $\kappa$ B dimers are retained in the cytoplasm by binding to specific inhibitors-the inhibitors of NF- $\kappa$ B (I $\kappa$ Bs). The classical pathway is IKK $\beta$  and IKK $\gamma$ -dependent and NF- $\kappa$ B activation occurs through the degradation of I $\kappa$ B proteins (77, 92). Activated IKK phosphorylates NF- $\kappa$ B-bound I $\kappa$ B proteins and targets them for polyubiquitination and rapid degradation. Proinflammatory cytokines such as TNF- $\alpha$  activate NF- $\kappa$ B through IKK $\beta$ -mediated site-specific phosphorylation and subsequent ubiquitination and degradation of inhibitory protein I $\kappa$ B $\alpha$  by the 26S proteasome. NF- $\kappa$ B complexes liberated from I $\kappa$ B inhibitory proteins then translocate to the nucleus leading to transcriptional activation of several target genes (92). In addition to this classical activation mechanism involving I $\kappa$ B degradation, post-translational modifications of p65 by phosphorylation, acetylation, and ubiquitination have been shown to modulate the trans-activation potential of NF- $\kappa$ B (92). Inhibition of NF- $\kappa$ B in differentiated muscle improves their regeneration in response to CTX-mediated injury (78) and in the mdx model of Duchenne muscular dystrophy (16). Coincidentally, we found that the DNA binding activity of NF- $\kappa$ B and the transcript levels of TNF- $\alpha$  and IL-1 $\beta$  were reduced in injured skeletal muscle of TRAF6<sup>mko</sup> mice (84). These results are also in agreement with our recently published report demonstrating that TRAF6 mediates the activation of NF- $\kappa$ B in skeletal muscle in response to catabolic stimuli such as denervation and cancer cachexia (41).

Cross-talk between NF- $\kappa$ B and Notch signaling pathways has been implicated in different cellular contexts (79, 80). Cytoplasmic sequestration of p65 by I $\kappa$ B $\alpha$  was shown to

both translocate nuclear corepressors SMRT (silence mediator for retinoic acid and thyroid receptors)/N-CoR (nuclear receptor corepressor) to the cytoplasm and upregulate transcription of Notch-dependent genes (93). Moreover, p65 and I $\kappa$ B $\alpha$  are able to directly bind SMRT, and this interaction can be inhibited in a dose-dependent manner by the CREB binding protein (CBP) coactivator and after TNF $\alpha$  treatment, suggesting that stimuli that promote I $\kappa$ B $\alpha$  degradation, p65 acetylation and NF- $\kappa$ B activation, such as TNF $\alpha$ , inhibit Notch-dependent transcriptional activity (93). More recently, it has been reported that TNF $\alpha$  is capable of inhibiting Notch1 in satellite cells and C2C12 myoblasts through NF- $\kappa$ B-dependent manner (94). Thus, the reduced expression of TNF- $\alpha$  and suppression of NF- $\kappa$ B activity may be another mechanisms for the increased Notch signaling in regenerating myofibers of TRAF6<sup>mk0</sup> mice.

While the role of TRAF6 in innate immune response has been extensively studied, there is a dearth of information on its mediation in activation of different phenotypes of macrophages. Accumulating evidence suggests that macrophage phenotype transition is critical for the regeneration of skeletal muscle upon injury because proinflammatory (M1) and anti-inflammatory (M2c) macrophages exert antagonistic effects on myogenesis (95). Initial activation of proinflammatory macrophages is mediated by inflammatory cytokines which is not influenced by muscle cells. However, as the regeneration progresses, cytokines produced by muscle cells may also contribute towards prolonged activation of macrophages (95). TNF- $\alpha$  and IL-1 $\beta$  are two inflammatory cytokines produced by both M1 macrophages and skeletal muscle cells (95-97). Increased levels of these cytokines facilitate the activation of M1 macrophages and inhibit transition from M1 to M2 phenotype. Our results demonstrate that the expression of both IL-1 $\beta$  and TNF $\alpha$  are decreased in injured myofibers

of TRAF6<sup>mk0</sup> mice which may be responsible for the reduced activation of M1 macrophages (84). In contrast, IL-4 and IL-10 are predominately anti-inflammatory cytokines which promote M2c phenotype of macrophages and induces the proliferation of satellite cells (98-100). While we did not find any major difference in mRNA levels of IL-10, the expression of IL-4 was increased in injured myofibers of TRAF6<sup>mk0</sup> compared to TRAF6<sup>f/f</sup> mice (84). This suggests that the inhibition of TRAF6 limits the levels of inflammatory cytokines which hastens the appearance of M2c macrophages resulting in increased proliferation of myogenic cells and rapid restoration of myofibers architecture.

It is also of interest to note that some of the pathways purported to be involved in skeletal muscle regeneration or synthesis of new myofibers were not affected by depletion of TRAF6. Ablation of TRAF6 did not have any major effect on the phosphorylation of Akt kinase and p38MAPK (84). While these data are in contrast to previous reports of TRAF6-dependent activation of Akt (36) and p38MAPK (101), they highlight TRAF6-mediated differential activation of downstream signaling pathways (102). This context-dependent role of TRAF6 supports our inference that in injury-induced regeneration of skeletal muscle, TRAF6 acts as a negative regulator of myogenesis.

While the TRAF6-mediated signaling in differentiated myofibers inhibits their regeneration upon injury, it is noteworthy that the role of TRAF6 could be quite different in muscle progenitor cells. A published report suggests that siRNA-mediated knockdown of TRAF6 in cultured C2C12 myoblasts inhibits their proliferation as well as differentiation into multinucleated myotubes (42). Using siRNA electroporation approach, Xiao et al (103) have recently investigated the *in vivo* role of TRAF6 in skeletal muscle regeneration. In contrast to our study, they reported that TRAF6 is essential for skeletal muscle regeneration

because its depletion through siRNA-mediated technique inhibited regeneration of injured myofibers (103). However, in their study, they performed electroporation of TRAF6 siRNA in TA muscle one day post CTX injection and continually performed the same procedure every day before studying muscle regeneration. This implies that they depleted TRAF6 in all cell types including satellite cells and immune and other cell types which infiltrate myofibers after injury (103). While the specific *in vivo* role of TRAF6 in satellite cell proliferation and differentiation requires further investigation using genetic mouse models, in the present study, we have shown that TRAF6 signaling that specifically originates in differentiated myofibers attenuates muscle regeneration program in response to injury.

In summary, TRAF6-mediated regulation of muscle regeneration unveiled by this study provides an unanticipated link Notch signaling and satellite cell activation and muscle formation in an injured tissue microenvironment. Considering the importance and limited availability of therapeutic interventions that can influence the balance between inflammation and myogenesis in pathological conditions such as muscular dystrophy, we believe that interventions targeting TRAF6-mediated signaling will enhance the ability to improve pathological conditions in inflammatory muscle disorders.

**FIGURE 2.1**

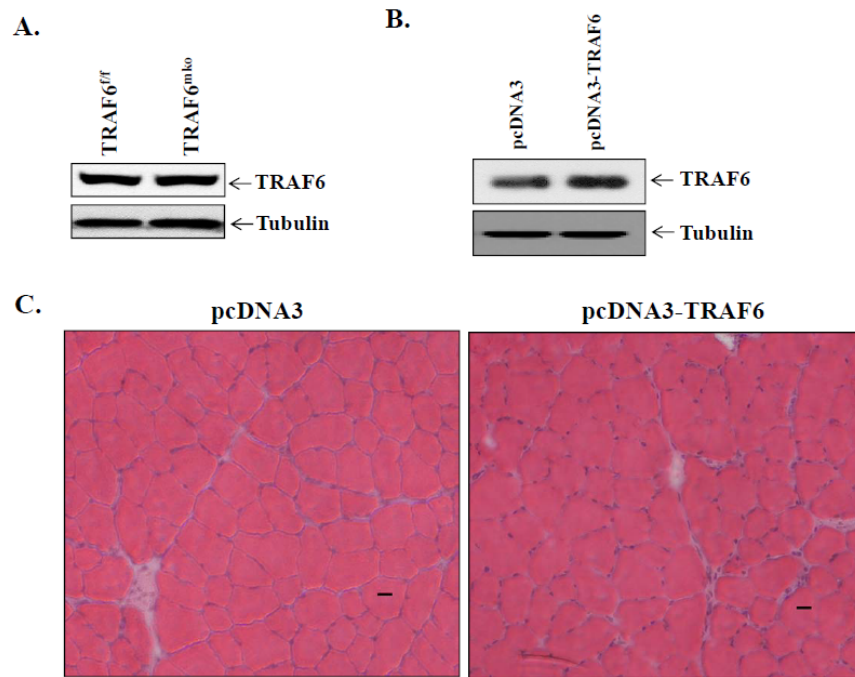


**FIGURE 2.1. Levels of TRAF6 in satellite cells of TRAF6<sup>f/f</sup> and TRAF6<sup>mko</sup> mice and effects of overexpression of TRAF6 in uninjured muscle of WT mice. (A).**

Representative immunoblots presented here demonstrate protein levels of TRAF6 and tubulin in cultured satellite cells of TRAF6<sup>f/f</sup> and TRAF6<sup>mko</sup> mice. **(B)** TA muscle of 10-week old C57BL6 mice was electroporated with pcDNA3 alone or pcDNA3-TRAF6 plasmid. After 7 days, the TA muscle was isolated and analyzed. Immunoblot presented here demonstrates increased levels of TRAF6 in pcDNA3-TRAF6 electroporated TA muscle. The level of an unrelated protein tubulin was comparable between TA muscle electroporated with pcDNA3 or pcDNA3-TRAF6 plasmids. **(C)**. Representative photomicrographs of H&E-stained transverse sections of TA muscle 7 days after electroporation with pcDNA3 or pcDNA3-TRAF6 plasmids. Scale bar: 20 $\mu$ m.

**FIGURE 2.2**

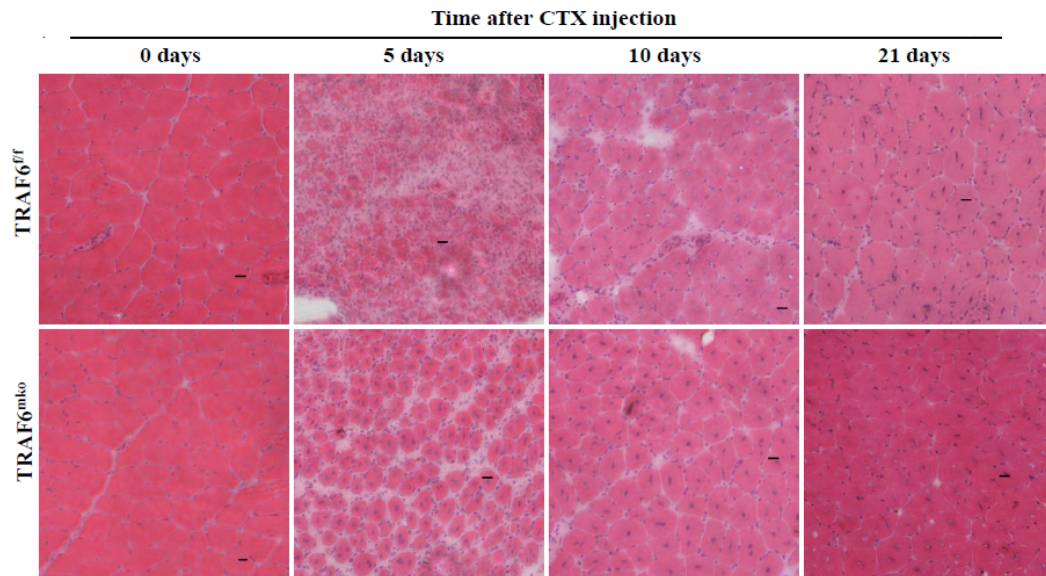


**FIGURE 2.2. Ablation of TRAF6 improves skeletal muscle regeneration in mice.** TA muscle of 8-week old WT mice was injected 100 $\mu$ l of saline alone or containing 10  $\mu$ M cardiotoxin (CTX) and analyzed at 5d. Representative immunoblots of TRAF6 and an unrelated protein tubulin in saline and CTX-injected tibial anterior (TA) muscle. N=3 at each time point. Scale bar: 20  $\mu$ m.

**FIGURE 2.3**

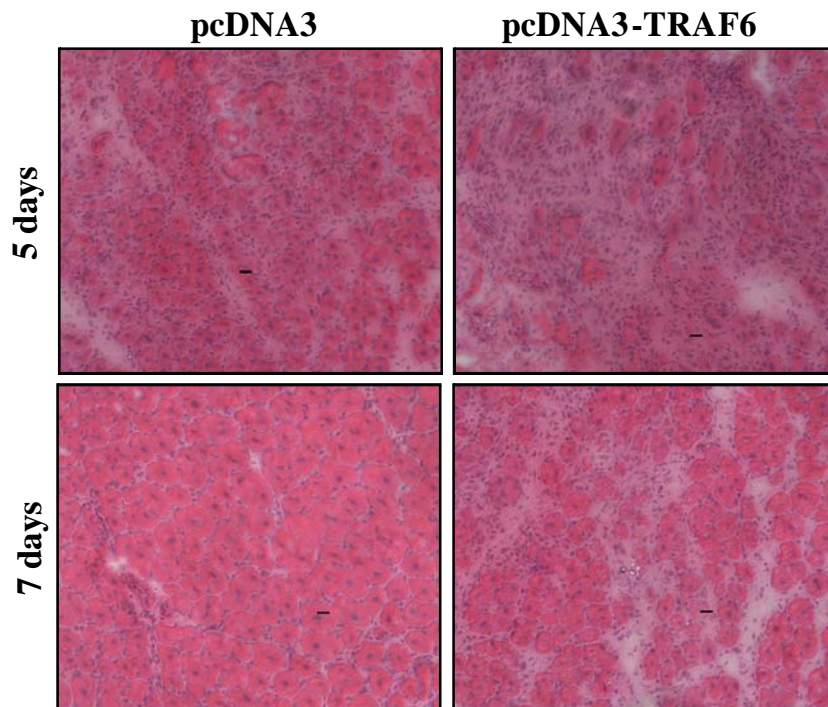
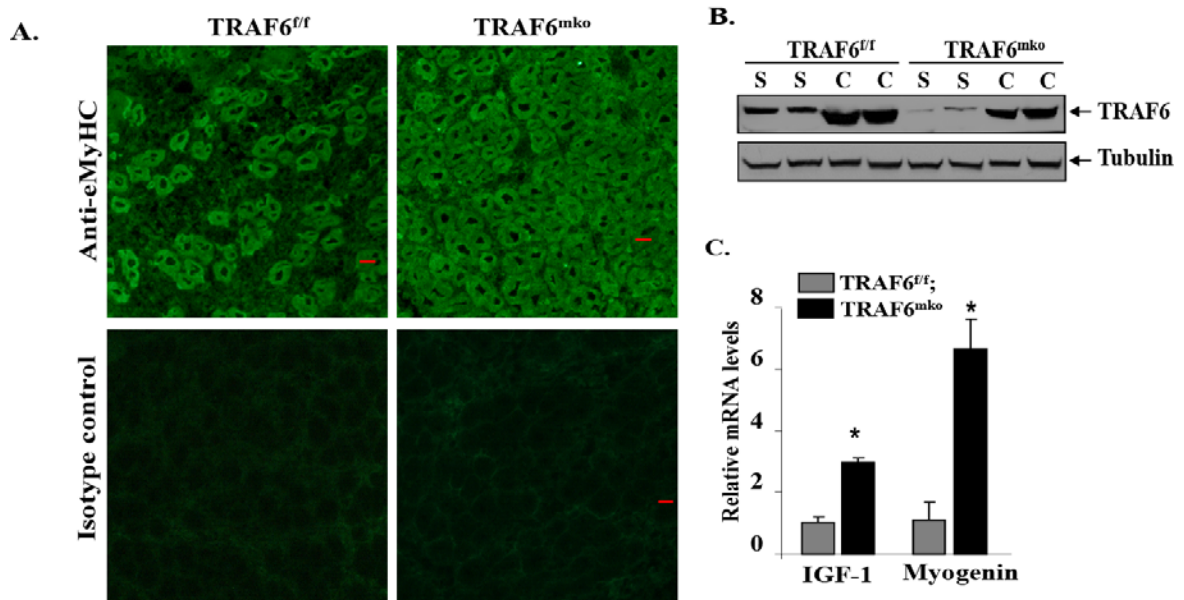


**FIGURE 2.3 Overexpression of TRAF6 reduces myofibers regeneration upon injury.**

TA muscle of WT mice was electroporated with pcDNA3 or pcDNA3-TRAF6 plasmids. After 7d, the muscle was injected with 100  $\mu$ l of 10  $\mu$ M CTX solution followed by their isolation and performing H&E staining. Representative photomicrographs of H&E-stained transverse sections at 5d and 7d post CTX injection are presented here. N=3 at each time point. Scale bar: 20  $\mu$ m.

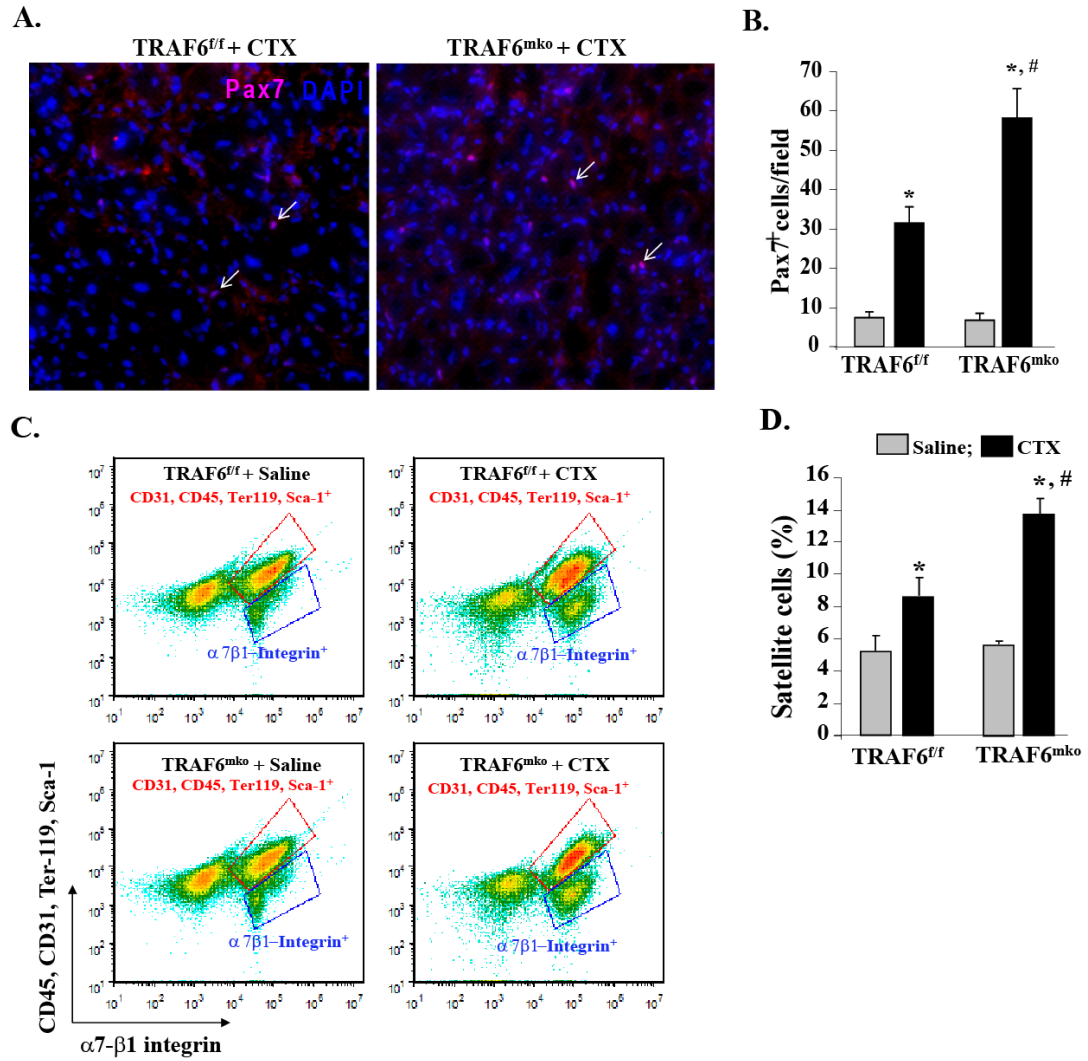


**FIGURE 2.4**



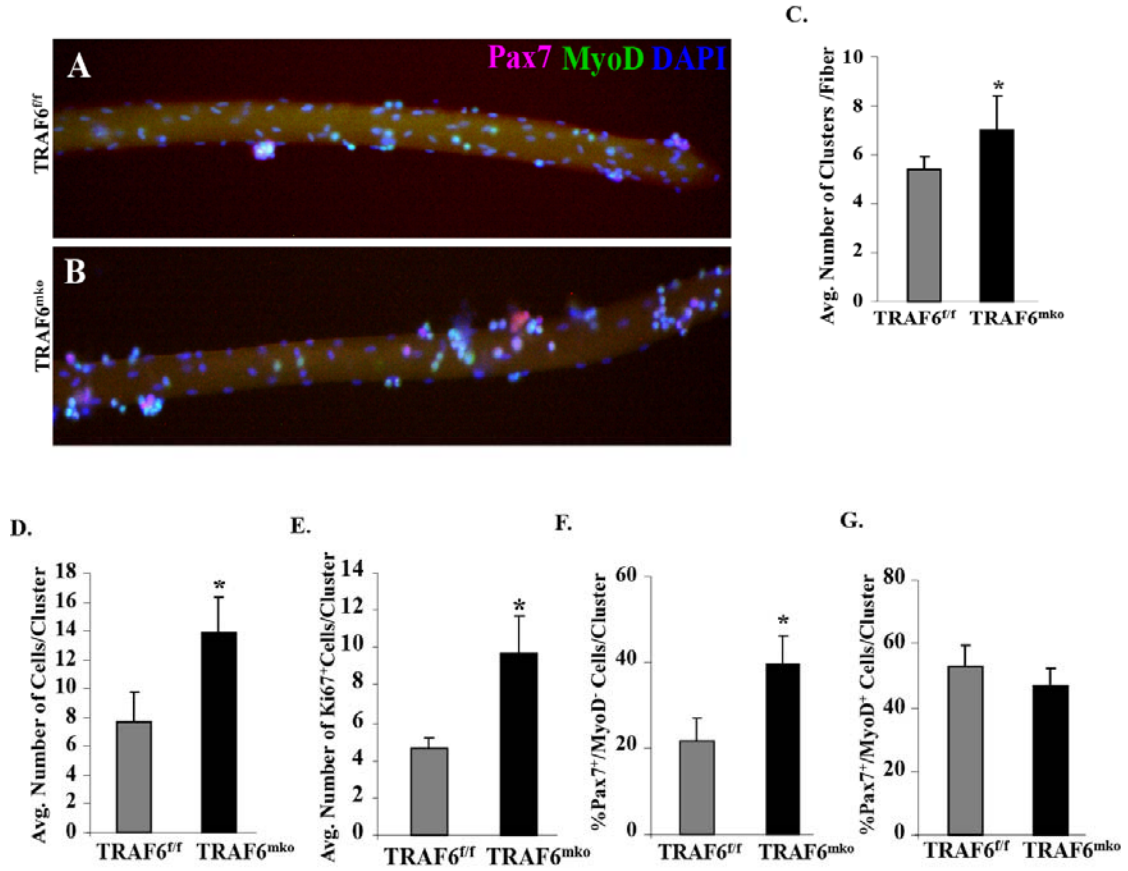
**FIGURE 2.4 Ablation of TRAF6 accelerates restoration of muscle architecture after injury.** TRAF6<sup>f/f</sup> and TRAF6<sup>mko</sup> mice were injected with saline or CTX in TA muscle followed by their isolation and analyses at 5d. . **(A)** Transverse sections of CTX-injured TA muscle from TRAF6<sup>f/f</sup> and TRAF6<sup>mko</sup> mice stained with anti-eMyHC (embryonic myosin heavy chain) or isotype control (mouse IgG). **(B)** Western blot analysis of expression levels of TRAF6, and tubulin in saline or CTX-injected TA muscle from TRAF6<sup>f/f</sup> and TRAF6<sup>mko</sup> mice. **(C)** Transcript levels of IGF-1 and myogenin in TA muscle of TRAF6<sup>f/f</sup> and TRAF6<sup>mko</sup> mice measured at 5d post CTX injection. Error bars represent SD. N=4 in each time point. \*p < 0.01, values significantly different from CTX-injected TA muscle of TRAF6<sup>f/f</sup> mice.

**FIGURE 2.5**



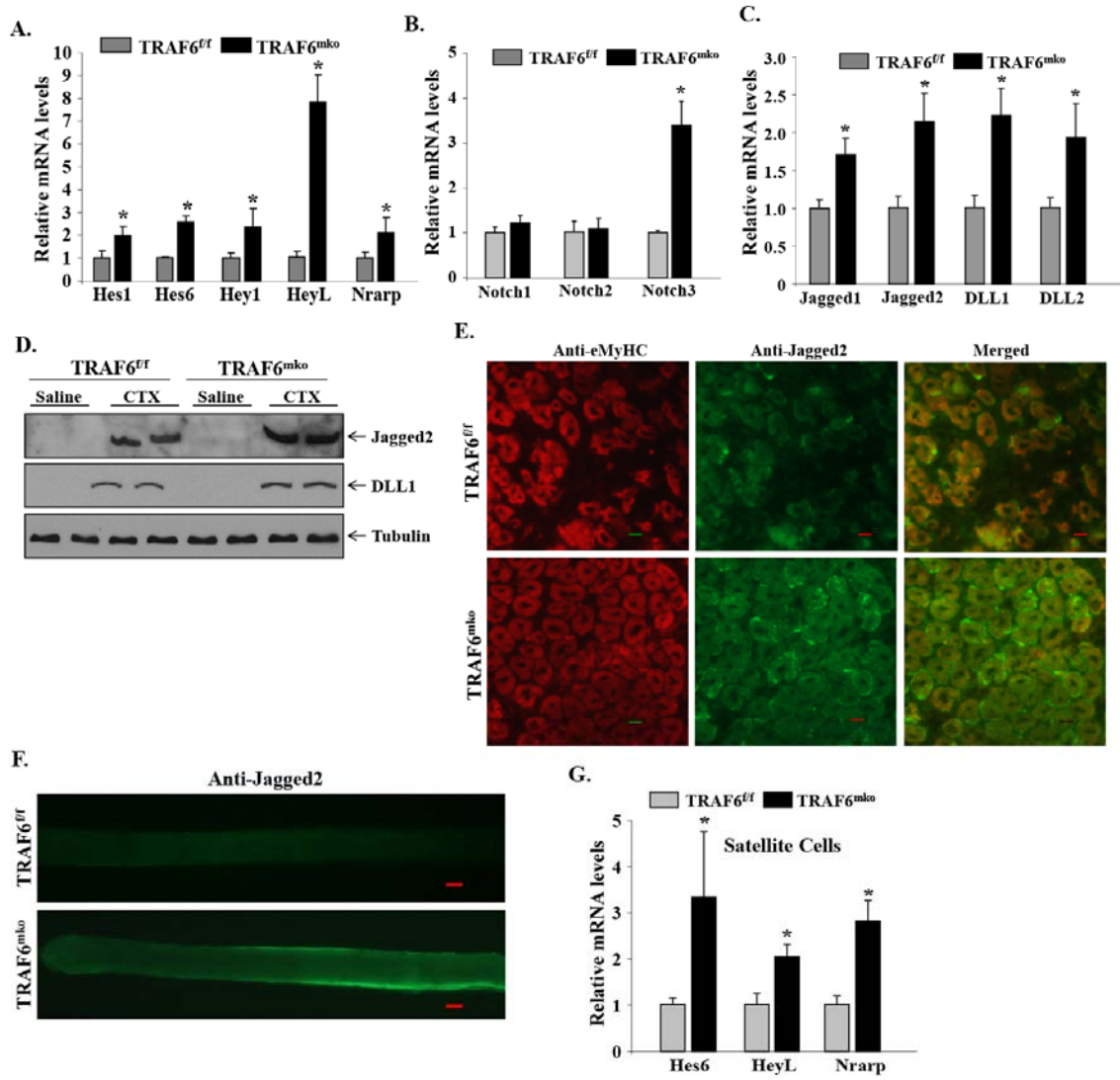
**FIGURE 2.5. Ablation of TRAF6 promotes the activation of satellite cells during muscle regeneration.** Three months old TRAF6<sup>f/f</sup> and TRAF6<sup>mk0</sup> were injected with saline or CTX in TA muscle and analyzed after five days. **(A)** Representative photomicrographs after immunostaining of transverse muscle sections with Pax7 antibody. Nuclei were identified by co-staining with DAPI. Arrows points to Pax7<sup>+</sup> cells. **(B)** Average number of Pax7<sup>+</sup> cells per field (~0.15 mm<sup>2</sup>) in saline and 5d CTX-injected TA muscle of TRAF6<sup>f/f</sup> and TRAF6<sup>mk0</sup> mice. **(C)** FACS analysis of saline or CTX-injected TA muscle for  $\alpha$ 7 $\beta$ 1-integrin-positive activated satellite cells in TRAF6<sup>f/f</sup> and TRAF6<sup>mk0</sup> mice. Representative dot plots are shown. Negative selection antibodies (CD45, CD31, Ter119, Sca-1) are gated in red whereas positive selection antibody ( $\alpha$ 7 $\beta$ 1-Integrin) is gated in blue. **(D)** Quantification of activated satellite cells in saline or CTX-injected TA muscles of TRAF6<sup>f/f</sup> and TRAF6<sup>mk0</sup> mice by FACS. Error bars represent SD. N=6 in each group. \*p < 0.01, values significantly different from contralateral saline-injected TA muscle; #p < 0.01, values significantly different from CTX-injected TA muscle of TRAF6<sup>f/f</sup> mice.

FIGURE 2.6



**FIGURE 2.6. Ablation of TRAF6 promotes proliferation and self-renewal of satellite cells.** Single myofiber cultures were established from EDL muscle of TRAF6<sup>f/f</sup> and TRAF6<sup>mko</sup> mice. **(A)** After 72h, myoblast clusters on the single myofibers were labeled with antibodies against Pax7 and MyoD. Nuclei were counterstained with DAPI. Representative merged images of Pax7, MyoD, and DAPI staining are presented here. **(B)** Average number of clusters (containing >4 cells per fiber) per myofiber of TRAF6<sup>f/f</sup> and TRAF6<sup>mko</sup> calculated from 35 myofibers in each group. **(C)** Number of myoblasts per cluster in TRAF6<sup>f/f</sup> and TRAF6<sup>mko</sup> mice (n=22). **(D)** In a separate experiment, myoblasts were also stained with proliferation marker Ki67 and DAPI and the number of Ki67<sup>+</sup> cells per cluster were enumerated. **(E and F)** Percentage of self-renewing (Pax7<sup>+</sup>MyoD<sup>-</sup>) and proliferating (Pax7<sup>+</sup>/MyoD<sup>-</sup>) myoblasts in TRAF6<sup>f/f</sup> and TRAF6<sup>mko</sup> myoblast colonies (calculated from 22 cultured colonies in each group). \*p < 0.01, values significantly different from CTX-injected TA muscle of TRAF6<sup>f/f</sup> mice.

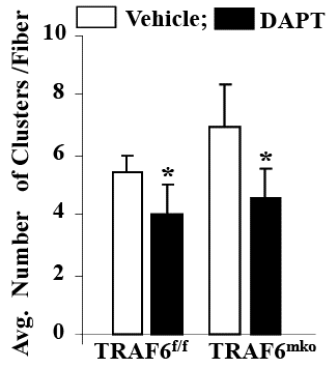
**FIGURE 2.7**



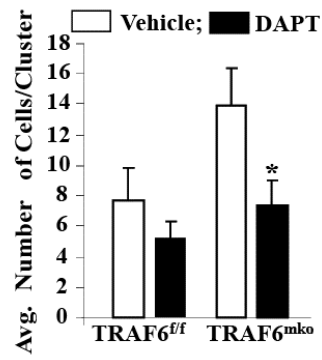
**FIGURE 2.7. Muscle-specific inhibition of TRAF6 activates Notch signaling upon injury.** TA muscle of TRAF6<sup>f/f</sup> and TRAF6<sup>mk0</sup> mice were injected with cardiotoxin (CTX) and 5d later the muscle were isolated and processed for QRT-PCR, Western blot, or immunostaining. Relative mRNA levels of (A) Notch target genes Hes1, Hes6, Hey1, HeyL, and Nrarp; (B) Notch receptors Notch1, Notch2, and Notch3; and (C) Notch ligands Jagged1, Jagged2, DLL1, and DLL2 in CTX-injected TA muscle of TRAF6<sup>f/f</sup> and TRAF6<sup>mk0</sup> mice. N=6 in each group. (D) Western blot analysis of Jagged2 and DLL1 protein in saline or CTX-injected TA muscle of TRAF6<sup>f/f</sup> and TRAF6<sup>mk0</sup> mice. (E) CTX-injected TA muscle transverse frozen sections were stained for embryonic myosin heavy chain (eMyHC) and Jagged2. Representative photomicrographs presented here demonstrate increased immunostaining for Jagged2 in myofibers of TRAF6<sup>mk0</sup> mice compared to TRAF6<sup>f/f</sup> mice. (F) Single myofiber cultures were prepared from TRAF6<sup>f/f</sup> and TRAF6<sup>mk0</sup> mice. After 24h in cultures, myofibers (n=12) were stained for Jagged2. (G) Relative mRNA levels of Notch-target genes Hes6, HeyL, and Nrarp in satellite cells isolated by FACS method from 5d CTX-injected TA muscle of TRAF6<sup>f/f</sup> (N=3) and TRAF6<sup>mk0</sup> (N=3) mice. Bars represent SD. \*p<0.05, values significantly different from corresponding TRAF6<sup>f/f</sup> mice.

FIGURE 2.8

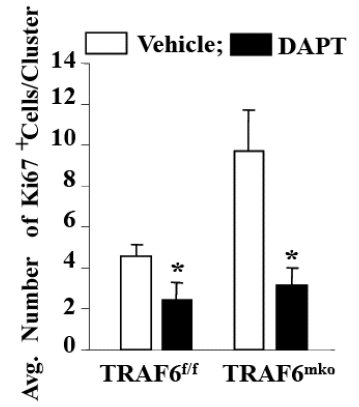
A.



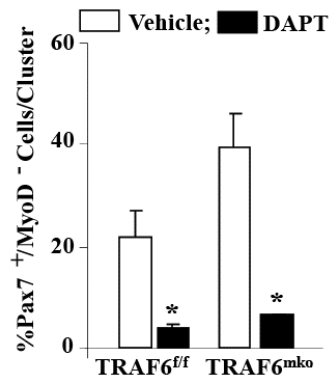
B.



C.



D.



E.

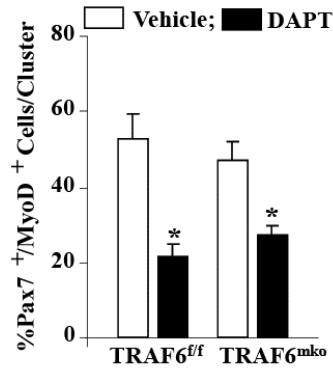




**FIGURE 2.8. Activation of Notch pathway causes activation and self-renewal of satellite cells on cultured myofibers of TRAF6<sup>mk0</sup> mice.** Single myofiber cultures were established from EDL muscle of TRAF6<sup>f/f</sup> and TRAF6<sup>mk0</sup> mice. After 48h, myofibers were treated with vehicle alone or along with 10 $\mu$ m for DAPT. Myoblasts on single myofibers were stained with antibodies against Pax7, MyoD, and/or Ki67 and nuclei were counter stained with DAPI. **(A)** Average number of clusters (containing >4 cells per fiber) per myofiber of DAPT-treated TRAF6<sup>f/f</sup> and TRAF6<sup>mk0</sup> myofiber cultures (calculated from 18 myofibers in each group). **(B)** Number of myoblasts per cluster in DAPT-treated myofiber cultures from TRAF6<sup>f/f</sup> and TRAF6<sup>mk0</sup> mice (n=16). **(C)** Number of Ki67<sup>+</sup> cells per cluster. **(D and E)** Percentage of self-renewing (Pax7<sup>+</sup>MyoD<sup>-</sup>) and proliferating (Pax7<sup>+</sup>/MyoD<sup>+</sup>) myoblasts in TRAF6<sup>f/f</sup> and TRAF6<sup>mk0</sup> myoblast colonies (calculated from 17 cultured colonies in each group). Bars represent SD. \*p<0.05, values significantly different from corresponding TA muscle of TRAF6<sup>f/f</sup> mice.

## CHAPTER 3

### DISTINCT ROLES OF TRAF6 AT EARLY AND LATE STAGES OF MUSCLE PATHOLOGY IN THE MDX MODEL OF DUCHENNE MUSCULAR DYSTROPHY

#### 3.1 INTRODUCTION

Duchenne muscular dystrophy (DMD) is a devastating and ultimately fatal disease characterized by progressive muscle wasting and weakness. The absence of dystrophin is a key factor in developing DMD (104). Dystrophin is a critical component of dystrophin-glycoprotein complex (DGC), which links the cytoskeleton to the extracellular matrix thus maintaining muscle fiber membrane integrity. (8). Although the primary genetic defect is known, the dystrophic process has not been clearly identified (10, 11). Studies in animal models and humans have shown that the primary deficiency of dystrophin results in the activation of several pathological cascades such as extracellular matrix breakdown, oxidative stress, cycles of fiber degeneration and regeneration, inflammatory response, and gradual replacement of muscle fibers with adipose and connective tissue (10, 12-15). Besides acting as a molecular scaffold serving mechanical function, accumulating evidence suggests that DGC also has an important signaling role in striated muscle. Loss of dystrophin in skeletal muscle leads to aberrant activation of a number of signaling pathways such as nuclear factor- $\kappa$ B (NF- $\kappa$ B), phosphatidylinositol 3-kinase (PI3K)/Akt, and mitogen-activated protein kinases (16-21). Interestingly, many of these signaling pathways are

activated even at pre-necrotic state and their modulation using molecular and pharmacological approaches considerably improves muscle pathology in models of DMD (16-18, 20, 21). However, given the progressive degenerative nature of DMD and the convoluted involvement of many secondary processes, developing a pan therapeutic strategy that proves beneficial during the course of the disease has been challenging. Despite the identification of many of the principal and auxiliary signaling pathways that contribute to myopathy, the proximal signaling events leading to the activation of such pathological cascades in dystrophic muscle remain unknown.

TNF receptor-associated factors (TRAFs) are a family of conserved adaptor proteins which act as signaling intermediates for several receptor-mediated signaling events leading to the context-dependent activation of a number of signaling pathways (48, 49). TRAF6 functions as a signal transducer to activate I $\kappa$ B kinase (IKK) and subsequently NF- $\kappa$ B activation in response to proinflammatory cytokines, bacterial products, Toll/IL-1 family and from receptors such as receptor activator of NF- $\kappa$ B (RANK) and CD40 (25, 27, 37, 49). TRAF6 is also an E3 ubiquitin ligase which undergoes autoubiquitination and catalyzes K63 polyubiquitination of TAK1 that is required for IKK activation (29, 105). TRAF6 interacts with ubiquitin conjugating enzymes UBE2N/UBC13 and UBE2V1/UEV1A to stimulate the formation of polyubiquitin chains on IKK. This protein also causes the K63-linked polyubiquitination of Akt which leads to its translocation to cell membrane, phosphorylation, and enzymatic activation (36). Other signaling proteins such as interleukin-1 receptor-associated kinase 1 (IRAK1), Src family kinase, and protein kinase C zeta (PKC $\zeta$ ) have also been found to interact with TRAF6 further signifying a central role of TRAF6 in cross-talk between different signaling pathways (27, 37, 49). Moreover, TRAF6 interacts with scaffold

protein p62/Sequestosome 1 which is involved in regulation of autophagy and TRAF6 trafficking of proteins to the proteasome (37-40). It has been also found that TRAF6 promotes the K63-linked ubiquitination of Beclin-1, which is critical for the induction of autophagy, in response to toll-like receptor 4 signaling (46). However, the role of TRAF6 signaling in muscular dystrophy remains unknown.

Accumulating evidence suggests that TRAF6 is a crucial regulator of skeletal muscle mass in catabolic states (41, 43, 84). Abundance and activation of TRAF6 are increased in skeletal muscle of mice in many atrophying conditions. Notably, inhibition of TRAF6 using genetic approaches attenuates muscle-wasting in response to denervation, cancer cachexia, and starvation (41, 43). Furthermore, specific inhibition of TRAF6 also improves myofiber regeneration upon cardiotoxin-mediated injury (84). One of the mechanisms by which TRAF6 mediates muscle-wasting is through stimulation of autophagy (41, 43). Autophagy is an important homeostasis mechanism which is essential for clearing of dysfunctional organelles and preventing tissue damage (106). While basal level of autophagy is required for the maintenance of skeletal muscle mass, excessive autophagosome formation generally leads to muscle-wasting (106-110). Interestingly, autophagy has been found to be impaired in muscle biopsies from patients with DMD and in skeletal muscle of mdx mice with concomitant accumulation of damaged organelles (111). However, the role of TRAF6 in regulation of autophagy in the “settings” of muscular dystrophy remains unknown.

In this study, we have investigated the role and the mechanisms by which TRAF6 affects disease progression in mdx (a mouse model of DMD) mice. Our results show that depletion of TRAF6 attenuates injury and inflammation and improves muscle structure and regeneration in young mdx mice. By contrast, continued inhibition of TRAF6 causes fiber

degeneration and fibrosis at later stages of mdx mouse development potentially through inhibition of autophagy.

### **3.2 MATERIALS AND METHODS**

**Mice.** Wild-type (strain: C57BL/10 ScSn) and mdx (strain: C57BL/10 ScSn DMD<sup>mdx</sup>) mice were purchased from Jackson Laboratory (Bar Harbor, ME, USA). Floxed TRAF6 (TRAF6<sup>f/f</sup>) and muscle-specific TRAF6-knockout (TRAF6<sup>mk0</sup>) mice have been previously described (41, 43). TRAF6<sup>mk0</sup> mice were crossed with mdx mice for 5-6 generations to generate littermate mdx;TRAF6<sup>f/f</sup> and mdx;TRAF6<sup>mk0</sup> mice. All genotypes were determined by PCR analysis from tail DNA. Mice were housed in the animal facility of the University of Louisville under conventional conditions with constant temperature and humidity and fed a standard diet. All experiments with animals were approved by the Institutional Animal Care and Use Committee of the University of Louisville.

**Creatine kinase (CK) assay:** The serum level of CK was determined using a commercially available kit (Stanbio Laboratory, TX).

**Histology and morphometric analysis.** Skeletal muscle tissues were isolated, frozen in isopentane cooled in liquid nitrogen, and sectioned in a microtome cryostat. For the assessment of tissue morphology, 10- $\mu$ m-thick transverse sections of each muscle were stained with Hematoxylin and Eosin (H&E), and staining was visualized on a microscope (Eclipse TE 2000-U), a digital camera (Digital Sight DS-Fi1), and NIS Elements BR 3.00 software (all from Nikon). The images were stored as JPEG files, and image levels were

equally adjusted using Photoshop CS2 software (Adobe). Pictures of the whole muscle sections were captured and the percentage of centrally nucleated fibers was counted in the entire muscle section. To quantify the variation in fiber size, fiber cross-sectional area was measured for every fiber in each section using Nikon NIS Elements BR 3.00 software (Nikon). Variability in cross-sectional areas between samples was expressed as the mean of the standard deviations for each population. Necrotic area in H&E-stained sections was determined by measuring percentage area filled with cellular infiltrate in whole muscle section. Mean minimum feret diameter of eMyHC<sup>+</sup> fibers was determined after measuring cross sectional area for each fiber. The extent of fibrosis in muscle cryosections was determined using a Trichrome staining kit following a protocol suggested by manufacturer (American Master Tech).

For Immunohistochemical detection of macrophages, rat anti-mouse F4/80 (Serotec) was used at at 1:500 dilution and horseradish peroxidase-labeled streptavidin biotin technique (DAKO K5001 with E468) was used as a detection system. The concentrations of F4/80<sup>+</sup> cells were expressed as the number of cells per volume of each section.

**Indirect Immunofluorescence.** For immunohistochemistry study, muscle sections were blocked in 1% bovine serum albumin in PBS for 1h, and incubated with anti-Pax7 (1:20, Developmental Studies Hybridoma Bank, University of Iowa, Iowa City, IA) or anti-E-MyHC (1:150, Developmental Studies Hybridoma Bank, University of Iowa, Iowa City, IA) in blocking solution at 4°C overnight under humidified conditions. The sections were washed briefly with PBS before incubation with Alexa Fluor® 488 or 594-conjugated secondary antibody (1:3000, Invitrogen) for 1h at room temperature and then washed 3

times for 5 minutes with PBS. The slides were mounted using fluorescence medium (Vector Laboratories) and visualized at room temperature on Nikon Eclipse TE 2000-U microscope (Nikon), a digital camera (Nikon *Digital Sight DS-Fi1*), and Nikon NIS Elements BR 3.00 software (Nikon). Image levels were equally adjusted using Adobe Photoshop CS2 software (Adobe). Damaged/ permeabilized fibers in muscle cryosections were identified by immunostaining with Cy3-labelled goat anti-mouse IgG (1:3000, Invitrogen).

**Immunoprecipitation and Western blotting.** Quantitative estimation of specific protein was done by Western blot using a method as previously described (112). Briefly, individual tissues were washed with phosphate-buffered saline (PBS) and homogenized in lysis buffer A [50 mM Tris-Cl (pH 8.0), 200 mM NaCl, 50 mM NaF, 1 mM dithiotheritol (DTT), 1 mM sodium orthovanadate, 0.3% IGEPAL, and protease inhibitors]. Approximately, 100 $\mu$ g protein was resolved on each lane on 10% SDS-PAGE, electrotransferred onto nitrocellulose membrane and probed using anti-TRAF6 (1:500 MBL International ), anti-TRAF2 (1:500; Santa Cruz Biotechnology, Inc.), anti-TRAF3 (1:500; Santa Cruz Biotechnology, Inc ), anti-LC3B (1:500; Cell signaling Technology), anti-Beclin (1:500; Cell signaling Technology), anti-p62 (1:500; MBL International), anti-phospho-Akt (1:500; Cell Signaling Technology), anti-Akt (1:500; Cell Signaling Technology), anti-phospho-mTOR (1:500; Cell Signaling Technology), anti-mTOR (1:500; Cell Signaling Technology), anti-phospho-p70-S6K (1:500; Cell Signaling Technology), anti-p70-S6K (1:500; Cell Signaling Technology), anti-GADPH (1:2000; Cell Signaling Technology) and anti-tubulin (1:2000, Cell Signaling Inc) and detected by chemiluminescence. To study the ubiquitination of TRAF6, muscle extract (400  $\mu$ g protein) was incubated overnight with 1  $\mu$ g of anti-Ubiqutin antibody (Santa cruz

Biotechnology, Inc.) in 600  $\mu$ l of lysis buffer, protein A-Sepharose beads were added, and the mixture was incubated at 4°C for an additional 2 h. The beads were washed four times with lysis buffer and finally suspended in 2 $\times$  Laemmli sample buffer. Proteins were resolved on 10% SDS-PAGE gel and immunoblotted using TRAF6 antibody (1:500; MBL International).

**Electrophoretic Mobility Shift Assay (EMSA).** The DNA binding activity of NF- $\kappa$ B transcription factor was measured using EMSA as detailed (21). Briefly, 20  $\mu$ g of nuclear extract prepared from skeletal muscle was incubated with 16 fmol  $^{32}$ P- $\gamma$  ATP-end-labeled NF- $\kappa$ B consensus double-stranded oligonucleotide (Promega, MA) for 20 min at 37°C. The incubation mixture included 2–3  $\mu$ g of poly dI.dC in a binding buffer (25 mM HEPES [pH 7.9], 0.5 mM EDTA, 0.5 mM dithiothreitol, 1% IGEPAL, 5% glycerol, 50 mM NaCl). The DNA-protein complex thus formed was separated from free oligonucleotides on a 7.5% native polyacrylamide gel. The gel was dried, and radioactive bands were visualized and quantitated by PhosphorImager using ImageQuant TL software (GE Healthcare, Piscataway, NJ).

**Quantitative real-time PCR (QRT-PCR):** Real-time PCR for individual genes was performed using an ABI Prism 7300 Sequence Detection System (Applied Biosystems) using a method as previously described (112, 113). Briefly, the first strand cDNA reaction (0.5  $\mu$ l) from gastrocnemius muscle of individual control or mdx mice (n=4 in each group) was subjected to real-time PCR amplification using gene-specific primers. The primers were designed according to ABI primer express instructions using Vector NTI software and were purchased from Sigma-Genosys (Spring, TX). The sequences of the primers used are as



follows: TNF- $\alpha$ , 5'-GCA TGA TCC GCG ACG TGGAA-3' (forward) and 5'-AGATCCATGCCGTTGGCC AG-3'(reverse); IL-1 $\beta$ , 5'-CTCCATGAGCTTTGTACAAGG-3' (forward) and 5'-TGCTGATGTACCAGTTGGGG-3' (reverse); IL-6, 5'-CCTTCTTGGGACTGATGCTGG-3' (forward) and 5'-GCCTCCGACTTGTGAAGTGGT-3' (reverse); MMP-9, 5'-GCGTGTCTGGAGATTCGACTT G-3' (forward) and 5'-CATGGTCCACCTTGTTACCTC-3' (reverse); LC3B, 5'-CTGGTGAATGGGCACAGCATG-3' (forward) and 5'-CGTCCGCTGGTAACATCCCTT-3' (reverse); Beclin1, 5'-TGAAATCAATGCTGCCTGGG-3' (forward) and 5'-CCAGAACAGTATAACGGCAACTCC-3' (reverse); p62, 5'-AGCACAGGCACAGAAGACAAGAGT-3' (forward) and 5'-AATGTGTCCAGTCATCGTCTCCTC-3' (reverse); Atrogin-1, 5'-GTCGCAGCCAAGAAGAGAAAGA-3' (forward) and 5'-TGCTATCAGCTCCAACAGCCTT-3' (reverse); MuRF1, 5'-TAACTGCATCTCCATGCTGGTG-3' (forward) and 5'-TGGCGTAGAGGGTGTCAAACCTT-3' (reverse); and beta-actin, 5' - CAGGCATTGCTGACAGGATG-3' (forward) and 5'-TGCTGATCCACATCTGCTGG-3' (reverse).

Approximately 25  $\mu$ l of reaction volume was used for the real-time PCR assays which consisted of 2 $\times$  (12.5  $\mu$ l) Brilliant SYBR Green QPCR Master Mix (Stratagene), 400 nm of primers (0.5  $\mu$ l each from the stock), 11  $\mu$ l of water, and 0.5  $\mu$ l of template. The thermal conditions consisted of an initial denaturation at 95  $^{\circ}$ C for 10 min followed by 40 cycles of denaturation at 95  $^{\circ}$ C for 15 s, annealing and extension at 60  $^{\circ}$ C for 1 min, and, for

a final step, a melting curve of 95 °C for 15 s, 60 °C for 15 s, and 95 °C for 15 s. All reactions were carried out in triplicate to reduce variation. The data were analyzed using SDS software version 2.0, and the results were exported to Microsoft Excel for further analysis. Data normalization was accomplished using two endogenous control ( $\beta$ -actin) and the normalized values were subjected to a  $2^{-\Delta\Delta C_t}$  formula to calculate the fold change between the control and experimental groups. The formula and its derivations were obtained from the ABI Prism 7900 Sequence Detection System user guide.

**Grip strength and wire hanging measurements.** A digital grip-strength meter (Columbus Instruments, Columbus, OH) was used to measure forelimb or total four-limb grip strength in mice. Mice were acclimatized for 5 minutes before starting test. The mouse was allowed to grab the metal pull bar with the forepaws and in a separate experiment with all four-paws. The mouse tail was then gently pulled backward in the horizontal plane until it could no longer grasp the bar. The force at the time of release was recorded as the peak tension. Each mouse was tested 5 times with a 20–40 seconds break between tests. The average peak tension from three best attempts normalized against total body weight was defined as forelimb grip strength. For wire hanging time evaluation, mice were placed on a grid in a starting upright position. The grid was then gradually inverted above a cage filled with bedding. Hanging time was determined as the longest time sustained hanging against gravity from three repetitions.

**Statistical analysis.** Results are expressed as mean  $\pm$  standard deviation (SD). Statistical analysis used Student's t-test (two tailed) to compare quantitative data populations with

normal distribution and equal variance. A value of  $P < 0.05$  was considered statistically significant unless otherwise specified.

### **3.3 RESULTS**

**3.3.1 TRAF6 levels are increased in skeletal muscle of mdx mice.** In mdx mice, muscle injury starts at around 2.5 weeks followed by peak necrotic phase in combination with inflammation between 3-4 weeks of age (114, 115). Regeneration starts around the age of 6 weeks and continues while alternating with ongoing degeneration until 12 weeks of age (116, 117). We first compared levels of TRAF6 in skeletal muscle of wild-type (WT) and mdx mice at both pre-necrotic and necrotic stages. Diaphragm and gastrocnemius (GA) muscle from 10, 14, 23, and 48 days old WT (i.e. C57BL10) and mdx mice were isolated and processed to measure protein levels of TRAF6 by performing Western blot. Consistent with our previously published results (41), the levels of TRAF6 were considerably higher in young mice and reduced at later stages of development. However, levels of TRAF6 protein were markedly higher in both diaphragm and GA muscle of mdx mice compared with WT mice at all the ages (**Figures 3.1A, 3.1B**). In a separate experiment, we measured protein levels of TRAF6 in quadriceps muscle of young (6-week) and old (9-month) WT and mdx mice. The levels of TRAF6 were significantly higher in quadriceps muscle of both 6-week and 9-month old mdx mice compared with their corresponding age-matched WT mice (**Figure 3.2**). Increased levels of TRAF6 at 10 and 14 days in mdx mice also suggests that levels of TRAF6 start increasing before the onset of fiber necrosis in mdx mice.

Since TRAF6 is an important E3 ubiquitin ligase which also undergoes autoubiquitination to induce cellular signaling (33, 34, 43), we next investigated the levels

of ubiquitinated TRAF6 protein in skeletal muscle of WT and mdx mice. Diaphragm was isolated from 10, 14, 21, 23, and 48 days old mice and muscle extracts prepared were immunoprecipitated using anti-ubiquitin followed by Western blot with anti-TRAF6. Results showed that the levels of ubiquitinated TRAF6 protein were significantly higher in mdx mice compared with WT mice at all the ages (**Figure 3.1C**). Together these data are suggestive that the levels and activation of TRAF6 are increased in skeletal muscle of mdx mice.

### **3.3.2 Targeted deletion of TRAF6 improves muscle strength in 7-week old mdx mice.**

We have previously generated and characterized muscle-specific TRAF6-knockout mice (TRAF6<sup>mk0</sup>) by crossing floxed TRAF6 (TRAF6<sup>f/f</sup>) mice with muscle creatine kinase (MCK)-Cre mice (41). MCK deletes floxed TRAF6 allele only in differentiated myofibers but not in other cell type such as satellite cells, endothelial cells, and fibroblasts (41, 84). For this study, we crossed TRAF6<sup>mk0</sup> mice with mdx mice to obtain littermate mdx;TRAF6<sup>f/f</sup> and mdx;TRAF6<sup>mk0</sup> mice. We first measured the levels of TRAF6 in skeletal muscle of mdx;TRAF6<sup>f/f</sup> and mdx;TRAF6<sup>mk0</sup> mice at the age of 2-week (before the onset of fiber necrosis). Levels of TRAF6 were found to be significantly reduced (~80%) in diaphragm and gastrocnemius (GA) muscle of mdx;TRAF6<sup>mk0</sup> mice compared with mdx;TRAF6<sup>f/f</sup> mice (**Figures 3.3A, 3.3B**). The depletion of TRAF6 in mdx;TRAF6<sup>mk0</sup> mice was specific because levels TRAF2 and TRAF3 were comparable between mdx;TRAF6<sup>f/f</sup> and mdx;TRAF6<sup>mk0</sup> mice (**Figure 3.3A**). We next investigated whether depletion of TRAF6 in skeletal muscle of mdx mice produces any developmental phenotype at pre-necrotic state. Hematoxylin and Eosin (H&E) staining of gastrocnemius (GA) muscle (**Figure 3.3C**) and

diaphragm (data not shown) showed that depletion of TRAF6 does not produce any overt phenotype in mdx mice at pre-necrotic state.

We next performed systematic evaluation of muscle function in mdx;TRAF6<sup>f/f</sup> and mdx;TRAF6<sup>mk0</sup> mice. We first sought to investigate whether depletion of TRAF6 affects muscle grip strength in mdx mice. Results showed that fore limb (**Figure 3.3D**) and total four limb (**Figure 3.3E**) grip strength was significantly higher in mdx;TRAF6<sup>mk0</sup> mice compared to mdx;TRAF6<sup>f/f</sup> littermates at the age of 7-week. Furthermore, mdx;TRAF6<sup>mk0</sup> mice performed significantly better compared to mdx;TRAF6<sup>f/f</sup> mice on a wire hanging test (**Figure 3.3F**) providing initial evidence that inhibition of TRAF6 signaling improves muscle function in young mdx mice.

### **3.3.3 Depletion of TRAF6 improves muscle histopathology in young mdx mice.**

Diaphragm, GA, quadriceps muscles of 7-week old mdx;TRAF6<sup>f/f</sup> and mdx;TRAF6<sup>mk0</sup> mice were isolated and processed for H&E staining. We observed typical features of dystrophic muscle including variability in fiber cross-section area, central nucleation, fiber necrosis, and cellular infiltrates within muscle cross-sections in skeletal muscle of mdx;TRAF6<sup>f/f</sup> mice. However, these dystrophic features were considerably reduced in skeletal muscles of mdx;TRAF6<sup>mk0</sup> mice compared with mdx;TRAF6<sup>f/f</sup> mice (**Figure 3.4A**). Morphometric analysis of H&E-stained muscle section showed that the necrotic area (i.e. that contains only cellular infiltrate and no myofibers) was significantly reduced in skeletal muscle of mdx;TRAF6<sup>mk0</sup> mice compared with mdx;TRAF6<sup>f/f</sup> mice (**Figure 3.4B**). Furthermore, proportion of centronucleated myofibers was also significantly reduced in skeletal muscle of mdx;TRAF6<sup>mk0</sup> mice compared with mdx;TRAF6<sup>f/f</sup> littermates (**Figure 3.4C**). Since serum

creatine kinase (CK) level is an important marker of muscle injury, we also measured the levels of CK in plasma. Our results showed that serum CK levels were significantly lower in mdx;TRAF6<sup>mk0</sup> mice compared with littermate mdx;TRAF6<sup>f/f</sup> mice (**Figure 3.4D**). By performing immunostaining with Cy3-labeled anti-mouse IgG on muscle sections, we further evaluated sarcolemmal injury in mdx;TRAF6<sup>f/f</sup> and mdx;TRAF6<sup>mk0</sup> mice. Consistent with serum CK activity, the number of IgG-filled fibers was significantly reduced in skeletal muscle of mdx;Traf6<sup>mk0</sup> mice compared with mdx;Traf6<sup>f/f</sup> mice (**Figure 3.5**). Taken together, these data are suggestive that the depletion of TRAF6 inhibits muscle injury in young mdx mice.

### **3.3.4 Inhibition of TRAF6 reduces macrophage accumulation, NF-κB activation, and expression of inflammatory cytokines in dystrophic muscle of young mdx mice.**

Inflammation is a major pathological feature that contributes significantly to disease progression in DMD (10, 118-120). To understand whether TRAF6 plays a role in exacerbating inflammatory response in skeletal muscle of *mdx* mice, by performing immunohistochemistry with F4/80 (a marker for macrophages) antibody, we studied the accumulation of macrophages in diaphragm of 7-8 weeks old mdx;TRAF6<sup>f/f</sup> and mdx;TRAF6<sup>mk0</sup> mice. Interestingly, concentration of F4/80<sup>+</sup> macrophages was found to be significantly reduced in diaphragm of mdx;TRAF6<sup>mk0</sup> mice compared with mdx;TRAF6<sup>f/f</sup> mice (**Figures 3.6A, 3.6B**). NF-κB is a major proinflammatory transcription factor that leads to the expression of a wide variety of inflammatory cytokines, chemokines, and matrix degrading enzymes (77, 121). To understand the mechanisms by which deletion of TRAF6 improves muscle inflammation in mdx mice, we studied the activation of NF-κB by

performing electrophoretic mobility shift assay (EMSA). DNA-binding activity of NF- $\kappa$ B was considerably reduced in both diaphragm and quadriceps muscle of mdx;TRAF6<sup>mko</sup> mice compared with mdx;TRAF6<sup>ff</sup> littermates (**Figures 3.6C, 3.6D**). Furthermore, transcript levels of proinflammatory cytokines TNF- $\alpha$ , IL-1 $\beta$ , and IL-6, and a matrix degrading enzyme, matrix metalloproteinase-9 (MMP-9) were significantly reduced in diaphragm of mdx;TRAF6<sup>mko</sup> mice compared with mdx;TRAF6<sup>ff</sup> mice (**Figure 3.6E**). These data demonstrate that TRAF6 mediates NF- $\kappa$ B activation and inflammatory response in myofiber of mdx mice.

### **3.3.5 Depletion of TRAF6 improves myofiber regeneration in 7-week old mdx mice.**

Accumulating evidence suggests that NF- $\kappa$ B and inflammatory cytokines inhibit skeletal muscle regeneration in mdx mice (16, 122, 123). We have also recently reported that inhibition of TRAF6 improves myofiber regeneration upon cardiotoxin-mediated injury (84). We next sought to investigate whether the inhibition of TRAF6 improves muscle regeneration in mdx mice. We performed immunostaining on quadriceps muscle section with an antibody that recognizes embryonic (developmental) myosin heavy chain (eMyHC). Our analysis showed that eMyHC-positive fibers were generally scattered and smaller in size in skeletal muscle mdx;TRAF6<sup>ff</sup> mice. By contrast, the eMyHC-positive fibers were more tightly packed in mdx;TRAF6<sup>mko</sup> compared to mdx;TRAF6<sup>ff</sup> mice (**Figure 3.7A, top**). Furthermore, the mean minimum Feret (MinFeret) diameter of eMyHC-positive fibers was significantly higher in mdx;TRAF6<sup>mko</sup> mice compared with TRAF6<sup>ff</sup> mice (**Figure 3.7B**). Since satellite cells are mainly responsible for repair of injured myofibers in adults, we also investigated whether depletion of TRAF6 in skeletal muscle of mdx mice affects the number

of satellite cells. Quadriceps muscle sections from 7-week old mdx;TRAF6<sup>f/f</sup> and mdx;TRAF6<sup>mk0</sup> mice were stained for Pax7, a marker for quiescent and proliferating satellite cells (2, 64, 82), and nuclei were counterstained with DAPI (**Figure 3.7A, bottom**). Results showed that the number of satellite cells was significantly increased in quadriceps of mdx;TRAF6<sup>mk0</sup> mice compared with mdx;TRAF6<sup>f/f</sup> mice (**Figure 3.7C**). These results suggest that the inhibition of TRAF6 improves satellite cells proliferation and myofiber regeneration in mdx mice.

**3.3.6 Inhibition of TRAF6 exaggerates myopathy in 9-month old mdx mice.** Upon confirming that the inhibition of TRAF6 improves muscle histopathology and regeneration in 7-week old mdx mice, we next sought to determine whether the inhibition of TRAF6 will also be effective in alleviating muscle pathology in older mdx mice. We first performed histological analysis of skeletal muscle at the age of 5 months. Intriguingly, we did not find any noticeable difference in muscle histopathology or level of fibrosis in skeletal muscle of 5-month old mdx;TRAF6<sup>f/f</sup> and mdx;TRAF6<sup>mk0</sup> mice (data not shown). We next analyzed skeletal muscle of these mice at the age of 9 months. Surprisingly, 9-month old mdx;TRAF6<sup>mk0</sup> mice showed increased muscle histopathology compared with mdx;TRAF6<sup>f/f</sup> mice (**Figure 3.8A**). Skeletal muscle of TRAF6<sup>mk0</sup> mice showed increased necrotic area, cellular infiltrate, and variability in fiber size (**Figures 3.8A-C**). To detect injured/permeable fibers in mdx mice, we also performed immunostaining with Cy3-labeled anti-mouse IgG on GA muscle sections (**Figure 3.8D**). The number of IgG-filled fibers was significantly higher in mdx;TRAF6<sup>mk0</sup> mice compared with mdx;TRAF6<sup>f/f</sup> mice (**Figure 3.8E**).



### **3.3.7 Muscle-specific depletion of TRAF6 increases fibrosis in 9-month old mdx mice.**

Fibrosis is a pathogenic factor characterized by chronic inflammation with persistent production of profibrotic cytokines and excessive deposition of ECM proteins, including collagens and fibronectin which can impair tissue function (124). Fibrosis is also a major pathological feature in muscular dystrophy which progressively deteriorates locomotor capacity, posture maintenance, and the vital function of respiratory muscles (125).

Progressive fibrosis is observed in diaphragm of the *mdx* mice which recapitulates clinical signs of DMD patients (115). We measured level of fibrosis by performing Trichrome staining on diaphragm and GA muscle sections. Accumulation of collagens was significantly increased in both diaphragm and GA muscle of 9-month old *mdx*;TRAF6<sup>mk0</sup> mice compared with age-matched *mdx*;TRAF6<sup>fl/fl</sup> littermates (**Figures 3.9A, 3.9B**). We next sought to investigate whether the deterioration in muscle histopathology observed in 9-month old *mdx*;TRAF6<sup>mk0</sup> mice is reflected in muscle function. Indeed, forelimb grip strength and total limb grip strength of *mdx*;TRAF6<sup>mk0</sup> mice were found to be significantly reduced compared with littermate *mdx*;TRAF6<sup>fl/fl</sup> mice (**Figures 3.9C, 3.9D**). Together, these results demonstrate that continued inhibition of TRAF6 exacerbates pathology and caused loss of muscle strength in old *mdx* mice.

### **3.3.8 Inhibition of TRAF6 reduces the markers of autophagy in dystrophic muscle of mdx mice.**

Recent studies have shown that inhibition of autophagy is one of the major causes for myopathy in various models of muscular dystrophy including *mdx* mice (111). Since TRAF6 is an important positive regulator of autophagy, we next sought to determine

whether the inhibition of TRAF6 further represses autophagy in mdx mice. Elevation in the level of LC3B-II protein is a hallmark of autophagy (106). We measured levels of LC3B-I and LC3B-II protein in skeletal muscle of mdx;TRAF6<sup>f/f</sup> and mdx;TRAF6<sup>mk0</sup> mice. The levels of LC3B-II were significantly reduced in skeletal muscle of 6-week mdx;TRAF6<sup>mk0</sup> mice compared with mdx;TRAF6<sup>f/f</sup> mice (**Figures 3.10A, 3.10B**). Moreover, the levels of another autophagy-related protein Beclin1 were significantly reduced in myofibers of mdx;TRAF6<sup>mk0</sup> mice compared with mdx;TRAF6<sup>f/f</sup> mice (**Figures 3.10A, 3.10B**). p62 protein undergoes degradation through autophagy-lysosomal system (41, 106). To further confirm the role of TRAF6 in induction of autophagy in myofiber of mdx mice, we also measured the levels of p62 protein. Results showed that levels of p62 protein were significantly higher in skeletal muscle of mdx;TRAF6<sup>mk0</sup> mice compared with mdx;TRAF6<sup>f/f</sup> littermates (**Figures 3.10A, 3.10B**).

TRAF6 has also been shown to induce the expression of ubiquitin-proteasome system (UPS) and autophagy-related molecules in skeletal muscle in many catabolic conditions (41, 43). To understand whether TRAF6 regulates the expression of the components of UPS and autophagy in dystrophic muscle, we performed QRT-PCR assay. Our results showed that the mRNA levels LC3B, Beclin1, and Atrogin-1 are significantly reduced in dystrophic muscle of 9-month old mdx;TRAF6<sup>mk0</sup> mice compared with mdx;TRAF6<sup>f/f</sup> mice (**Figure 3.10C**). Together these results suggest that the inhibition of TRAF6 represses autophagy and UPS which may be responsible for accumulation of damaged proteins and organelles leading to increased myopathy at later stages of disease progression in mdx mice.

**3.3.9 Inhibition of TRAF6 reduces the activation of Akt in dystrophic muscle of mdx mice.** Previous studies have shown that the Akt-mTOR signaling pathway inhibits autophagy in skeletal muscle (106). There is also evidence that TRAF6 activates Akt in some cell types (36). Moreover, it has been also reported that the activity of Akt-mTOR pathway is increased in skeletal muscle of mdx mice compared to wild-type controls (18, 126). We investigated whether TRAF6 affects the activation of Akt in skeletal muscle of mdx mice. Protein extracts prepared from GA muscle of mdx;TRAF6<sup>f/f</sup> and mdx;TRAF6<sup>mk0</sup> mice were subjected to immunoblotting to detect phosphorylated and total protein levels of Akt, mTOR, and p70S6 kinase. Results showed that the phosphorylation of Akt, mTOR, and p70S6 kinase was significantly reduced in myofibers of mdx;TRAF6<sup>mk0</sup> compared to mdx;TRAF6<sup>f/f</sup> mice (**Figure 3.11A, 3.11B**). Collectively these results indicate that TRAF6 is involved in the activation of Akt; however, TRAF6 regulates autophagy independent of Akt signaling.

### **3.4 DISCUSSION**

Recent studies using genetic mouse models and pharmacological approaches have provided strong evidence that the modulation of activity of specific signaling pathways has enormous potential to reduce the severity of disease progression in muscular dystrophy (16, 17, 127). While the role of anomalous myogenic signaling has become increasingly clear, the proximal signaling events which lead to the activation of different pathways in dystrophic muscle remain less understood. Furthermore, the effect of long-term inhibition of different signaling pathway in disease progression in models of DMD has not been yet investigated. Since TRAF6 is an important upstream regulator of many proinflammatory signaling

pathways, we investigated the role of TRAF6 in pathogenesis of DMD. Our study demonstrates that the expression and activity of TRAF6 are increased in dystrophin-deficient skeletal muscle (**Figure 3.1**). While muscle-specific depletion of TRAF6 signaling reduces injury and improves muscle histopathology (**Figure 3.4**) and regeneration (**Figure 3.7**) in young mice (7-8 weeks), long-term inhibition of TRAF6 results in deterioration of myopathy and loss of function in mdx mice (**Figures 3.8 and 3.9**).

One of the mechanisms by which muscle-derived TRAF6 signaling causes dystrophy in young mdx mice is by promoting chronic inflammatory response. Initial fiber necrosis due to sarcolemmal instability causes severe inflammatory response in skeletal muscle which includes infiltration of macrophages and neutrophils in dystrophic muscle and increased levels of proinflammatory cytokines leading to hastening of fiber necrosis and disease progression in DMD (17, 127). Muscle-derived factors appear to be some of the important contributors of chronic inflammation in mdx myofibers supported by the findings that the activation of proinflammatory transcription factors such as NF- $\kappa$ B and activator protein-1 (AP-1) and levels of various inflammatory cytokines (e.g. TNF- $\alpha$  and IL-1 $\beta$ ) start increasing before the onset of fiber necrosis (16, 18, 20, 21). Our results demonstrate that muscle-specific inhibition of TRAF6 leads to diminished activation of NF- $\kappa$ B in dystrophic muscle of young mdx mice (**Figure 3.6C, 3.6D**). It is notable that in addition to proinflammatory cytokines, NF- $\kappa$ B also induces the expression of a number of chemokines which causes extravasation and migration of leukocytes (77, 121). Consistently, we have found that the accumulation of macrophages and transcript levels of inflammatory cytokines were also significantly reduced in skeletal muscle of mdx;TRAF6<sup>mk0</sup> mice compared to mdx;TRAF6<sup>ff</sup> mice (**Figure 3.6**). These results are consistent with previous reports

demonstrating that muscle-specific depletion of TRAF6 inhibits activation of NF- $\kappa$ B in the conditions of denervation and cancer cachexia and cardiotoxin-mediated muscle injury (41, 84). Although depletion of TRAF6 in skeletal muscle reduces inflammation, in the present study, we have not investigated the role of TRAF6 in immune cells. It is possible that TRAF6 signaling emanating from immune compartments might also contribute to the inflammatory processes in dystrophic muscles and concurrent inhibition of TRAF6 in skeletal muscle and immune cells may lead to further improvement in dystrophinopathy. Future research should clarify the role of the TRAF6 signaling in immune cells in pathogenesis of DMD.

Another mechanism by which TRAF6 signaling causes dystrophy is through the repression of myofiber regeneration. Inhibition of TRAF6 increases the formation of new myofibers in mdx mice (**Figures 3.7**). These results are in agreement with our previous findings demonstrating that the depletion of TRAF6 improves whereas its overexpression represses the regeneration of myofiber in response to acute injury in wild-type mice (84). Muscle regeneration after injury is a complex process which involves the activation of quiescent satellite cells, their differentiation into myoblasts, and finally fusion of myoblasts to damaged myofibers (1, 3). Although the exact mechanisms remain enigmatic, the results of the present study suggest that TRAF6 signaling from injured myofibers limit the activation of satellite cells and may interfere with their differentiation and fusion into myotubes. It has been consistently observed that inflammatory cytokines such as TNF- $\alpha$ , IL-1 $\beta$ , and IL-6 inhibit the differentiation of myoblasts by repressing the levels of MyoD (76, 113, 128-130). Furthermore, there is a positive feed-back loop between inflammatory cytokines and NF- $\kappa$ B transcription factor. Elevated levels of inflammatory cytokines

activate NF- $\kappa$ B, which in turn induces the expression of inflammatory cytokines leading to sustained activation of NF- $\kappa$ B (77, 121). Acharyya et al have previously reported that NF- $\kappa$ B inhibits myofiber regeneration in mdx mice (16). Our results demonstrate that TRAF6 is an upstream activator of NF- $\kappa$ B and expression of inflammatory cytokines in dystrophic muscle (**Figure 3.6**). Therefore, it is reasonable to speculate that the inhibition of TRAF6 improves muscle regeneration through blocking NF- $\kappa$ B and reducing repertoire of inflammatory cytokines in dystrophic muscle.

A striking observation of the present study is that the long-term inhibition of TRAF6 signaling exacerbates muscle pathology in mdx mice. Analysis of myofibers of 9-month old mdx;TRAF6<sup>mk0</sup> mice revealed the presence of significantly increased number of necrotic fibers and replacement of muscle fibers by collagens (**Figures 3.8 and 3.9**). Although the exact mechanisms remain enigmatic, inhibition of autophagy appears to be one of the important reasons for increased myopathy in mdx;TRAF6<sup>mk0</sup> mice. Autophagy is an important homeostasis mechanism which is critical for clearing dysfunctional organelles and to preventing tissue damage (106, 131). Recently, the role of autophagy in pathogenesis of muscular dystrophy has been investigated using multiple approaches. Autophagy has been found to be impaired in muscle biopsies from patients with DMD and in mdx mice with concomitant accumulation of damaged organelles (111). Notably, reactivation of autophagy by feeding low-protein diet improved muscle strength and various pathological features including fiber necrosis, pathological hypertrophy, and fibrosis in mdx mice (111). Similarly, forced activation of autophagy using AMPK agonist, AICAR (5-aminoimidazole-4-carboxamide-1- $\beta$ -d-ribofuranoside) led to improvements in mdx diaphragm histopathology and in force-generating capacity (132).

TRAF6 is an essential component of autophagy in mammalian cells. TRAF6 interacts with LC3B through p62. It has been recently demonstrated that TRAF6 causes the Lys-63–linked ubiquitination of Beclin1 (the mammalian homologue of yeast Atg6), which is essential for autophagosome formation in response to Toll-like receptor 4 signaling (46). We have previously reported that muscle-specific depletion of TRAF6 inhibits expression of autophagy-related molecules and autophagosome formation in atrophying skeletal muscle (41, 43). Our results demonstrate that the levels of autophagy markers are considerably reduced in dystrophic muscle of mdx;TRAF6<sup>mko</sup> compared to mdx;TRAF6<sup>f/f</sup> mice suggesting that TRAF6 is required for the activation of autophagy in mdx mice (**Figures 3.10A, 3.10B**). While autophagy is also inhibited in young mdx;TRAF6<sup>mko</sup> mice, there is still significant improvement in muscle pathology compared with mdx;TRAF6<sup>f/f</sup> littermates. We envision that inflammation plays a predominant role in initial muscle injury and regeneration and that there may not be sufficient load of damaged organelles to clear through autophagy pathway in young mdx mice. It is notable that excessive autophagy causes muscle wasting in many catabolic states (106). Thus the initial inhibition of autophagy in young mdx;TRAF6<sup>mko</sup> mice may be a protective mechanism to preserve skeletal muscle mass. However, due to the progressive nature of myopathy in mdx mice, autophagy becomes essential for clearance of defunct cellular organelles at later stages and hence continued inhibition of autophagy exaggerates dystrophic phenotype in mdx mice. Moreover, our results demonstrate that depletion of TRAF6 inhibits both NF-κB and Akt signaling in skeletal muscle of mdx mice (**Figures 3.6C, 3.6D, 3.11A, 3.11B**). While specific inhibition of NF-κB has been shown to ameliorate dystrophy in young mdx mice (16), the effects of long-term inhibition of NF-κB have not been yet investigated. Both NF-

$\kappa$ B and Akt are known to play critical roles in cell survival mechanisms (121, 133).

Therefore, it is possible that prolonged inhibition of NF- $\kappa$ B and Akt in mdx;TRAF6<sup>mk<sup>o</sup></sup> mice also directly induces muscle cell death. Indeed, it has been previously reported that forced activation of Akt prevents myofiber degeneration and improves regeneration in mdx mice (134).

Akt signaling is also an important regulator of autophagy in skeletal muscle. Activation of Akt inhibits autophagy through repressing the activity of FOXO family transcription factors (106). Recently, De Palma et al. have suggested that the activation of Akt signaling is responsible for inhibition of autophagy in mdx mice (111). However, our results demonstrate that TRAF6 regulates autophagy independent of Akt signaling. Muscle-specific inhibition of TRAF6 also inhibited Akt pathway in myofibers of mdx mice (**Figures 3.11A, 3.11B**). It is also notable that the inhibition of TRAF6 signaling did not affect the activation of Akt kinase in regenerating myofibers in response to cardiotoxin-mediated injury (84). However, in some other cell types, TRAF6 has been found to be an important upstream activator of Akt kinase (36). Together these findings further highlight the role of TRAF6 in context-dependent activation of various signaling pathways.

In summary, our study has provided novel mechanistic insights in dystrophic progression by identifying the role of TRAF6 in mdx mice. It is now increasingly clear that muscular dystrophy is a complex disorder and that a single therapeutic intervention may not be sufficient to treat patients with muscular dystrophy. Recent studies further support this notion by providing experimental evidence that combinatorial approaches correcting more than one parameter of pathological cascade can produce more robust improvement in myopathy in mouse models of muscular dystrophy (135). Our results demonstrate that the



inhibition of TRAF6 is effective in reducing inflammatory response and initial fiber necrosis in mdx mice. However, it is also evident that the inhibition of TRAF6 can also produce deleterious effects due to further repression of autophagy in dystrophic muscle. Nevertheless, it is reasonable to speculate that a combinatorial approach involving pharmacological inhibitors of TRAF6 and activators of autophagy can provide an effective treatment strategy for patients with DMD.

**FIGURE 3.1**

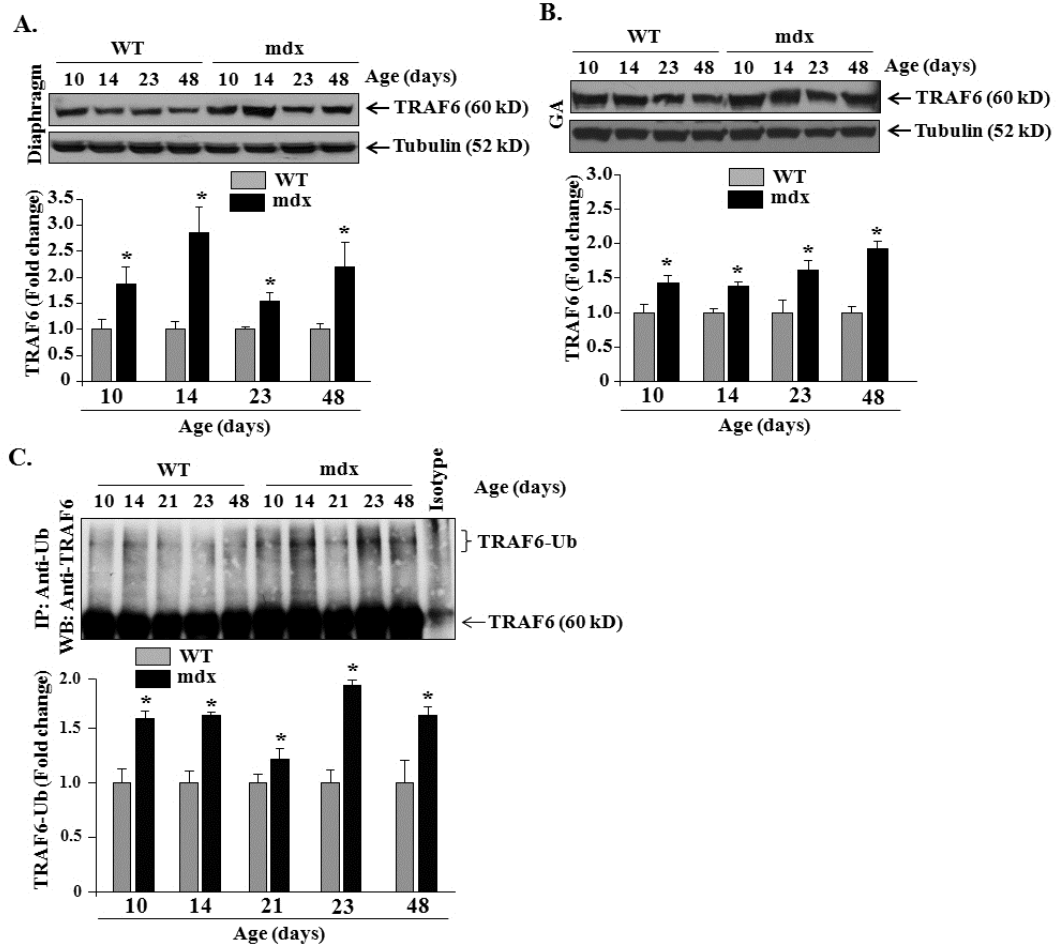


**FIGURE 3.1. Activation of TRAF6 in skeletal muscle of mdx mice.** Levels of TRAF6 protein in (A) Diaphragm and (B) Gastrocnemius muscle of wild-type (WT) and mdx mice at different stages of development measured by Western blotting. Representative immunoblots and densitometry quantification of data are presented here. (C) Diaphragm extracts from 10, 14, 21, 23 and 48-day old WT and mdx mice were immunoprecipitated with anti-ubiquitin followed by Western blotting using anti-TRAF6. Representative immunoblot and quantification of fold change in the levels of ubiquitinated TRAF6 protein are depicted here. N=3 or 4 at indicated age of mice. Error bars represent SD. \* $p < 0.05$ , values vary significantly from corresponding age-matched WT mice.

**FIGURE 3.2**

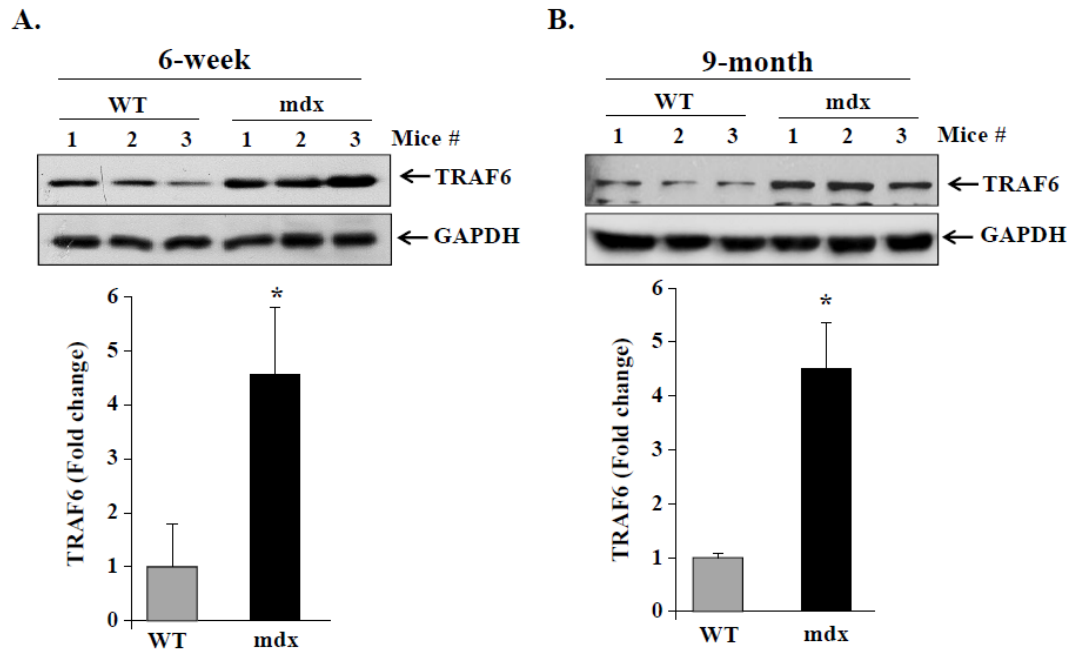


**FIGURE 3.2. Levels of TRAF6 in skeletal muscle of young and old WT and mdx mice.**

Representative immunoblots and densitometry quantification demonstrating that TRAF6 protein levels are upregulated in quadriceps muscle of (A) 6-week old and (B) 9-month old mdx mice compared with age-matched WT mice. N=3 in each age group. Error bars represent SD. \* $p < 0.05$ , values vary significantly from corresponding age-matched WT mice.

**FIGURE 3.3**

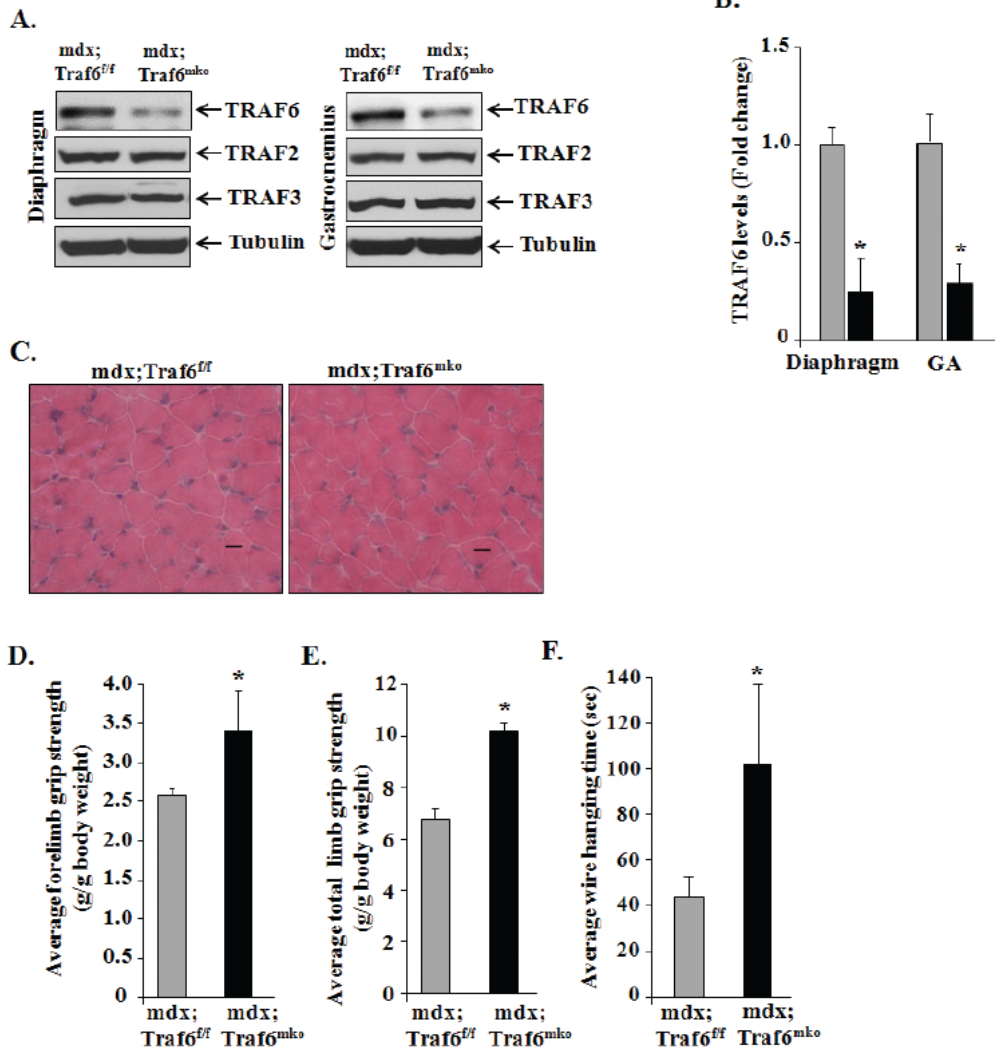


**FIGURE 3.3. Targeted depletion of TRAF6 improves muscle strength in 7-week old mdx mice.** (A) Western blot analysis of TRAF2, TRAF3, and TRAF6 protein levels in diaphragm and gastrocnemius (GA) muscle of 2-week old mdx;TRAF6<sup>f/f</sup> and mdx;TRAF6<sup>mk0</sup> mice. (B) Densitometry quantification of TRAF6 levels in diaphragm and GA muscle of 2-week old mdx;TRAF6<sup>f/f</sup> and mdx;TRAF6<sup>mk0</sup> mice. N=4 in each group. (C) Representative photomicrographs of H&E-stained GA muscle sections of 2-week old mdx;TRAF6<sup>f/f</sup> and mdx;TRAF6<sup>mk0</sup> mice. Scale bar: 20µm. Muscle strength was evaluated through a series of functional tests in 7-week old mdx;TRAF6<sup>f/f</sup> and mdx;TRAF6<sup>mk0</sup> mice. Bar diagrams represent (D) Fore limb grip strength normalized to body weight; (E) Total four limb grip strength; and (F) Wire hanging time (in seconds). N=8 in each group. Error bars represent SD. \*p < 0.05, values vary significantly from mdx;TRAF6<sup>f/f</sup> littermate.

**FIGURE 3.4**

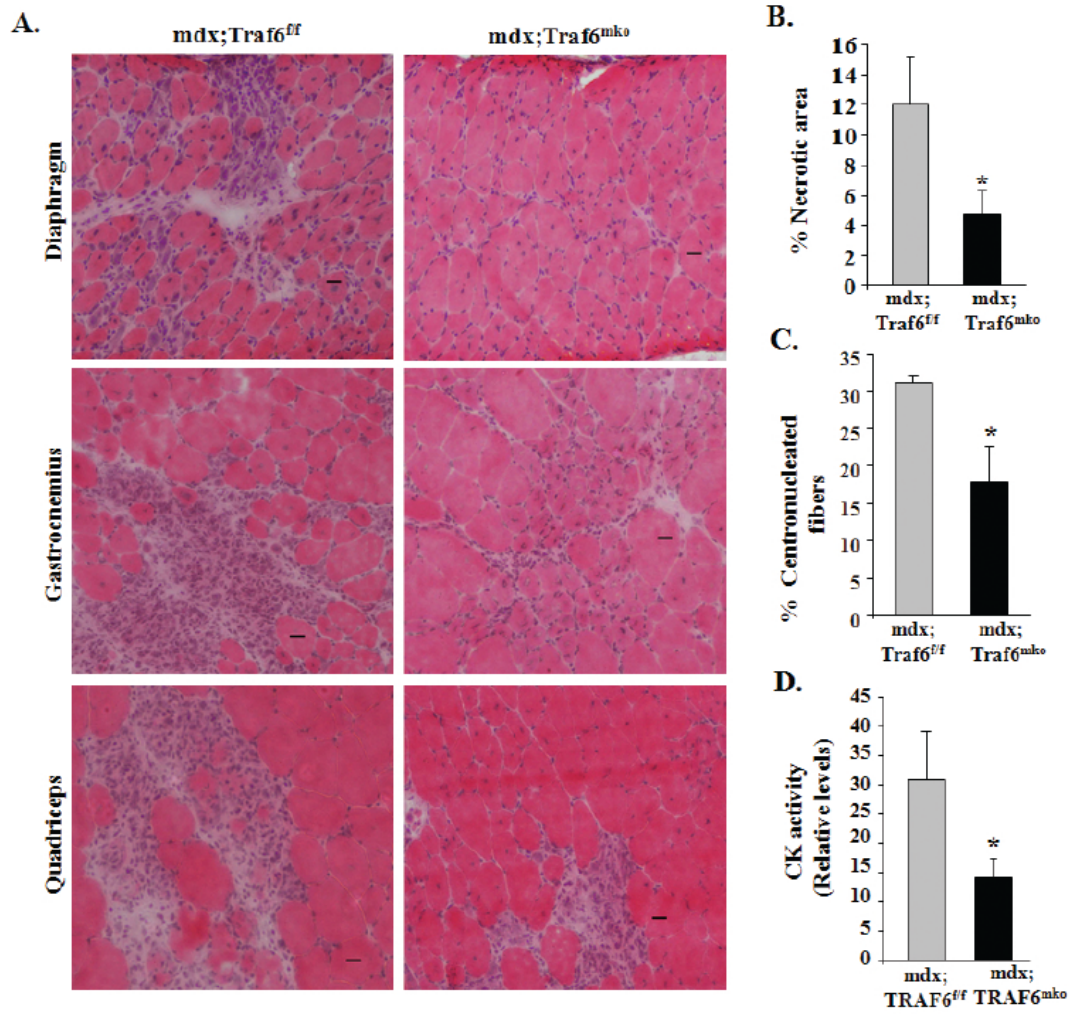


**FIGURE 3.4. Depletion of TRAF6 improves muscle histopathology in 7-week old mdx mice.** (A) Skeletal muscle of 7-week old mdx;TRAF6<sup>mko</sup> and littermate mdx; TRAF6<sup>f/f</sup> mice were isolated and processed for H&E staining. Representative photomicrographs of H&E-stained diaphragm (top), GA (middle) and quadriceps (bottom) muscles displaying manifestations of pathology. Scale bar: 20  $\mu$ m. (B) Percentage necrotic area in quadriceps muscle of 7-week old mdx;TRAF6<sup>f/f</sup> and mdx;TRAF6<sup>mko</sup> littermates. (C) Percentage of fibers with one or more centrally localized nuclei in quadriceps muscle of 7-week old mdx;TRAF6<sup>f/f</sup> and mdx;TRAF6<sup>mko</sup> mice. (D) Relative fold change in creatine kinase (CK) activity in serum of 7-week old mdx;TRAF6<sup>f/f</sup> and mdx;TRAF6<sup>mko</sup> mice. N=7 in each group. Error bars represent SD. \* $p < 0.05$ , values vary significantly from mdx;TRAF6<sup>f/f</sup> mice.



**FIGURE 3.5**

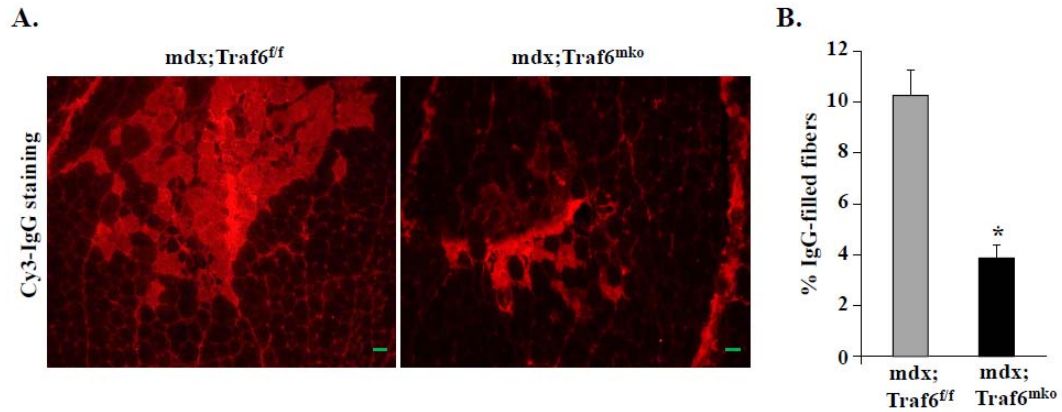


**FIGURE 3.5. Deletion of TRAF6 reduces sarcolemmal injury in mdx mice. (A)**

Quadriceps muscle sections from 7-week old mdx;TRAF6<sup>f/f</sup> and mdx;TRAF6<sup>mko</sup> mice were immunostained with Cy3-labeled goat anti-mouse IgG to detect permeable/damaged fibers. Representative photomicrographs are presented here. **(B)** Quantification of IgG-positive fibers in quadriceps muscle sections from 7-week old mdx;TRAF6<sup>f/f</sup> and mdx;TRAF6<sup>mko</sup> mice. N=7 in each group. Scale bar: 20µm. Error bars represent SD. \*p < 0.05, values vary significantly from mdx;TRAF6<sup>f/f</sup> mice.

**FIGURE 3.6**

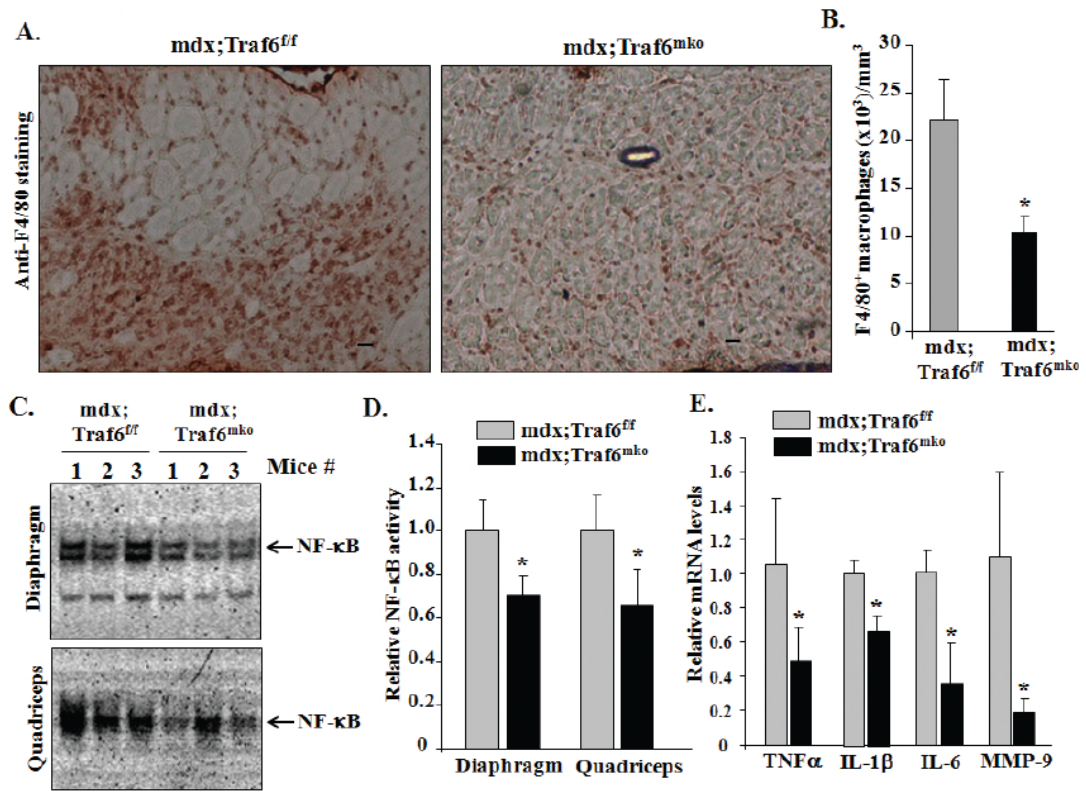


**FIGURE 3.6. Muscle-specific depletion of TRAF6 attenuates inflammatory processes in dystrophic muscle of 7-week old mdx mice.** (A) Representative photomicrographs demonstrating F4/80<sup>+</sup> macrophages in diaphragm section of 7-week old mdx;TRAF6<sup>f/f</sup> and mdx;TRAF6<sup>mk0</sup> mice. Scale bar: 20μm. (B) Quantification of F4/80<sup>+</sup> cells in diaphragm of 7-week old mdx;TRAF6<sup>mk0</sup> and mdx; TRAF6<sup>f/f</sup> mice. N=7 or 8 in each group. (C) Representative EMSA gels presented here demonstrate that the DNA-binding activity of NF-κB is reduced in diaphragm (upper panel) and quadriceps (lower panel) muscle in 7-week-old mdx;TRAF6<sup>mk0</sup> mice compared to littermate mdx; TRAF6<sup>f/f</sup> mice. (D) Quantification of fold change in DNA-binding activity of NF-κB in diaphragm and quadriceps muscle of 7-week old mdx;TRAF6<sup>mk0</sup> mice and mdx; TRAF6<sup>f/f</sup> littermates. N=3 in each group. (E) Relative mRNA levels of IL-1β, IL-6, TNFα and MMP-9 measured by QRT-PCR in diaphragm of 7-week old mdx; TRAF6<sup>f/f</sup> and mdx;TRAF6<sup>mk0</sup> mice. N= 4 in each group. Error bars represent SD. \*p < 0.05, values significantly different from littermate mdx;TRAF6<sup>f/f</sup> mice.

**FIGURE 3.7**

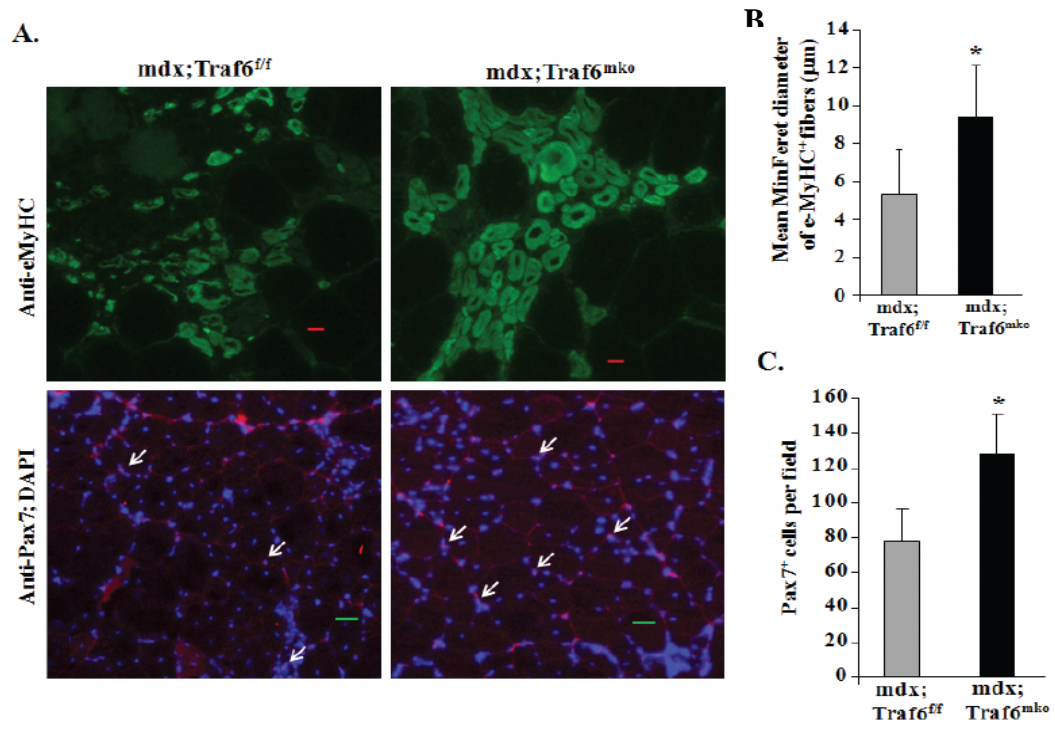


**FIGURE 3.7. Depletion of TRAF6 improves myofiber regeneration in young mdx mice.**

(A) Quadriceps muscle from 7-week-old mdx;TRAF6<sup>f/f</sup> and mdx;TRAF6<sup>mk0</sup> mice were isolated and processed for e-MyHC (top) and Pax7 (bottom) staining. Nuclei were identified by co-staining with DAPI. Representative photomicrographs are presented here. Arrows point to Pax7<sup>+</sup> cells. (B) Quantification of mean minimum Feret (MinFeret) diameter of eMyHC<sup>+</sup> fibers in quadriceps muscle of mdx;TRAF6<sup>f/f</sup> and mdx;TRAF6<sup>mk0</sup> mice. (C) Average number of Pax7<sup>+</sup> cells per field (~0.15 mm<sup>2</sup>) in quadriceps muscle of 7-week old mdx;TRAF6<sup>f/f</sup> and mdx;TRAF6<sup>mk0</sup> mice. N=8 in each group. Scale bar: 20μm. Error bars represent SD. \*p < 0.05, values significantly different from mdx;TRAF6<sup>f/f</sup> mice.

**FIGURE 3.8**

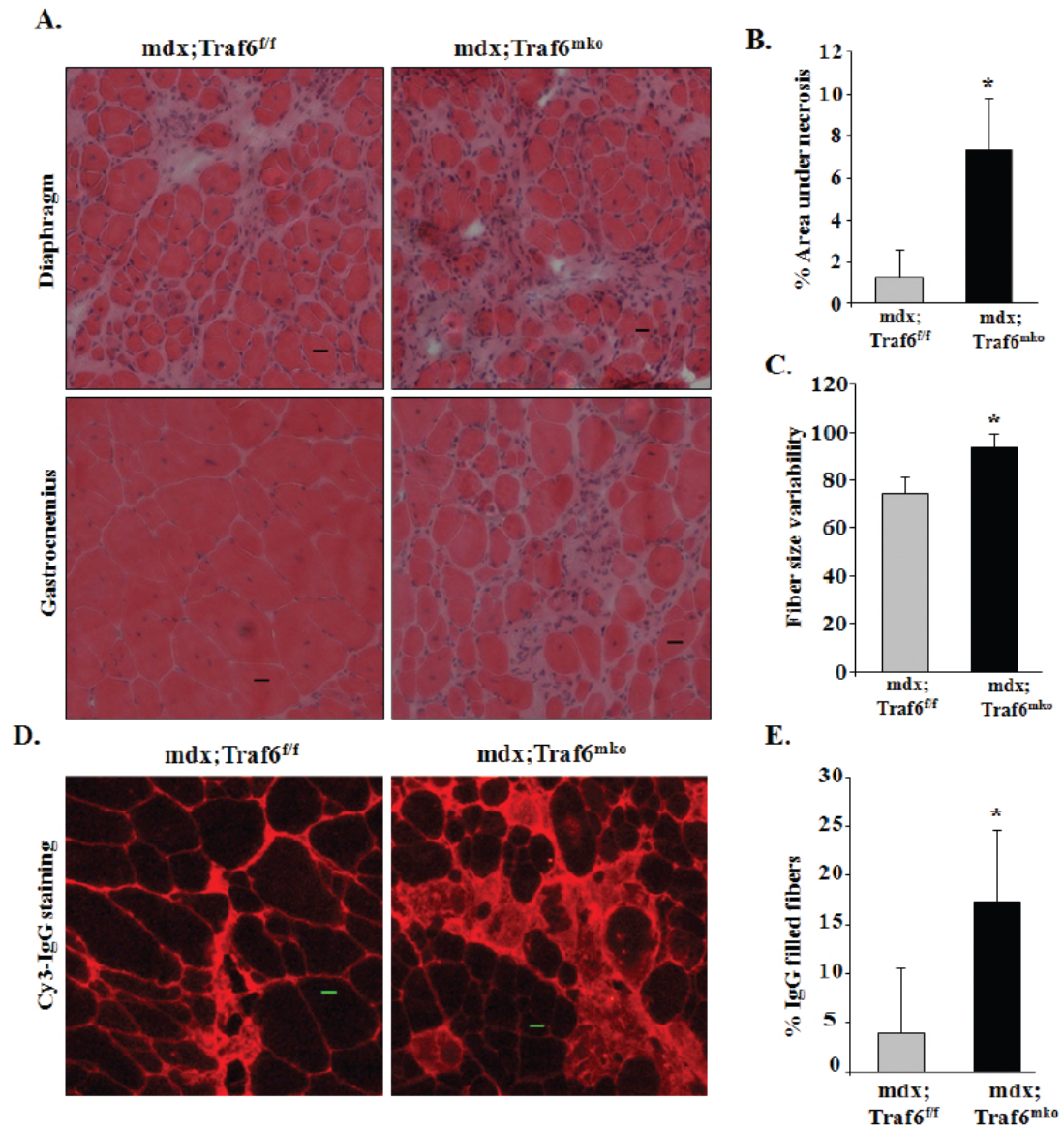


**FIGURE 3.8. Inhibition of TRAF6 exacerbates myopathy in 9-month old mdx mice.**

Diaphragm and GA muscles were isolated from 9-month old mdx; TRAF6<sup>f/f</sup> and mdx;TRAF6<sup>mk0</sup> mice and processed for H&E staining. (A) Representative photomicrographs of H&E-stained transverse sections of diaphragm (top) and GA (bottom) muscle. Scale bar: 20  $\mu$ m. (B) Percentage area under necrosis in H&E-stained sections of GA muscle of 9-month old mdx;TRAF6<sup>f/f</sup> and mdx;TRAF6<sup>mk0</sup> littermates. (C) Quantification of variability in fiber cross-sectional area (CSA) in GA muscle of 9-month old mdx;TRAF6<sup>f/f</sup> and mdx;TRAF6<sup>mk0</sup> mice. (D) GA muscle sections from 9-month old mdx;TRAF6<sup>f/f</sup> and mdx;TRAF6<sup>mk0</sup> mice were immunostained with Cy3-labeled goat anti-mouse IgG to detect permeable/damaged fibers. Representative photomicrographs are presented here. (E) Quantification of IgG-positive fibers in GA muscle sections from 9-month old mdx;TRAF6<sup>f/f</sup> and mdx;TRAF6<sup>mk0</sup> mice. N=7 or 8 in each group. Scale bar: 20 $\mu$ m. Error bars represent SD. \*p < 0.05, values vary significantly from mdx;TRAF6<sup>f/f</sup> mice.



**FIGURE 3.9**

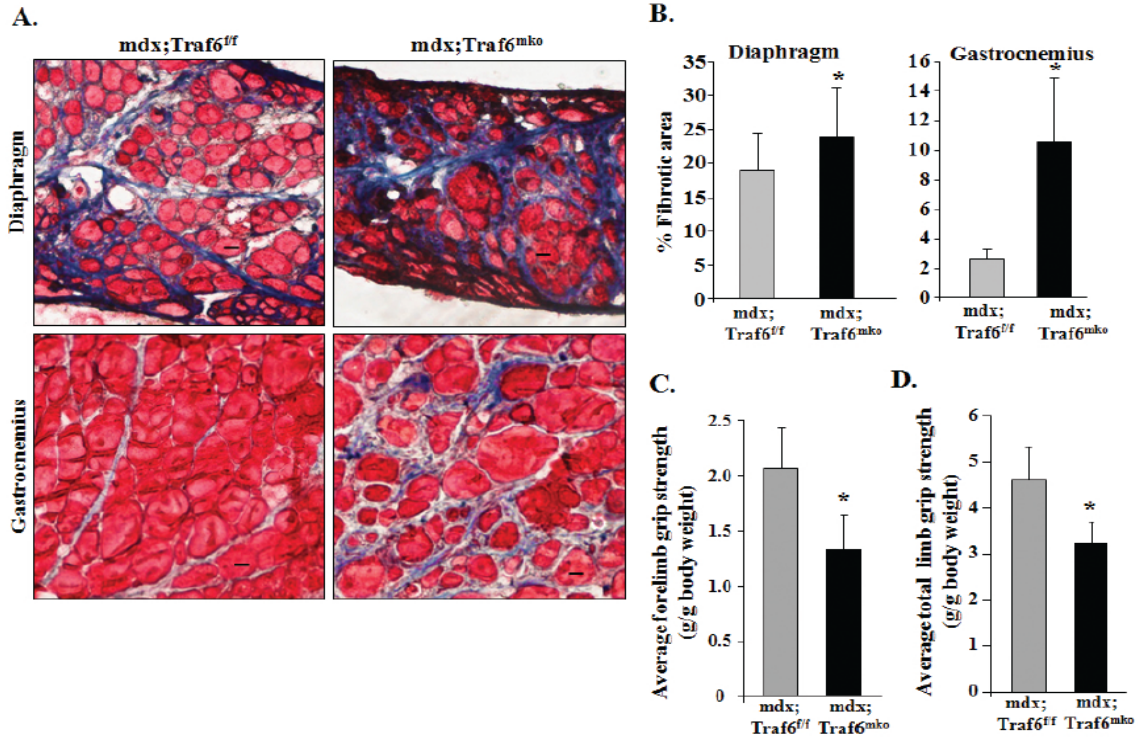


**FIGURE 3.9. Muscle-specific depletion of TRAF6 increases fibrosis in 9-month old**

**mdx mice.** (A) Diaphragm and GA muscle were isolated from 9-month old mdx; TRAF6<sup>f/f</sup> and mdx;TRAF6<sup>mko</sup> mice and transverse muscle sections made were processed for Mason's Trichrome staining for detection of collagen accumulation. Representative photomicrographs are presented here. Scale bar: 20µm. (B) Quantification of fibrotic area in diaphragm and GA muscle of 9-month old mdx;TRAF6<sup>f/f</sup> mice and mdx;TRAF6<sup>f/f</sup> littermates. Muscle strength of 9-month old mdx;TRAF6<sup>f/f</sup> and mdx;TRAF6<sup>mko</sup> mice was evaluated. Bar diagrams representing (C) forelimb grip strength and (D) total four limb grip strength normalized to body weight. N=8 in each group. Scale bar: 20µm. Error bars represent SD. \*p < 0.05, values significantly different from mdx; TRAF6<sup>f/f</sup> mice.



**FIGURE 3.10**

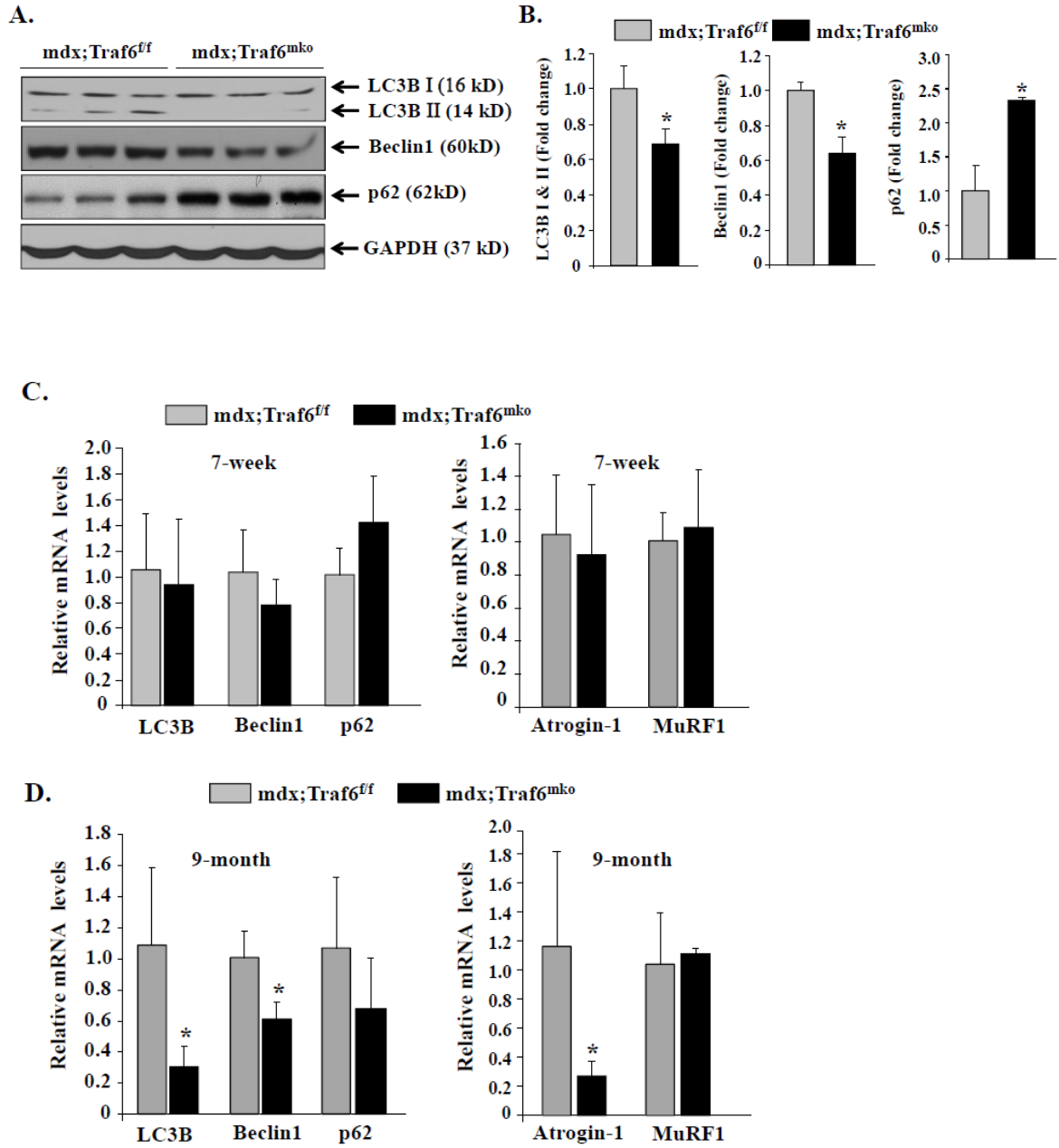


**FIGURE 3.10. Depletion of TRAF6 in inhibits autophagy in mdx mice. (A)**

Representative immunoblots present here demonstrate the levels of LC3B I and LC3B II and Beclin1, p62, and an unrelated protein GAPDH (glyceraldehyde 3-phosphate dehydrogenase). **(B)** Densitometry quantification of LC3B I & II, Beclin1, and p62 protein levels in GA muscle of 6-week old mdx;TRAF6<sup>f/f</sup> and mdx;TRAF6<sup>mk0</sup> mice. N=6 in each group. Error bars represent SD. \*p < 0.05, values significantly different from mdx;TRAF6<sup>f/f</sup> mice. Relative mRNA levels of autophagy related genes (LC3B, Beclin1 and p62) and ubiquitin-proteasome system-related genes (Atrogin-1 and MuRF1) measured by QRT-PCR in quadriceps muscle of **(C)** 7-week old and **(D)** 9-month old mdx;TRAF6<sup>f/f</sup> and mdx;TRAF6<sup>mk0</sup> mice. N= 4 in each age group. Error bars represent SD. \*p < 0.05, values significantly different from littermate mdx;TRAF6<sup>f/f</sup> mice.

**FIGURE 3.11**

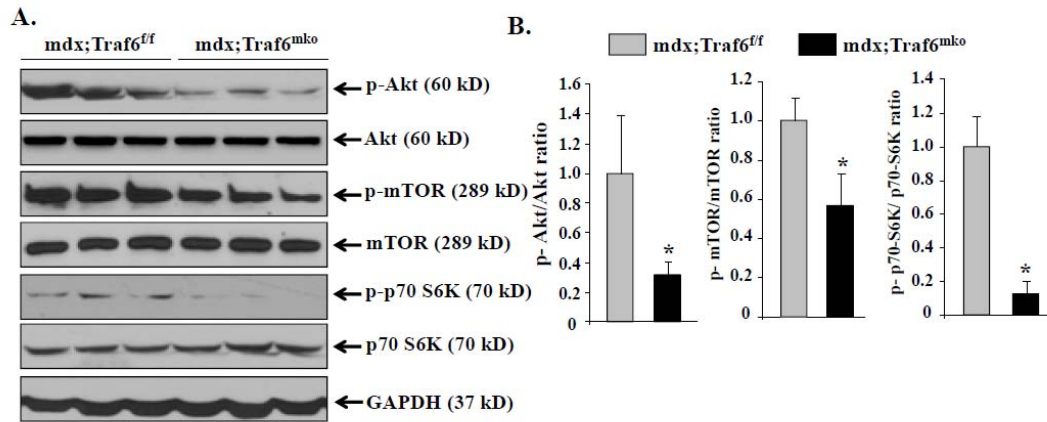


**FIGURE 3.11. Role of TRAF6 in activation of Akt signaling pathway in mdx mice.** GA muscle of 6-week old mdx;TRAF6<sup>fl/fl</sup> and mdx;TRAF6<sup>mk/mk</sup> mice were processed for Western blotting. **(A)** Representative immunoblots present here demonstrate the levels of phosphorylated (p) and total Akt, mTOR, p70 S6 kinase (p70 S6K), and GAPDH protein. **(B)** Quantification of phosphorylated versus total Akt, mTOR, p70 S6K ratio in GA muscle of 6-week old mdx;TRAF6<sup>fl/fl</sup> and mdx;TRAF6<sup>mk/mk</sup> mice. N=6 in each group. Error bars represent SD. \*p < 0.05, values significantly different from mdx;TRAF6<sup>fl/fl</sup> mice.

## CHAPTER 4

### TRAF6 IS CRITICAL FOR SATELLITE CELL FUNCTION AND SKELETAL MUSCLE REGENERATION UPON INJURY

#### 4.1. INTRODUCTION

Satellite cells are skeletal muscle resident stem cells which reside between the plasma membrane and basal lamina in a quiescent state characterized by low-metabolic activity and reversible mitotic arrest (136). These cells are primarily responsible for growth, maintenance, and repair of injured adult myofibers (3, 137). In response to myofiber injury, satellite cells are rapidly activated to reenter the cell cycle, undergo proliferation, and differentiate into myoblasts which eventually fuse with each other or pre-existing myofibers to complete the repair process (138, 139). While most of the activated satellite cells differentiate into myogenic lineage, a small portion of them self-renew and return to quiescent state to respond to next round of muscle injury and repair (138, 139).

Paired-box transcription factor Pax7 is a critical regulator for satellite cell biogenesis, survival, specification, and self-renewal. Skeletal muscle of Pax7-null mice lack satellite cells and show reduced muscle growth and defects in regenerative response after injury (82, 87). Furthermore, quiescent satellite cells express high level of Pax7 whereas the expression of other myogenic regulatory factors such as Myf5 and MyoD is undetectable. In proliferating satellite cells, Pax7 persist at lower levels whereas expression of Pax7 is completely repressed in myogenic lineage cells which commit to terminal differentiation (64, 138, 140). The critical role of Pax7 in maintaining satellite cell quiescence or self-

renewal is also evident by the findings that forced expression of Pax7 inhibits myogenesis and cell cycle progression in satellite cells resulting in the maintenance of their inactivated state (141). In addition to its imperative role in maintaining the pool of quiescent satellite cells (142), a temporal expression of Pax7 is also required for sustaining the myogenic potential of activated satellite cells to drive the events of muscle regeneration (143, 144). Genetic deletion of Pax7 in satellite cells of adult mice led to failure of myofiber regeneration due to precocious differentiation (144).

A number of factors have now been identified which regulate satellite cell homeostasis through modulating the myogenic activity of Pax7. For example, arginine methyltransferase Carn1 has been found to methylate multiple arginine residues in the N terminus of Pax7. Methylated Pax7 then recruits the ASH2L:MLL1/2:WDR5:RBBP5 histone H3K4 methyltransferase complex to the promoter region of Myf5 leading to the induction of Myf5 during satellite stem cell asymmetric division and entry into the myogenic program (145, 146). Furthermore, both Pax7<sup>+</sup>/Myf5<sup>-</sup> satellite stem cells and Pax7<sup>+</sup>/Myf5<sup>+</sup> committed myogenic precursors express EZH2, the enzymatic subunit of the Polycomb-repressive complex 2 (PRC2). Conditional deletion of Ezh2 in satellite cells of mice results in reduced number of Pax7<sup>+</sup> cells and diminished regeneration of injured skeletal muscle signifying that Ezh2 is essential to maintaining satellite cell pool in adult skeletal muscle (147). Furthermore, post-transcriptional mechanisms involving microRNAs (miRs) are involved in the repression of Pax7 during the transition from proliferating satellite cells to differentiating satellite cells. In particular, miR-1 and miR-206, which are highly up-regulated during satellite cell differentiation, bind to the 3' untranslated region of Pax7 transcript to repress the levels of Pax7 (148). While it is increasingly clear that both

protein modifications and post-transcriptional mechanisms (e.g. miRs) regulate Pax7 activity, the molecular mechanisms which govern the gene expression of Pax7 in satellite cells remain largely unknown.

Several lines of evidence suggest that Notch signaling plays a critical role in self-renewal and differentiation of satellite cells (2, 74, 84, 137). Overexpression of Notch 1 intracellular domain (N1ICD) increases self-renewal of satellite cells on cultured myofibers (149). Activation of Notch pathway also inhibits differentiation through repressing the levels of MyoD (150). Moreover, a  $\gamma$ -secretase inhibitor reduces the proportion of Pax7<sup>+</sup>/MyoD<sup>-</sup> cells and increases Pax7<sup>-</sup>/MyoD<sup>+</sup> cells on cultured myofibers (64, 84). Furthermore, inactivation of RBP-J $\kappa$  through genetic approach dramatically reduces the proportion of Pax7<sup>+</sup> cells by spontaneously increasing terminally differentiated cells in both normal and injured skeletal muscle of mice (72, 73). It has been found that N1ICD stimulates the expression of Pax7 through interaction with RBP-J $\kappa$ , which binds to two consensus sites in the promoter region of Pax7 gene (149). Moreover, signaling through the Wnt7a/Fzd7 planar-cell-polarity pathway drives the symmetric expansion satellite stem cell to enhance regeneration of injured myofibers (151). Finally, angiotensin-1 produced by fibroblasts and vascular cells binds to Tie-2 receptor on satellite cells to stimulate ERK pathway leading to increased number of quiescent satellite cells (152). However, it remains unknown whether there are additional pathways which regulate the abundance of satellite stem cells in skeletal muscle.

Tumor necrosis factor (TNF) receptor-associated factor (TRAF6) is a crucial adaptor protein that mediates signaling events from TNF receptor superfamily (TNFRSF), interleukin-1 receptor (IL-1R) family, and toll-like receptor (TLR) family (27). TRAF6 is

also a non-conventional RING finger E3 ligase, which catalyzes formation of K63-linked ubiquitin chains (33, 36). Signals coupled through TRAF6 lead to activation of a cascade resulting in the activation of nuclear factor- $\kappa$ B (NF- $\kappa$ B) and activator protein 1 (AP1) transcription factors, through activation of upstream kinases, including inhibitor of kappa B kinase (IKK) and the mitogen-activated protein kinase (MAPKs, i.e. ERKs, JNKs, and p38MAPK) family (27, 33, 36, 153). TRAF6 plays critical roles in innate immune responses and regulate the function of antigen-presenting cells such as macrophages and dendritic cells and the CD40-induced B cell responses (81, 153). TRAF6-deficient mice die between 2-3 weeks due to severe osteopetrosis and deficit of tooth eruption because of defective signaling through the receptor activator of NF- $\kappa$ B (RANK), a member of TNF receptor superfamily which is required for osteoclast formation (44, 45). TRAF6-deficient mice also show significant hematopoietic abnormalities (154). Furthermore, TRAF6 has also been found to play crucial role in a lymph node organogenesis, formation of skin appendices, and development of nervous system (153). While TRAF6 is expressed in the cells of myogenic lineage (41, 42, 84, 103), the role of TRAF6 in satellite stem cell homeostasis and function has not been yet investigated.

In this study, using a conditional knockout approach we have investigated the role of TRAF6 in regulation of satellite stem cell homeostasis. Our results demonstrate TRAF6 is critical for the gene expression of Pax7, maintaining the satellite stem cell pool, and regeneration of injured skeletal muscle. The ablation of TRAF6 in satellite cells of mdx mice (a model for Duchenne muscular dystrophy) exaggerates dystrophic phenotype due to impairment in myofiber regeneration. Furthermore, our results demonstrate that TRAF6-mediated signaling is required for the activation of ERK and JNK which causes the

phosphorylation of transcription factor c-Jun which in turn binds to the proximal region of Pax7 promoter to augment the gene expression of Pax7.

## **4.2. MATERIALS AND METHODS**

**Animals.** Satellite cells specific TRAF6-knockout mice (henceforth TRAF6<sup>scko</sup>) were generated by crossing Pax7<sup>CreER</sup> mice (Jax Strain: B6;129-Pax7<sup>tm2.1(cre/ERT2)Fan/J</sup>) with floxed TRAF6 (i.e. TRAF6<sup>ff</sup>) mice. Similarly, mdx mice were crossed with TRAF6<sup>scko</sup> to generate mdx;TRAF6<sup>scko</sup> mice and littermate mdx;TRAF6<sup>ff</sup> mice. All mice were in the C57BL6 background and their genotype was determined by PCR from tail DNA. Tamoxifen administration was started at 6 weeks of age and the mice were maintained on tamoxifen diet during the duration of the experiment. At the age of 8 weeks, 100  $\mu$ l of 1.2% BaCl<sub>2</sub> (Sigma Chemical Co.) dissolved in phosphate-buffered saline (PBS) was injected into the TA muscle of mice to induce necrotic injury. At various time points, TA muscle was collected from euthanized mice for biochemical and histology studies. All experimental protocols with mice were approved in advance by the Institutional Animal Care and Use Committee (IACUC) at the University of Louisville.

**Histology and Morphometric Analysis.** Hind limb muscle from mice were isolated and frozen in isopentane cooled in liquid nitrogen and sectioned in a microtome cryostat. For the assessment of tissue morphology, 10 $\mu$ m thick transverse sections of tibial anterior (TA) muscle were stained with Hematoxylin and Eosin (H&E) and examined under Nikon Eclipse TE 2000-U microscope (Nikon). Fiber cross-sectional area (CSA) was analyzed in H&E-stained TA muscle sections using Nikon NIS Elements BR 3.00 software (Nikon). For each



muscle, the distribution of fiber CSA was calculated by analyzing 200 to 250 myofibers as described (41). The extent of fibrosis in transverse cryosections of TA muscle determined using Masson's Trichrome staining kit following a protocol suggested by the manufacturer (Richard-Allan Scientific).

**Indirect Immunofluorescence:** For immunohistochemistry study, frozen TA muscle section sections or paraformaldehyde-fixed cultured myotubes were blocked in 1% bovine serum albumin in PBS for 1h, and incubated with anti-Pax7 (1:20, Developmental Studies Hybridoma Bank, DSHB, University of Iowa, Iowa City, IA), anti-E-MyHC (1:50, DSHB, University of Iowa, Iowa City, IA), anti-MF20 (1:250, DSHB, University of Iowa, Iowa City, IA) in blocking solution at 4°C overnight under humidified conditions. The sections were washed briefly with PBS before incubation with Alexa Fluor® 488 or 594-conjugated secondary antibody (1:3000, Invitrogen) for 1h at room temperature and then washed 3 times for 30 minutes with PBS. The slides were mounted using fluorescence medium (Vector Laboratories) and visualized at room temperature on Nikon Eclipse TE 2000-U microscope (Nikon), a digital camera (Nikon *Digital Sight DS-Fi1*), and Nikon NIS Elements BR 3.00 software (Nikon). Image levels were equally adjusted using Adobe Photoshop CS2 software (Adobe).

**Isolation, Culture, and Staining of Single Myofibers.** Single myofibers were isolated from the extensor digitorum longus (EDL) muscles after digestion with collagenase A (Sigma Chemical Company) and trituration as previously described (83, 84). Suspended fibers were cultured in 60-mm horse serum-coated plates in Dulbecco's modified Eagle's medium

supplemented with 10% fetal bovine serum (FBS; Invitrogen), 2% chicken embryo extract (Accurate Chemical, Westbury, NY), and 1% penicillin-streptomycin for 3 days. Freshly isolated fibers and cultured fibers were then fixed in 4% PFA and stained for Pax7 and MyoD.

**Satellite Cell Cultures.** Satellite cells were isolated from the hind limbs of 8-week-old mice following a protocol as described (22). Briefly, mice were sacrificed and TA and gastrocnemius muscles were isolated. Excess connective tissues and fat were cleaned in sterile PBS followed by mincing of skeletal muscle in DMEM and enzymatic dissociation with 0.1% Pronase. The digested slurry was spun, pelleted, and triturated several times and then passed through a 70- $\mu$ m cell strainer (BD Falcon). The filtrate was spun at 1000  $\times$  g and resuspended in myoblast growth medium (Ham's F-10 medium with 20% FBS supplemented with 5 ng/ml of basic fibroblast growth factor). Cells were first re-fed after 3 days of initial plating. During the first few passages, cells were also enriched by pre-plating for selection of pure myoblast population. Upon selection, the cells were cultured in a 1:1 ratio of myoblast growth medium and growth medium (DMEM with 20% FBS) until 80% confluence was reached.

**Cell Proliferation Assay.** Satellite cell proliferation was assayed using Click-iT® EdU Cell Proliferation Assay kit (Invitrogen). In brief, satellite cells were seeded on 24-well cell culture plates coated with 10% Matrigel. 5-Ethynyl-2'-deoxyuridine (10  $\mu$ M, Invitrogen) was added in culture medium for the 90 minutes. Cells were then fixed with 3.7% paraformaldehyde for 15 min and permeabilized with 0.5% Triton X-100. The 5-ethynyl-2'-

deoxyuridine<sup>+</sup> cells were identified using Click-iT reaction mixture. Nuclei were counterstained with 1× Hoechst 33342 for 30 min at room temperature. Images were visualized on Nikon Eclipse TE 2000-U microscope (Nikon), a digital camera (Nikon Digital Sight DS-Fi1), and analyzed using Nikon NIS Elements BR 3.00 software (Nikon).

**Generation of short hairpin RNA (shRNA) constructs.** The pLKO.1-mCherry-Puro plasmid was kindly provided by Dr. Renzhi Han of Loyola University. The shRNA oligonucleotides were synthesized to contain the sense strand of target sequences for TRAF6, short spacer (AACG or TTCAAGAGA) and the reverse complement sequences followed by five thymidines as an RNA polymerase III transcriptional stop signal. Oligonucleotides were annealed and cloned into pLKO.1-mCherry-Puro with AgeI/EcoRI sites. The insertion of shRNA sequence was confirmed by sequencing of the plasmid.

**Gene Transfer by Electroporation.** To overexpress specific proteins in primary satellite cells, plasmid DNA was introduced into cells by electroporation (1500 V, 10 ms for duration, 3 pulses) using the Neon transfection system following a protocol suggested by the manufacturer (Invitrogen).

**Western Blot.** Quantitative estimation of specific protein was performed by Western blot using a method as described (41, 50). TA muscle were washed with PBS and homogenized in lysis buffer [50 mM Tris-Cl (pH 8.0), 200 mM NaCl, 50 mM NaF, 1 mM dithiotheritol (DTT), 1 mM sodium orthovanadate, 0.3% IGEPAL, and protease inhibitors]. Approximately, 100 µg protein was resolved on each lane on 8-10 % SDS-PAGE,

electrotransferred onto nitrocellulose membrane and probed using anti-TRAF6 (1:1000, Millipore), anti-Pax7 (1:1000, Developmental Studies Hybridoma Bank), anti-E-MyHC (1:1000, Developmental Studies Hybridoma Bank), (anti-phospho-c-Jun (Cell Signaling Technology), anti-c-Jun (Santa Cruz Biotechnology), anti-phospho-ERK1/2 (Cell Signaling Technology), anti-ERK1/2 (Cell Signaling Technology), anti-phospho-JNK1/2 (Cell Signaling Technology), anti-JNK1/2 (Cell Signaling Technology), anti-phospho-p38 MAPK (Cell Signaling Technology), anti-p38 MAPK (Cell Signaling Technology), anti-phospho-ERK5 (Cell Signaling Technology), anti-ERK5 and anti- $\alpha$ -GAPDH (1:2000, Cell Signaling, Inc.) and detected by chemiluminescence.

**Fluorescence Activated Cell Sorting (FACS).** Satellite were analyzed by FACS as previously described (64, 83). Approximately  $2 \times 10^6$  cells were incubated in DMEM (supplemented with 2% FBS and 25 mM 4-(2-hydroxyethyl)-1-piperazineethanesulfonic acid) and dead cells (positive for Propidium iodide staining) which were around ~1% were excluded from all FACS analysis. For satellite cell quantification from heterogeneous cell population, cells were immunostained with antibodies against, CD45, CD31, and Ter-119 for negative selection (all PE conjugated, eBiosciences), and with  $\alpha 7$ -integrin (MBL International) for positive selection. A tandem conjugate of R-PE (Alexa 647, Molecular Probes) was used as a secondary antibody against  $\alpha 7$ -integrin. FACS analysis was performed on a C6 Accuri cytometer equipped with three lasers. The output data was processed and plots were prepared using FCS Express 4 RUO software (De Novo Software).

**RNA Isolation and Quantitative Real-time PCR (QRT-PCR).** RNA isolation and QRT-PCR were performed using a method as previously described (41).

**Statistical Analyses.** Results are expressed as mean  $\pm$  standard deviation (SD). Statistical analyses used Student's *t*-test to compare quantitative data populations with normal distribution and equal variance. A value of  $P < 0.05$  was considered statistically significant unless otherwise specified.

### 4.3 RESULTS

**Ablation of TRAF6 in satellite cells impairs regeneration of injured myofibers in adult mice.** Following acute muscle injury, muscle satellite cells are activated to drive the events of muscle repair in a manner that mimics embryonic development (1, 4). Our previous study revealed that the levels of TRAF6 are highly up regulated following muscle injury and the ablation of TRAF6 under the control of muscle creatine kinase (MCK) promoter (i.e. TRAF6<sup>mko</sup>) improves muscle regeneration possibly due to overall reduction in inflammatory response (84). However, an interesting observation was that while ablation of TRAF6 in myofibers reduced the levels of TRAF6 in control muscle, TRAF6 protein levels remained relatively high in contralateral injured muscle of TRAF6<sup>mko</sup> mice (84) indicating that myofibers are not the only source for TRAF6 in injured skeletal muscle. TRAF6 is known to be expressed by a number of other cell types including immune cells (27, 81) and proliferating myoblasts (41, 42) which occupy injured muscle microenvironment. To delineate the contribution of satellite cells in the elevated levels of TRAF6 in injured muscle, we crossed TRAF6<sup>f/f</sup> mice with tamoxifen inducible Pax7 Cre mice (Pax7<sup>CreER</sup>

mice) to generate satellite-cell specific TRAF6-knockout (henceforth, TRAF6<sup>scko</sup>) mice (**Figure 4.1A**). 8-week old littermate TRAF6<sup>f/f</sup> and TRAF6<sup>scko</sup> mice were injected intraperitoneally with tamoxifen (10 mg/mL in corn oil) for four consecutive days and kept on tamoxifen-containing standard chow (1 mg tamoxifen per day/20g body weight). TA muscle of these mice then was given intramuscular injection of 100 $\mu$ l solution of 1.2% BaCl<sub>2</sub> or saline alone. After 5 days, the levels of TRAF6 were measured by performing Western blot. Results showed that while injured muscle of TRAF6<sup>f/f</sup> mice displayed a dramatic increase in TRAF6 protein levels compared to saline injected control muscle (**Figure 4.1B**) as previously described (84), BaCl<sub>2</sub>-injected muscle of TRAF6<sup>scko</sup> showed comparatively smaller up-regulation in the levels of TRAF6 protein (**Figure 4.1B**) suggesting that satellite cells are major source of TRAF6 in injured skeletal muscle of mice. To confirm that TRAF6 is expressed in the satellite cells, primary myogenic cells prepared from C57BL6 mice were FACS sorted for  $\alpha$ 7-integrin (a marker for satellite cells) after eliminating possible infiltrating cells. This analysis showed that TRAF6 is highly enriched in the  $\alpha$ 7-integrin<sup>+</sup> population (**Figure 4.2A**). Furthermore, immunohistochemical analysis showed that TRAF6 is expressed in cultured Pax7<sup>+</sup> myogenic cells (**Figure 4.2B**). To determine whether there is any correlation in the levels of TRAF6 and Pax7 during myogenic differentiation, we next measured the protein levels of TRAF6 and Pax7 at different time points after induction of differentiation in primary cultures. Results showed that levels of both Pax7 and TRAF6 are repressed and followed similar kinetics after addition of differentiation medium in cultured satellite cells (**Figure 4.2C**).

We next investigated the role of TRAF6 in satellite cells during skeletal muscle regeneration. TA muscle of adult TRAF6<sup>f/f</sup> and TRAF6<sup>scko</sup> mice was injured through

intramuscular injection of 1.2% BaCl<sub>2</sub> solution. The muscle was isolated at 3, 5, 10 and 21 days post-BaCl<sub>2</sub> injection and analyzed by performing H&E staining. Histological examination of H&E-stained TA muscle sections revealed equal necrosis of TA muscle of TRAF6<sup>scko</sup> and TRAF6<sup>ff</sup> mice 3 days post-BaCl<sub>2</sub> injection (**Figure 4.3A**). Strikingly, muscle regeneration was dramatically reduced in TRAF6<sup>scko</sup> mice. At day 5 after BaCl<sub>2</sub>-mediated injury, newly formed centronucleated fibers populated regenerating TA muscle of TRAF6<sup>ff</sup> mice. By contrast, TA muscle of corresponding TRAF6<sup>scko</sup> mice showed poor signs of regeneration evident by reduced myofiber cross-sectional area (CSA) and number of centronucleated fibers (**Figures 4.3A-B**) with robust persistence of cellular infiltrate (**Figure 4.3A**). Manifestations of defective muscle repair in TRAF6<sup>scko</sup> mice were evident even at 21 days after muscle injury where regenerated muscle of control TRAF6<sup>ff</sup> displayed complete subsidence of inflammatory cells and reconstitution of normal muscle (**Figure 4.3A**). Signs of impaired muscle regeneration in TRAF6<sup>scko</sup> mice were even more pronounced when TA muscle was subjected to a second round of injury using BaCl<sub>2</sub> injection (**Figure 4.4A**). Regenerating areas of TRAF6<sup>scko</sup> muscle were notably void of newly formed muscle fibers and displayed massive deposition of fibrotic and adipogenic tissue at 5 days of second injury (**Figure 4.4B**). These results suggest that TRAF6 is required for satellite cell function during regenerative myogenesis.

**Ablation of TRAF6 in satellite cells impairs myofiber formation upon injury.** Proper muscle regeneration involves differentiation and fusion of proliferating myogenic cells to restore the architectural structure of the injured muscle. This process involves intrinsic regulation of transcription factors and expression markers that drive progression of activated

satellite cells through the myogenic lineage (53). Hierarchical expression of myogenic regulatory factors Myf5, MyoD, and myogenin and embryonic/developmental isoform of myosin heavy chain (eMyHC) is required for completing the myogenic program (53, 64). To determine at which stage of myogenesis TRAF6 signaling in satellite cells is required, we performed immunostaining for eMyHC, an isoform that is expressed by newly formed muscle fibers. Regenerating muscle from TRAF6<sup>scko</sup> mice contained drastically reduced number and smaller size eMyHC<sup>+</sup> fibers (**Figures 4.5A-C**) compared to corresponding TRAF6<sup>ff</sup> at 3 and 5 days post-injury. Moreover, the mRNA levels of eMyHC were significantly reduced in injured TA muscle of TRAF6<sup>scko</sup> mice compared to corresponding TRAF6<sup>ff</sup> mice (**Figure 4.5D**). Furthermore, transcript levels of Myf5, MyoD and myogenin were also found to be significantly reduced in injured TA muscle of TRAF6<sup>scko</sup> mice compared to injured TA muscle of TRAF6<sup>ff</sup> mice (**Figure 4.5E**). Intriguingly, transcript levels of Myf5 were also found to be significantly reduced in contralateral uninjured TA muscle of TRAF6<sup>scko</sup> mice (**Figure 4.5E**) leading to conjure that TRAF6 has a pivotal role in regulating the early stages of myogenesis in satellite stem cells.

**TRAF6 is required for maintenance of satellite cell pool in skeletal muscle.** The reduced number and size of e-MyHC<sup>+</sup> fibers accompanied with down-regulation of transcript levels of myogenic regulatory factors in injured muscle of TRAF6<sup>scko</sup> mice suggest the possibility of reduced number of activated satellite cells available to participate in the myogenic program or an intrinsic defect in the satellite cells ability to progress through the myogenic lineage to form fusion competent myoblasts. It has been unarguably evident that Pax7 expression is vital for maintaining satellite cell function (143, 144). A fundamental



characteristic of adult stem cells is the ability to serve as source of tissue-specific differentiated cells while retaining the capacity to self-renew and repopulate the stem-cell niche. Such potential is inherent in muscle satellite cells by a timely regulated expression of Pax7 (82, 142, 144). Quiescent satellite cells are Pax7<sup>+</sup>/MyoD<sup>-</sup> (84, 142). In response to activating stimuli, satellite cells start expressing MyoD giving rise to proliferating myoblasts (149, 155). Sustained expression of Pax7 alongside MyoD is essential for generating adequate amount of myogenic progeny to drive proper muscle repair. Conditional inactivation of Pax7 in adult mice led to defective muscle regeneration following injury and progressive loss of the satellite cell pool due to premature differentiation of Pax7-null satellite cells (144). To understand the role of TRAF6 in regulation of Pax7 expression in satellite cells, muscle section from 5d saline or BaCl<sub>2</sub>-injected TRAF6<sup>scko</sup> and TRAF6<sup>ff</sup> mice were immunostained for Pax7 (**Figure 4.6A**). While injured muscle of TRAF6<sup>ff</sup> demonstrated efficient activation of satellite cells evident by a dramatic up-regulation in Pax7<sup>+</sup> cells, such increase was not observed in corresponding TRAF6<sup>scko</sup> muscle (**Figures 4.6A, 4.6B**). Strikingly, the number of Pax7<sup>+</sup> cells was also significantly reduced in contralateral uninjured muscle of TRAF6<sup>scko</sup> mice compared to that of TRAF6<sup>ff</sup> mice (**Figures 4.6A, 4.6B**). Consistent with reduced number of Pax7<sup>+</sup> cells, we found that protein and mRNA levels of Pax7 along with eMyHC protein were dramatically reduced in injured TA of TRAF6<sup>scko</sup> mice compared with TRAF6<sup>ff</sup> mice (**Figure 4.6C, 4.6D**). Moreover, mRNA levels of Pax7 were also found to be significantly reduced in uninjured TA muscle of TRAF6<sup>scko</sup> mice compared with TRAF6<sup>ff</sup> mice (**Figure 4.6D**). To further clarify the role of TRAF6 in satellite cells, we FACS analyzed satellite cells content in uninjured and 5d injured TA muscle of TRAF6<sup>scko</sup> and TRAF6<sup>ff</sup> mice using  $\alpha$ 7-integrin as a marker of

satellite cells and excluding CD31, CD45, Sca1, and Ter119<sup>+</sup> populations (**Figure 4.6E**). Consistent with immunohistological results, TA muscle of TRAF6<sup>scko</sup> demonstrated a modest up regulation in  $\alpha$ 7-integrin<sup>+</sup> cells following injury compared to that of TRAF6<sup>f/f</sup> mice (**Figures 4.6E, 4.6F**). Furthermore, number of  $\alpha$ 7-integrin<sup>+</sup> cells was found to be reduced in uninjured muscle of TRAF6<sup>scko</sup> mice compared with corresponding TRAF6<sup>f/f</sup> mice (**Figure 4.6F**).

We also measured the transcript levels of a few target genes of Notch pathway, a known regulator of satellite cell dynamics in both quiescent and activated states (57, 72, 73). Notably, mRNA levels of Hey, HeyL, Hes1, and Hes6 were significantly reduced in injured muscle of TRAF6<sup>scko</sup> mice (**Figure 4.7**). It has been reported that Hes1 and HeyL are involved in maintaining the quiescent status of satellite cells (72). Interestingly, we found that the transcript levels of HeyL and Hes1 were diminished in uninjured muscle of TRAF6<sup>scko</sup> compared to uninjured muscle of TRAF6<sup>f/f</sup> mice (**Figure 4.7**). These results suggest that TRAF6 is required the maintenance of satellite stem cell pool and their function *in vivo*.

### **Ablation of TRAF6 inhibits satellite cell self-renewal and causes premature**

**differentiation.** We next investigated dynamics of TRAF6-null satellite cells in cultures. Single myofibers were established from EDL muscle of TRAF6<sup>f/f</sup> and TRAF6<sup>scko</sup> mice and the satellite cells associated with them were analyzed immediately or 72h after culturing. Consistent with our *in vivo* results, a substantial reduction in the number of quiescent Pax7<sup>+</sup> satellite cells was clearly noticeable in freshly isolated fibers of TRAF6<sup>scko</sup> mice (**Figures 4.8A, 4.8B**). Intriguingly, the majority of Pax7<sup>+</sup> cells associated with TRAF6<sup>scko</sup> myofibers

were also expressing MyoD (**Figures 4.8A, 4.8B**). Corresponding fibers from TRAF6<sup>f/f</sup> mice contained an average of 6 satellite cells that were predominantly Pax7<sup>+</sup>/MyoD<sup>-</sup> (**Figure 4.8C**). The reduced number of Pax7<sup>+</sup> satellite cells on freshly isolated myofibers of TRAF6<sup>scko</sup> mice and the untimely expression of MyoD implies a pre-mature inclination of TRAF6-null satellite cells towards entering the cell cycle and failure to self-renew.

To further understand the myogenic potential of TRAF6-deficient satellite cells, myofibers and associated cells were fixed after 72h in suspension culture and immunostained for Pax7 and MyoD. Myofiber-associated TRAF6<sup>f/f</sup> satellite cells displayed a normal activation profile characterized by formation of satellite cell clusters and normal distribution of self-renewing (Pax7<sup>+</sup>/MyoD<sup>-</sup>), proliferating (Pax7<sup>+</sup>/MyoD<sup>+</sup>), and differentiating (Pax7<sup>-</sup>/MyoD<sup>+</sup>) cells (**Figures 4.8D-F**). However, myofibers from TRAF6<sup>scko</sup> mice exhibited scattered distribution of singlet and couplet cells and no evident clusters originating from a single clone (**Figures 4.8D-F**). Moreover, majority of cells were Pax7<sup>-</sup>/MyoD<sup>+</sup> and a few cells that were Pax7<sup>+</sup> were unanimously MyoD<sup>+</sup> with diminished expression of both proteins (**Figures 4.8D-F**).

We also investigated whether deficiency of TRAF6 also compromises the fusion potential of myogenic cells. Primary myoblasts prepared from TRAF6<sup>f/f</sup> and TRAF6<sup>scko</sup> mice were plated at high density and differentiation was induced through serum withdrawal. TRAF6-deficient myoblast were capable of fusion evident by normal myotube formation (**Figure 4.9**). These results suggest that TRAF6 is required for self-renewal and maintaining the myogenic potential of satellite cells.

**TRAF6 mediates proliferation and gene expression of Pax7 in satellite cells.** Lack of satellite cell clusters on culture myofibers of *Traf6*<sup>sko</sup> mice indicates a requirement of TRAF6 for maintaining satellite cells' replicative capacity. To directly address this issue, we prepared primary myoblasts from hind limb muscle of C57BL6 mice and transfected them with vector alone (pcDNA3), full length TRAF6 (TRAF6-FL), or a dominant negative (DN) mutant of TRAF6 (TRAF6-DN). The number of satellite cells was measured after Pax7 staining whereas cellular proliferation was studied by EdU incorporation. Interestingly, forced expression of TRAF6-FL significantly increased the number of Pax7<sup>+</sup> cells (**Figures 4.10A, 4.10B**) and the incorporation of EdU in myoblast cultures (**Figure 4.10C**). By contrast, number of Pax7<sup>+</sup> or EdU<sup>+</sup> cells was significantly reduced in the cultures transfected with TRAF6-DN (**Figures 4.10A-C**).

To determine whether TRAF6 is required for the gene expression Pax7 in satellite cells, we measured the transcript levels of Pax7 in myoblast cultures transfected with TRAF6-FL or TRAF6-DN. Interestingly, forced expression of TRAF6-FL had no effect on Pax7 mRNA levels whereas the cells transfected with TRAF6-DN exhibited a significant reduction in mRNA levels of Pax7 (**Figure 4.10D**). We also investigated the effects of knockdown of TRAF6 on mRNA levels of Pax7. Results showed that shRNA-mediated knockdown of TRAF6 significantly reduced the mRNA levels of Pax7 in primary myogenic cultures (**Figure 4.10E**). These results give rise to two possibilities: (a) TRAF6 regulates the proliferative capacity of Pax7<sup>+</sup> cells with no direct effect on the gene expression on Pax7, or (b) TRAF6 is a signaling intermediate through which upstream molecular configurations lead to the activation of Pax7 locus and hence the forced expression of TRAF6 in isolation of a parallel overexpression of a docking molecule does not increase the gene expression of

Pax7. To address this issue, we studied the effects of interleukin-1 $\beta$  (IL-1 $\beta$ ) on the levels of Pax7 and cellular proliferation. In response to IL-1 $\beta$ , TRAF6 is recruited to the IL-1 receptor (IL-1R) serving as a scaffold protein which lead to the activation of downstream signaling molecules (101). Therefore, we postulated if TRAF6 is the liaison for a higher hierarchal interaction that initiates downstream expression of Pax7, stimulation of such pathway should lead to the increased gene expression of Pax7 in satellite cells. Indeed, primary myoblasts treated with IL-1 $\beta$  displayed a dramatic up-regulation in levels of Pax7 protein (**Figure 4.10F**). Intriguingly, IL-1 $\beta$  did not affect the levels of TRAF6 in satellite cells (**Figure 4.10F**) further confirming that TRAF6 is a possible transducer of a signaling pathway that leads to the increased expression of Pax7 in satellite cells. Moreover, cells treated with IL-1 $\beta$  displayed enhanced replicative capacity evident by increased EdU incorporation (**Figures 4.10G, 4.10H**). Collectively, these findings imply that TRAF6 is an integral component of a pathway that is required for the gene expression of Pax7 and proliferation of satellite cells.

**TRAF6 regulates the expression of Pax7 in satellite cells through activation of ERKs and JNK.** Recently, signaling from MAPKs has been linked to various stages of satellite cell-cycle regulation. ERK1/2-mediated signaling in satellite cells promoted a G0-like phenotype (152) while signaling through p38 MAPK stimulated their activation and terminal differentiation (102, 156). Functional outcome of either pathway has been shown to take place through direct or indirect regulation of Pax7 expression (152, 156). Our attempts to directly isolate primary myoblasts from skeletal muscle of tamoxifen-treated TRAF6<sup>sko</sup> mice were unsuccessful due to reduced number of myofiber-associated satellite cells in these mice and failure of the cells to grow in culture upon seeding. We then isolated

satellite cells from hind limb muscle of non-tamoxifen treated TRAF6<sup>sko</sup> mice and expanded them in the cultures followed by treatment with vehicle alone or 4-hydroxytamoxifen (4-OHT) to induce tamoxifen-mediated Cre recombination. Treatment with 4-OHT drastically reduced the protein levels of TRAF6 in myoblast cultures (**Figure 4.11A**). Consistent with in vivo results, a substantial reduction in Pax7 protein levels was noticeable in TRAF6<sup>sko</sup> cultures treated with 4-OHT compared to those treated with vehicle alone (**Figure 4.11A**). Interestingly, phosphorylation levels of ERK1/2 and JNK1/2 were considerably reduced while no such effect was observed on ERK5 phosphorylation (**Figure 4.11B**). The reduction in ERK1/2 phosphorylation is in line with previously published reports indicating the involvement of ERK1/2 pathway in regulating proliferation and self-renewal of satellite cells in a context-dependent manner (152, 157, 158). Intriguingly, ablation of TRAF6 using 4-OHT drastically increased the levels of p38 phosphorylation (**Figure 4.11B**) aligning with a role of p38 in promoting progression through the myogenic lineage (102, 159). More importantly, total and phosphorylated levels of c-Jun, a direct phosphorylation target of ERK1/2 and JNK (160), were also diminished as a result of deletion of TRAF6 (**Figure 4.11C**). IL-1 $\beta$ , which increases the levels of Pax7, also increased the phosphorylation of c-Jun in satellite cell cultures (**Figure 4.11D**). Furthermore, we also found that in vivo ablation of TRAF6 in satellite cells (i.e. tamoxifen-treated TRAF6<sup>sko</sup>) reduced the phosphorylation of c-Jun in injured skeletal muscle of mice (**Figure 4.11E**).

To understand the direct role of various MAPK pathways in Pax7 expression, primary myoblasts prepared from WT mice were treated with specific MAPK inhibitors: PD184352 which inhibits ERK1/2, SP6100125 which inhibits JNK, and SB203580 which

inhibits the p38MAPK pathway. After 48 hours of treatment, mRNA and protein levels of Pax7 were measured. Interestingly, cells treated with ERK1/2 or JNK inhibitors significantly reduced mRNA and protein levels of Pax7 while those treated with p38 inhibitor had no effect on Pax7 expression (**Figure 4.11F**). Furthermore, cells treated with ERK1/2 and JNK inhibitors (but not p38 inhibitor) exhibited a sharp decrease in c-Jun phosphorylation (**Figure 4.11G**). To understand the role of c-Jun in regulation of Pax7 expression, we performed loss-of-function and gain-of-function experiments. In correlation with the preceding findings, shRNA-mediated knock down of c-Jun sharply reduced the levels Pax7 mRNA in primary myoblast cultures from WT mice (**Figure 4.11H**). By contrast, overexpression of c-Jun significantly increased the mRNA levels of Pax7 in myoblast cultures (**Figure 4.11I**). Notably, c-Jun is known to form homo- or hetro- dimers with other Jun or Fos family members giving rise to AP1 transcription factor (161). Since c-Jun possesses a transactivation domain, we contemplated that c-Jun regulates Pax7 expression through direct binding of Pax7 promoter. Our *in silico* analysis of 3.5 kb region upstream of transcription start site in Pax7 promoter revealed 11 potential consensus sequence for AP1/c-Jun transcription factor (data not shown). To understand whether c-Jun enrich the Pax7 promoter, we performed chromatin immunoprecipitation (ChIP) assay. Intriguingly, 4 out of 11 potential sites displayed high enrichment in Pax7 promoter in primary myoblasts (**Figure 4.11J**). All together, these findings demonstrate that TRAF6-mediated signaling augments Pax7 levels through the activation ERK1/2 and JNK which in turn activate c-Jun transcription that directly interacts with the promoter region of Pax7.

**Ablation of TRAF6 augments the levels of muscle-specific microRNAs (myomiRs) in satellite cells.** MicroRNAs are a class of short (19-22 bp) non-coding RNAs that function as post-transcriptional regulators of gene expression (162). By hybridizing to complementary binding sites in the 3' untranslated region (UTR) of target mRNAs, miRNAs inhibit protein translation through mRNA cleavage or steric hindrance (162-164). Recently, a group of muscle specific miRNAs (MyomiRs) consisting of mir-1, miR-206 (163-165), miR-133a, and miR-133b has been shown to be critical in regulating skeletal muscle development. Expression levels of miR-1, miR-206 and miR-133 were found to be sharply upregulated during myogenesis (164). Furthermore, miR-1 and miR-206 have been shown to promote satellite cell differentiation through direct targeting of Pax7 mRNA (148). To investigate if TRAF6 also regulates Pax7 abundance in a microRNA-mediated manner, we measured the levels of miR-1, miR-206, and miR-133a in TRAF6-deficient primary myoblasts. Strikingly, expression levels of all three miRNAs were found to be dramatically increased upon ablation of TRAF6 (**Figure 4.12A**). Since our preceding findings draw a possible role of c-Jun in mediating TRAF6 regulation of Pax7 transcription, we further delineated whether TRAF6-mediated regulation of MyomiRs is also brought about through a c-Jun dependent mechanism. We found that overexpression of c-Jun repressed the levels of miR-206 and miR-133a in cultured satellite cells (**Figure 4.12B**). Collectively, these results are suggestive of a possible post-transcriptional role of TRAF6-MAPK-AP1 axis in mediating Pax7 expression.

**Deletion of TRAF6 in satellite cells exacerbates myopathy in mdx mice.** Functional inactivation of the dystrophin gene is the primary cause of Duchenne muscular dystrophy



(DMD) in humans and in mdx mice (a mouse model of DMD) (8). Dystrophic muscle undergoes repetitive rounds of degeneration and regeneration (8, 14). To further examine the role of TRAF6-mediated signaling in satellite cells, we investigated the effects of ablation of TRAF6 in satellite cells of mdx mice on myopathy. TRAF6<sup>sko</sup> mice were crossed with mdx mice to generate mdx;TRAF6<sup>sko</sup> and littermate mdx;TRAF6<sup>fl/fl</sup> mice. In mdx mice, acute muscle injury starts at around 2.5 weeks and peaks between the age of 3-4 weeks (14) after which alternating cycles of regeneration and degeneration persists till the age of 12 weeks. Accordingly, tamoxifen mediated Cre recombination was initialized at 3 weeks of age and analysis was conducted at the age of 8 weeks. We found a significant decrease in size and body weight of mdx;TRAF6<sup>sko</sup> mice compared with littermate mdx;TRAF6<sup>fl/fl</sup> mice (**Figures 4.13A, 4.13B**). Furthermore, mdx;TRAF6<sup>sko</sup> mice displayed reduced functional output evident by decreased forelimb grip strength and total four-limb grip strength (**Figure 4.13C**). Wet weight of gastrocnemius (GA) and quadriceps muscles was also found to be significantly reduced in mdx;TRAF6<sup>sko</sup> mice compared to littermate mdx;TRAF6<sup>fl/fl</sup> mice (**Figure 4.13D**). Analysis of H&E-stained muscle sections of mdx;TRAF6<sup>sko</sup> mice showed signs of exacerbated myopathy marked by increased necrotic areas and failure of regeneration manifested by the lack of centronucleated fibers and exaggerated pseudo-muscle hypertrophy (**Figure 4.13E**). Increased myopathy was also reflected by significantly higher levels of creatine kinase (CK) in plasma of mdx;TRAF6<sup>sko</sup> mice compared to mdx;TRAF6<sup>fl/fl</sup> mice (**Figure 4.13F**). Consistent with our findings in the BaCl<sub>2</sub>-mediated model of injury, these results suggest that TRAF6 is required for satellite cell function in dystrophic muscle.

#### 4.4 DISCUSSION

Under normal conditions Pax7 expressing satellite cells reside in quiescence beneath the basal lamina of adult muscle (52). In response to activating stimuli such as injury, satellite cells rapidly enter the cell cycle by up regulating MyoD giving rise to a population of proliferating myoblasts (85, 155). The majority of activated satellite cells progress through the myogenic lineage and undergo terminal differentiation leading to the forming new mature muscle, while a subpopulation homes back to the muscle niche to replenish the reservoir of satellite cells (85, 142). This process is driven by coordinated regulation of intrinsic and extrinsic factors that culminate in controlling the expression status of Pax7 which in turn determines the fate of satellite cells (64, 70, 152). Thus, the precise regulation of Pax7 is pivotal for maintaining satellite cell function in skeletal muscle.

Our findings in this study illustrate a satellite cell autonomous role of TRAF6 in regulating Pax7 function in adult skeletal muscle. Conditional deletion of TRAF6 in satellite cells led to defective muscle regeneration following BaCl<sub>2</sub>-mediated injury (**Figures 4.3, 4.4**). Satellite cells from regenerating muscle of TRAF6<sup>scko</sup> mice failed to provide sufficient competent myogenic cells capable of driving proper regeneration program (**Figure 4.6**). Diminished number of activated Pax7<sup>+</sup> cells led to inadequate muscle formation evident by reduced number and size of eMyHC<sup>+</sup> fibers upon deletion of TRAF6 (**Figure 4.5**).

Failure of TRAF6-KO satellite cells to drive proper regeneration could be attributed to: (a) failure in activation and exiting quiescence, (b) proper activation and entry to the cell cycle but impaired replicative capability, (c) proper activation and proliferation capacities but fusion incompetency, (d) improper activation and proliferation but fusion competency, or (e) improper activation and proliferation associated with fusion incompetence. Excluding

(c), reduced number of activated Pax7<sup>+</sup> satellite cells in regenerating muscle of TRAF6<sup>sko</sup> mice (Figure 3) gives rise to any of the remaining possibilities. Nevertheless, decreased expression of Pax7 and reduced number of Pax7<sup>+</sup> satellite cells in sham muscle (**Figure 4.6**) and freshly isolated myofibers of TRAF6<sup>sko</sup> mice accompanied with MyoD expression (**Figure 4.8**) also rules out the first possibility, as abatement of Pax7 expression indicates loss of quiescence and upregulated MyoD levels implies activation. Furthermore, lack of cell cluster formation associated with cultured TRAF6<sup>sko</sup> myofibers (**Figure 4.8**) and reduced EdU incorporation in DN-TRAF6 transfected myoblast (**Figure 4.10**) are direct evidence for elimination of probability (b), leaving the possibility of (d) or (e). However, normal myotube formation displayed by TRAF6-KO myoblasts plated at high confluency (Figure S5) indicates preserved fusion capacity giving strong plausibility to the interpretation in (d). Our systematic examination of the expression profile and activation and proliferation dynamics implicates loss of myogenic lineage upon deletion of TRAF6 due to deregulation of Pax7 expression, which in turn leads to precocious differentiation.

Our results further demonstrate that TRAF6 regulates Pax7 expression in a context dependent manner. While knockdown of TRAF6 considerably reduced the mRNA levels of Pax7 (**Figures 4.10D, 4.10E**), over expression of TRAF6 alone had no effect on Pax7 transcription (**Figure 4.10D**). Forced activation of TRAF6-mediated signaling by treatment with IL-1 $\beta$  enhanced the expression levels of Pax7 with no notable effect on TRAF6 levels (Figure **4.10G**). These findings led us to contemplate that TRAF6 is an essential mediator of upstream signaling that regulates downstream expression of Pax7 and that loss of TRAF6-mediated signaling transduction brings halt to the Pax7 activating pathway.

Moreover, our study indicates that TRAF6 regulates Pax7 function of satellite cells through conditional activation and deactivation of specific MAPK family signaling pathways (**Figure 4.11**). Increased expression of p38 MAPK in TRAF6-KO myoblasts (**Figure 4.11B**) lends further support to the premise that loss of TRAF6 in myogenic cells leads to precocious differentiation. Signaling from p38MAPK has been shown to play an essential role in regulating the later stages of myogenesis (156, 166). Quiescent satellite cells treated with p38 inhibitors failed to enter the cell cycle upon induction of activation. In contrast, overexpression of p38 promotes exit from quiescence and premature induction of terminal differentiation (156, 159). Conversely, phosphorylation levels of ERK1/2 were dramatically reduced in TRAF6-KO cells (**Figure 4.11B**) consistent with the published role of ERK1/2 signaling in regulating proliferation and self-renewal of satellite cells in a context-dependent manner (152, 157, 158). Additionally, our results implicate a parallel role of JNK signaling in regulation of satellite cells, as phosphorylated JNK protein levels were also reduced upon deletion of TRAF6 (**Figure 4.11B**) and inhibition of JNK independently reduced Pax7 expression levels mirroring ERK1/2 inhibition (**Figures 4.11F, 4.11G**). Of note, JNK signaling has been shown to counteract p38 activity; therefore it is possible that reduced JNK signaling brought about by deletion of TRAF6 leads to hyperactivation of p38 signaling in satellite cells which in part promotes exit from quiescence and precocious differentiation. Our findings also suggest that Pax7 regulation through ERK1/2 and JNK signaling takes place in a c-Jun dependent manner. TRAF6-KO primary myoblasts exhibited a dramatic reduction in total and phosphorylated levels of c-Jun protein (**Figure 4.11C**) and inhibition of ERK1/2 and JNK pathways similarly reduced phosphorylation of c-Jun in WT myoblasts (**Figure 4.11F**). Importantly, cells knocked-

down of c-Jun displayed a phenotypic outcome that resembled that of TRAF6-KO myoblast (**Figure 4.11H**). Our ChIP data further validates the inference that TRAF6 regulates gene expression of Pax7 in myoblasts through direct binding of c-Jun to multiple sites in the mouse Pax7 promoter (**Figure 4.11J**).

Interestingly, our findings further suggest a potential post transcriptional role of c-Jun in modulating Pax7 levels. Pax7 has been identified as one of the direct regulatory targets of miR-1 and miR-206 (148), both of which were found to be upregulated in TRAF6-KO myoblasts (**Figure 4.12A**) and diminished upon c-Jun overexpression (**Figure 4.12B**). However, further investigations will be required to determine whether the alterations observed in MyomiRs are mere phenotypic outcomes or possible auxiliary regulatory facets that modulate Pax7 expression in TRAF6 context.

The role of TRAF6 in regulating satellite cell function is further supported by our findings in the mdx mouse (**Figure 4.13**). In resemblance to various injury models, satellite cells drive the events of muscle regeneration in dystrophic muscle. Deletion of TRAF6 in satellite cells of mdx mice led to exacerbated myopathy as a result of impaired regeneration (**Figure 4.13**). Exhaustion of satellite cell myogenic capacity accompanies progression of dystrophinopathy leading to cessation of muscle regeneration. Although therapies aimed at improving the muscle microenvironment have demonstrated to be transiently advantageous, extensive investigations have shown that premature loss of satellite cell function in dystrophic muscle is due to a cell autonomous defect. Modulating TRAF6 levels in satellite cells of dystrophic muscle or donor cells may prove to be beneficial in prolonging the myogenic potential and replenishing the reservoir of satellite cells.

In summary, our present study has identified a previously unrecognized role of TRAF6 in regulation satellite cell function. TRAF6-mediated regulation of satellite cells to takes place through regulating the expression of Pax7. TRAF6 is also necessary to maintaining the quiescent state of satellite cells under unchallenged conditions, sustaining the myogenic potential upon stimulation, and regulating self-renewal following activation.

**FIGURE 4.1**

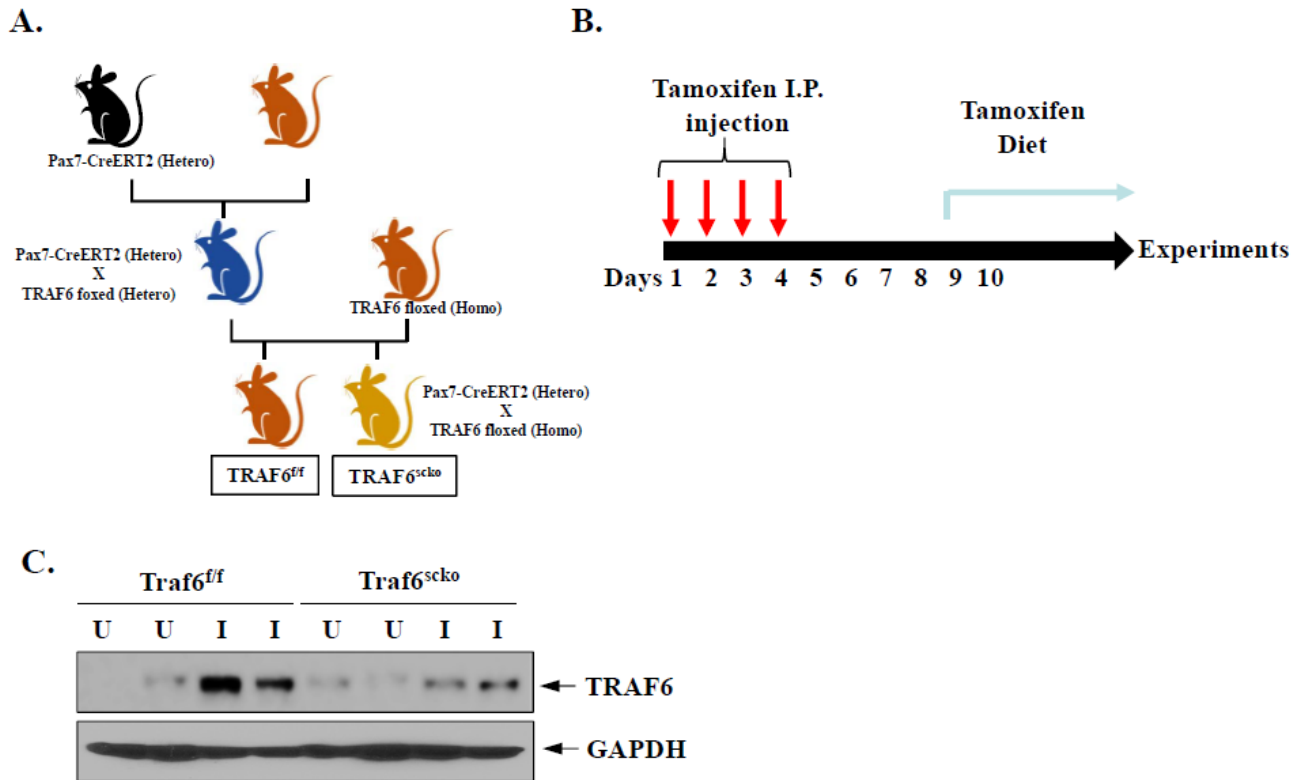
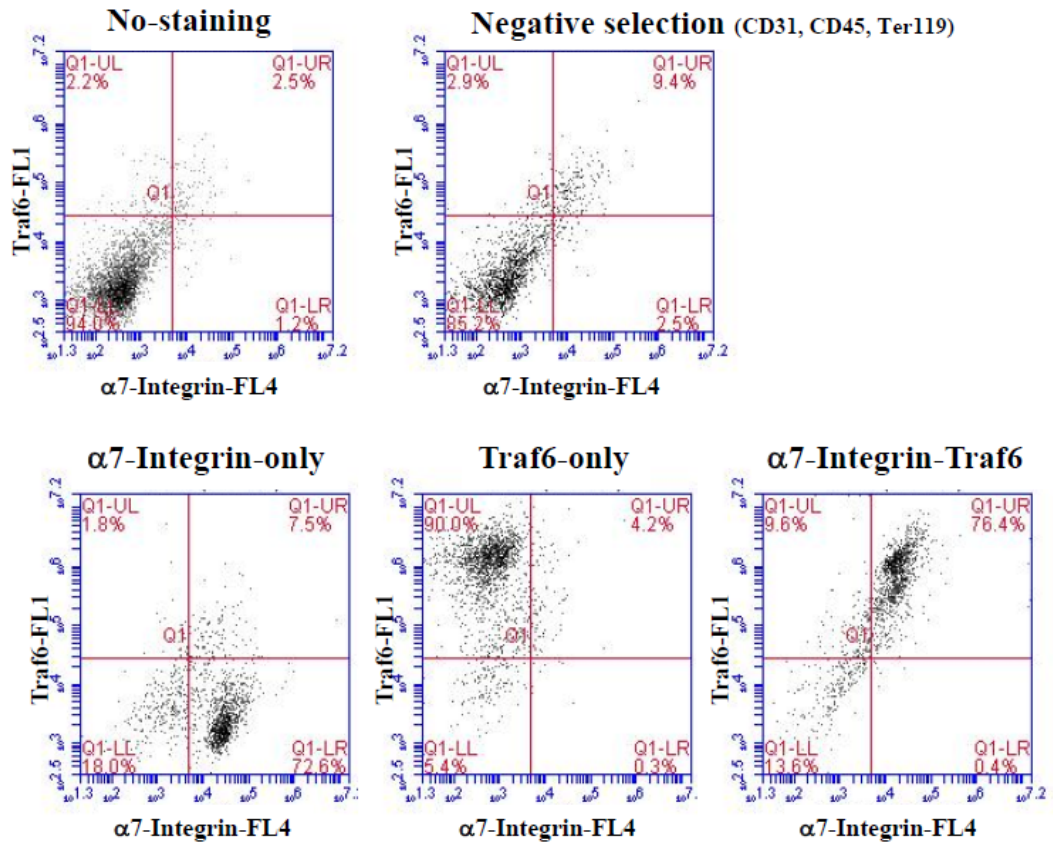


**FIGURE 4.1. Generation of conditional satellite cell-specific TRAF6-knock out**

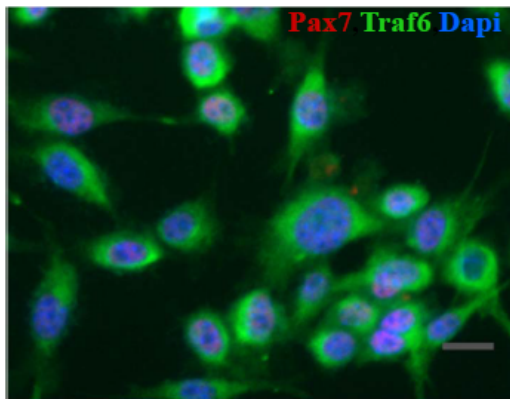
**(TRAF6<sup>sc<sup>ko</sup>)</sup>** mice. (A) Schematic illustration of the breeding strategy to obtain TRAF6<sup>sc<sup>ko</sup> and littermate TRAF6<sup>fl/fl</sup> mice. (B) Representation of the time line of tamoxifen mediated Cre-recombination. (C) Representative immunoblot displaying TRAF6 protein levels in injured and naïve TA muscle 5 days post BaCl<sub>2</sub> injection following Cre-recombination.</sup>

**FIGURE 4.2**

**A.**



**B.**



**C.**

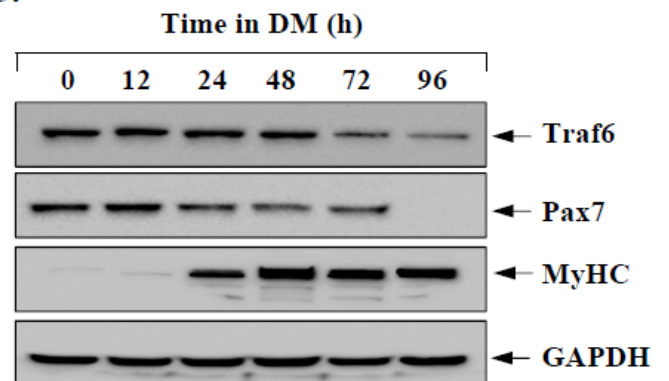




**FIGURE 4.2. TRAF6 is expressed in satellite cells.** Primary myoblasts were isolated from hind limb muscle of BL6 mice and FACS sorted based on  $\alpha 7$ -Intigrin expression. **(A)** Representative dot plot displaying enrichment of TRAF6<sup>+</sup> cells amongst  $\alpha 7$ -intigrin<sup>+</sup> population. **(B)** Primary myoblast seeded in matrigel coated plates were fixed and labeled with antibodies that recognize TRAF6 and Pax7. Representative photomicrograph illustrating co-localization of TRAF6 and Pax7 in mouse primary myoblasts are presented here. In a separate experiment primary myoblasts were induced to differentiate by serum withdrawal for various time points after which protein extracts were prepared **(C)** Representative immunoblots demonstrating regulation of TRAF6, Pax7, and MyHC levels during myogenesis.

**FIGURE 4.3**

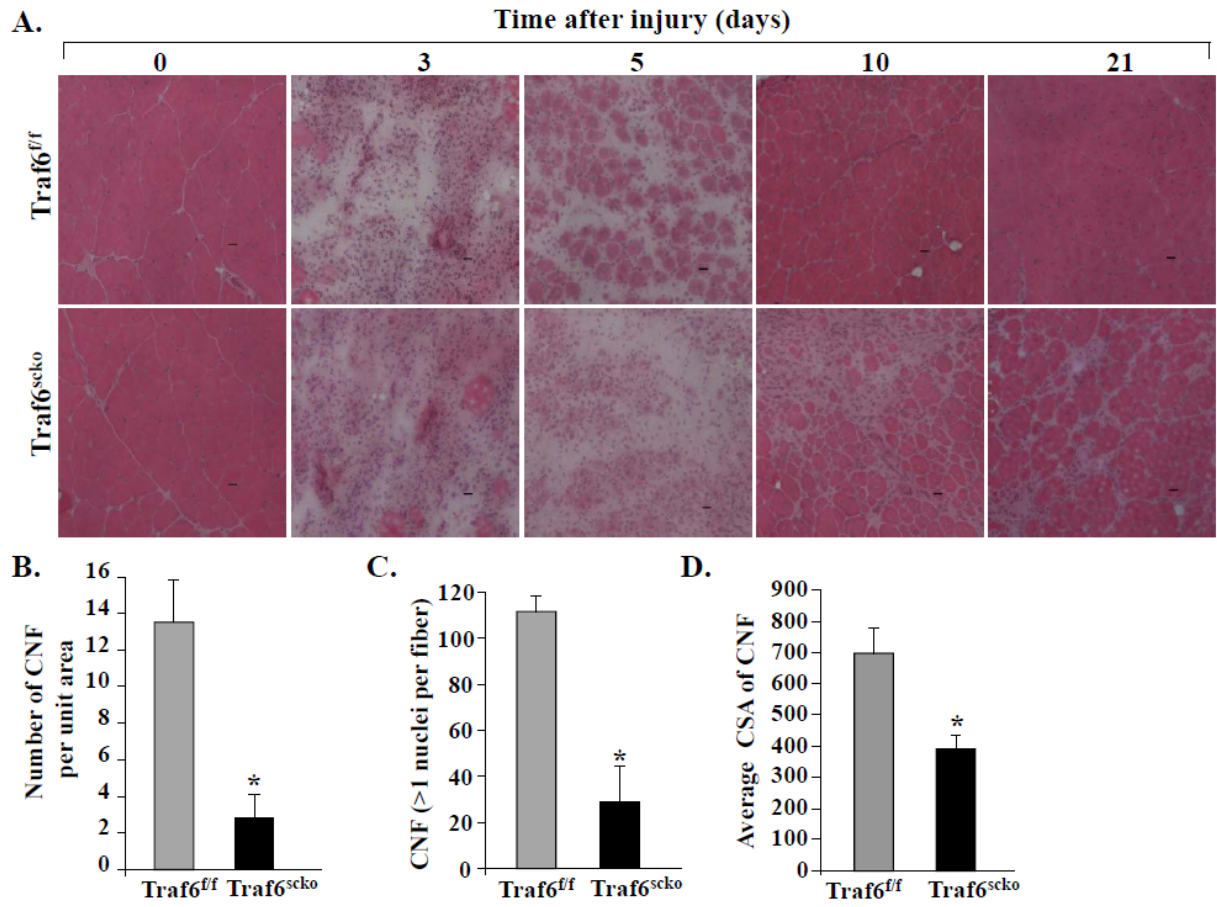
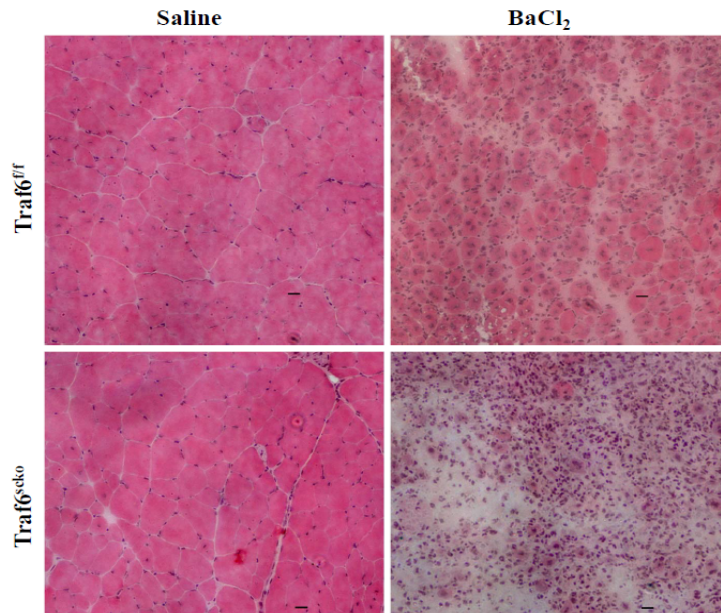


**FIGURE 4.3. TRAF6 is required for skeletal muscle regeneration.** Following tamoxifen-mediated Cre recombination, TA muscle of adult TRAF6<sup>f/f</sup> and TRAF6<sup>scko</sup> mice were injected with 100μl of 1.2% BaCl<sub>2</sub> solution after which muscles were isolated and analyzed at different time points. **(A)** Representative photomicrographs of H&E-stained sections illustrating a severe regeneration defect in injured muscle of TRAF6<sup>scko</sup> mice compared with TRAF6<sup>f/f</sup> littermates. Quantification of **(B)** number of centrally nucleated fibers (CNF) per unit area **(C)** number of myofibers containing more than one central nuclei and **(D)** Cross sectional area (CSA) of centrally nucleated fibers 5d post BaCl<sub>2</sub>-mediated injury. Error bars represent SD. N=3 in each group. \*p < 0.05 vs. saline injected TA muscle TRAF6<sup>f/f</sup> mice and #p<0.05 vs. saline injected TA muscle of TRAF6<sup>scko</sup> mice.

**FIGURE 4.4**

**A.** 1<sup>st</sup> BaCl<sub>2</sub> injury — 21 days — 2<sup>nd</sup> BaCl<sub>2</sub> injury — 5 days — Analysis



**B.** Saline BaCl<sub>2</sub>

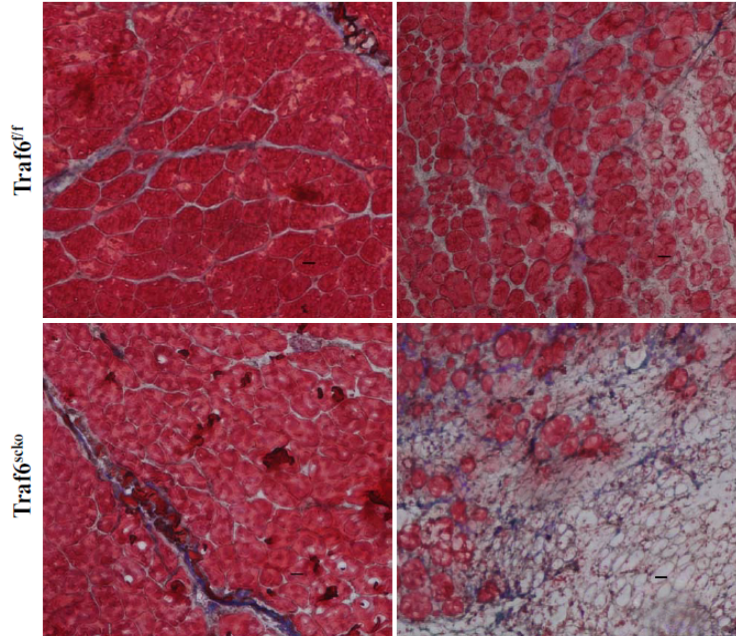


**FIGURE 4.4. Loss of muscle tissue following double injury in TRAF6<sup>scko</sup> mice.** TA muscle of TRAF6<sup>scko</sup> and TRAF6<sup>f/f</sup> mice were subjected to a first BaCl<sub>2</sub> injection and injured muscles were allowed to heal for 21 days after which a second round of muscle injury was induced and muscle regeneration was analyzed 5 days following the second BaCl<sub>2</sub> injection. **(A)** Representative photomicrograph of H&E stained TA muscles of TRAF6<sup>scko</sup> and TRAF6<sup>f/f</sup> mice. **(B)** Representative photo micrograph of trichrome-stained TA muscle of TRAF6<sup>scko</sup> and TRAF6<sup>f/f</sup> mice.

**FIGURE 4.5**

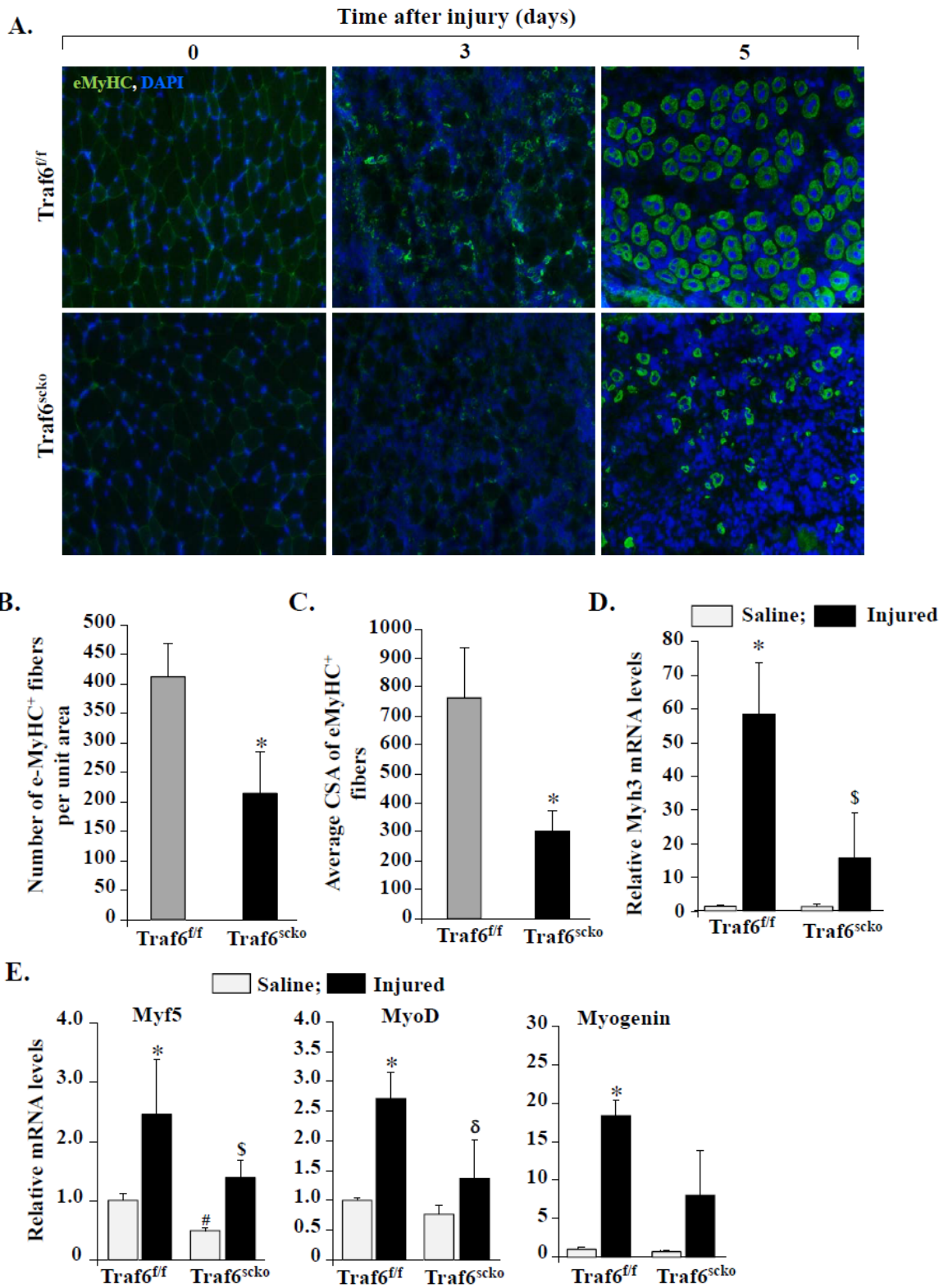


**FIGURE 4.5. Ablation of TRAF6 in satellite cells inhibits formation of new myofibers (eMyHC<sup>+</sup>) following injury. (A)** Representative photomicrograph of eMyHC-stained sections prepared from TA muscle of TRAF6<sup>f/f</sup> and TRAF6<sup>scko</sup> mice collected at various time points following BaCl<sub>2</sub> injection. **(B)** Number and **(C)** CSA of eMyHC<sup>+</sup> fibers are presented here. In a separate experiment, TA muscle of TRAF6<sup>f/f</sup> and TRAF6<sup>scko</sup> mice were injected with 1.2% BaCl<sub>2</sub> or saline. After 3 days, the TA muscle was isolated and processed for qRT-PCR. Relative mRNA levels of **(D)** eMyHC and **(E)** Myf5, MyoD, and myogenin are presented here. Error bars represent SD. n=3 in each group. \* p < 0.05 vs. saline injected TRAF6<sup>f/f</sup> muscle and #p<0.05 vs. saline injected TRAF6<sup>scko</sup> muscle.



**FIGURE 4.6**

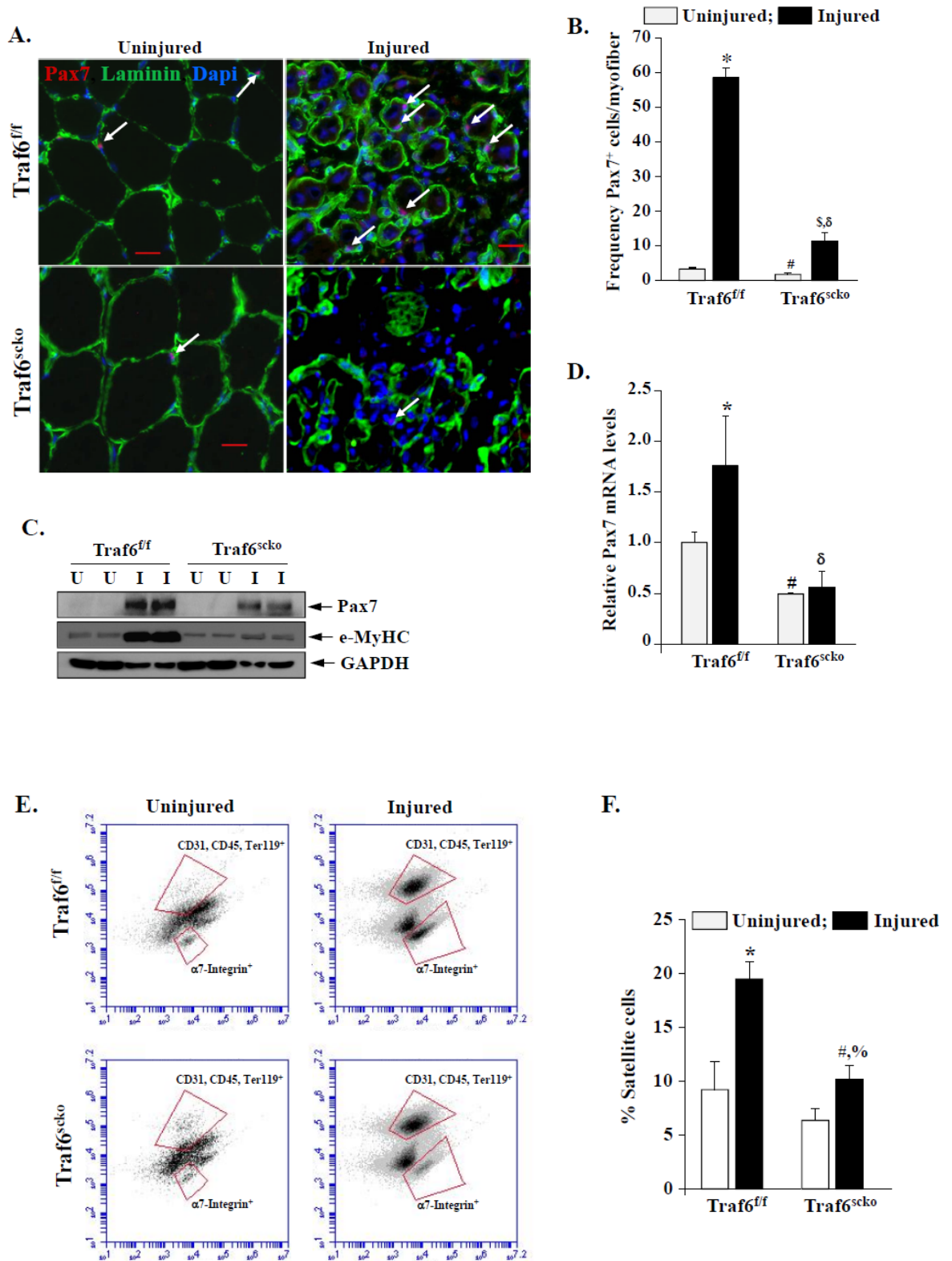




**FIGURE 4.6. TRAF6 is required for maintenance of satellite cell pool in skeletal muscle.** TA muscle of TRAF6<sup>f/f</sup> and TRAF6<sup>scko</sup> mice were injected with 1.2% BaCl<sub>2</sub> or saline for 5 days after which muscles were isolated and processed for histological and biochemical analysis. **(A)** Representative photomicrographs of Pax7-stained sections. Nuclei were identified by co-staining with DAPI. Arrows point to Pax7<sup>+</sup> cells. **(B)** Quantification of average number of Pax7<sup>+</sup> cells per myofiber in BaCl<sub>2</sub> and saline injected muscle of TRAF6<sup>f/f</sup> and TRAF6<sup>scko</sup> mice. **(C)** mRNA, and **(D)** protein levels of Pax7 are presented here. **(E)** Representative FACS dot plots demonstrating the percentage of a7-integrin<sup>+</sup> cells in saline and BaCl<sub>2</sub> injected TA muscle of TRAF6<sup>f/f</sup> and TRAF6<sup>scko</sup> mice. **(F)** Quantification of a7-integrin<sup>+</sup> satellite cells in saline- or BaCl<sub>2</sub>-injected TA muscle of TRAF6<sup>f/f</sup> and TRAF6<sup>scko</sup> mice by FACS. Error bars represent SD. N=3 or 4 in each group. \*p < 0.05 vs. saline injected TRAF6<sup>f/f</sup> muscle. #p<0.05 vs. saline injected TRAF6<sup>scko</sup> muscle.

**FIGURE 4.7.**

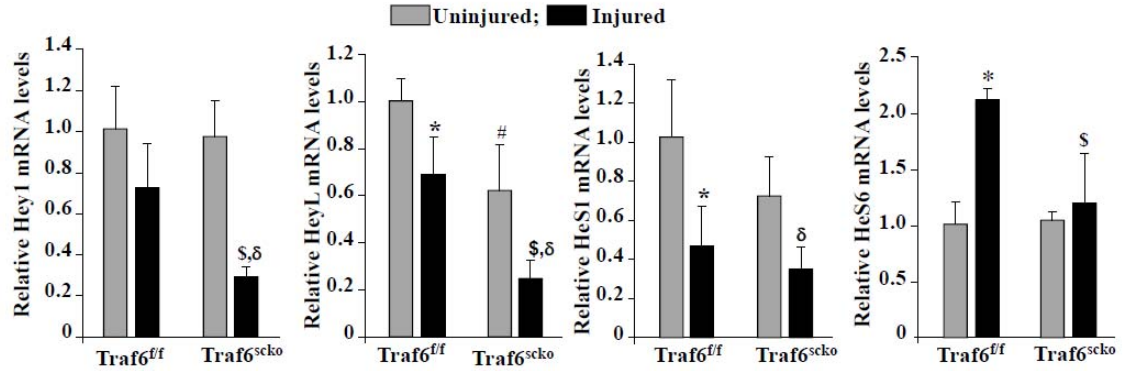


**FIGURE 4.7. Notch signaling is compromised in skeletal muscle of TRAF6<sup>scko</sup> mice.** TA muscle of TRAF6<sup>scko</sup> and TRAF6<sup>f/f</sup> mice were injured with BaCl<sub>2</sub> injection and 3 days later muscles were collected and processed for qRT-PCR analysis. Representative bar diagrams illustrating relative mRNA levels of Notch pathway target genes in naive and injured TA muscles of TRAF6<sup>scko</sup> and TRAF6<sup>f/f</sup> mice. Error bars represent SD. N=3 in each group. \*p < 0.05 vs. saline injected TRAF6<sup>f/f</sup> muscle and #p < 0.05 vs. saline injected TRAF6<sup>scko</sup> muscle.

**FIGURE 4.8**

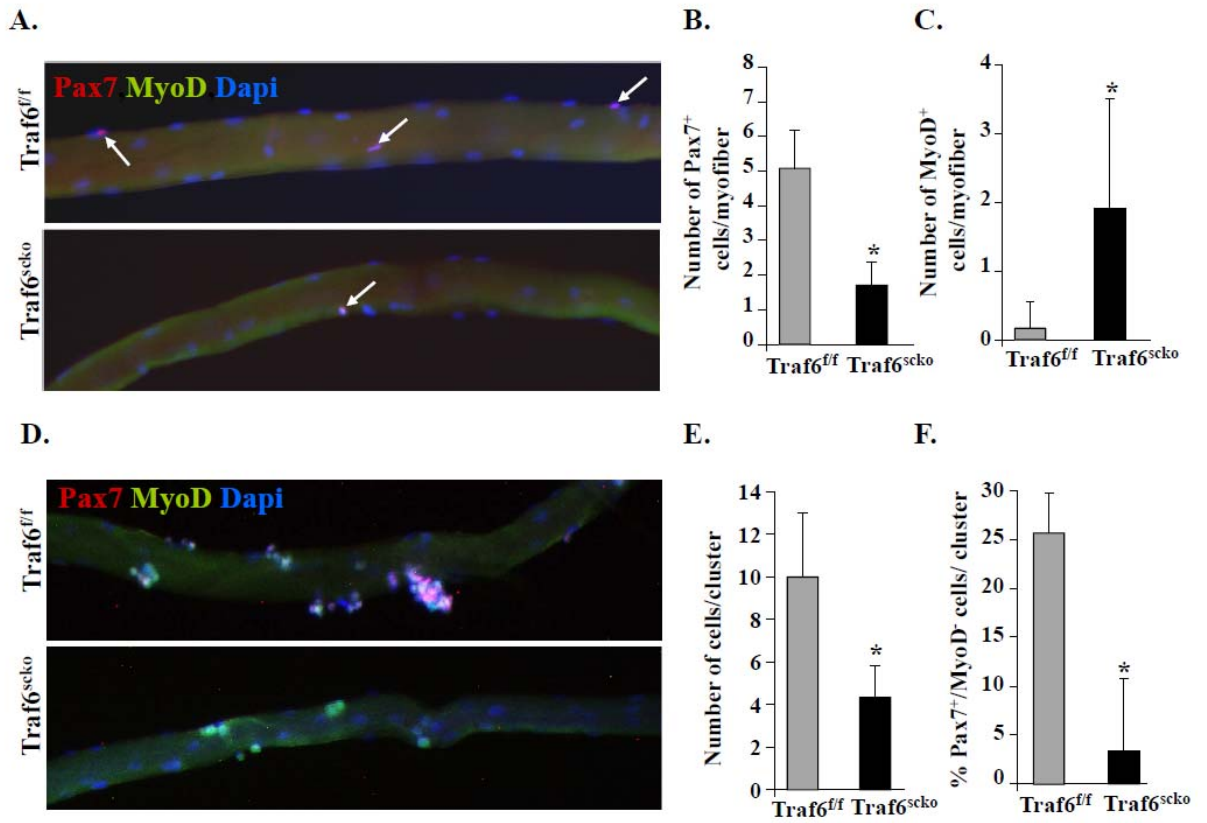


**FIGURE 4.8 Deletion of TRAF6 in satellite cells leads to premature differentiation.**

Single myofibers were isolated from EDL muscle of TRAF6<sup>f/f</sup> and TRAF6<sup>scko</sup> mice. At 0h and 72h of culture, myofibers were collected and labeled with antibodies against Pax7 and MyoD. Nuclei were counter stained with DAPI. **(A)** Representative merged images of freshly isolated myofibers from TRAF6<sup>f/f</sup> and TRAF6<sup>scko</sup> mice stained with Pax7, MyoD and DAPI. Quantification of number of **(B)** Pax7<sup>+</sup>/MyoD<sup>-</sup> and **(C)** Pax7<sup>+</sup>/MyoD<sup>+</sup> cells per fiber are presented here. **(D)** Representative merged images of myofibers isolated from TRAF6<sup>f/f</sup> and TRAF6<sup>scko</sup> mice after 72h of suspension culture. Bar histograms representing **(E)** number of cells per cluster and **(F)** percentage of self-renewing Pax7<sup>+</sup>/MyoD<sup>-</sup> cells per myofibers following 72h of culture. Error bars represent S.D. \*, p < 0.05, values significantly different from TRAF6<sup>f/f</sup> myofibers.

**FIGURE 4.9**

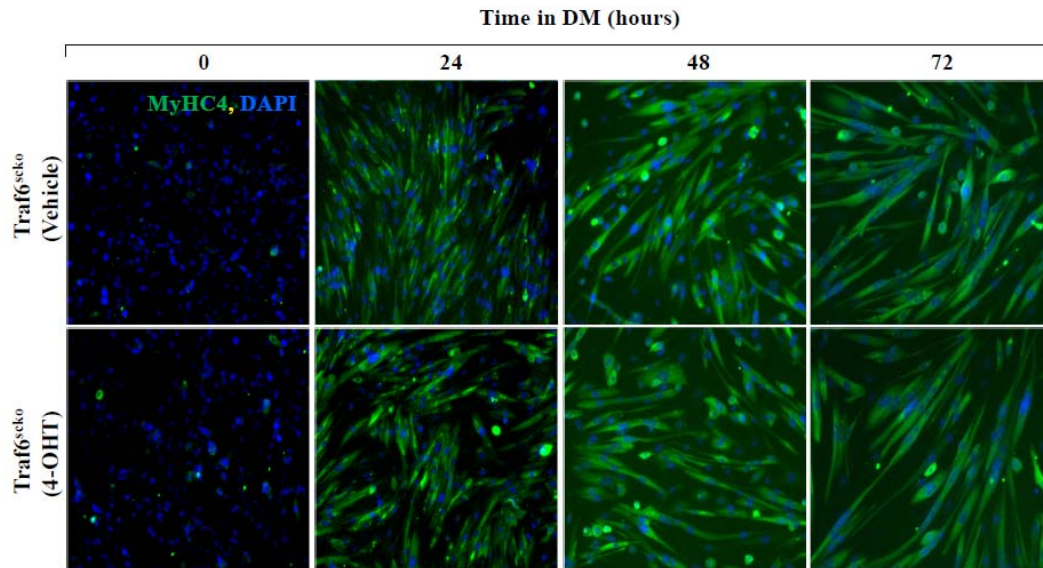


**FIGURE 4.9. Fusion capacity is preserved in TRAF6 deficient myoblasts.** Primary myoblast were prepared from hind limb muscle of non-tamoxifen administered TRAF6<sup>sko</sup> mice. Following purification, cells were treated with vehicle or 10ng/ml 4-OHT to induce Cre-recombination. 7 days post 4-OHT treatment, cells were plated at high density and induced for differentiation via serum withdrawal. Photomicrograph of vehicle and 4-OHT treated myoblasts stained with MF-20 at various time points of differentiation.

**FIGURE 4.10**

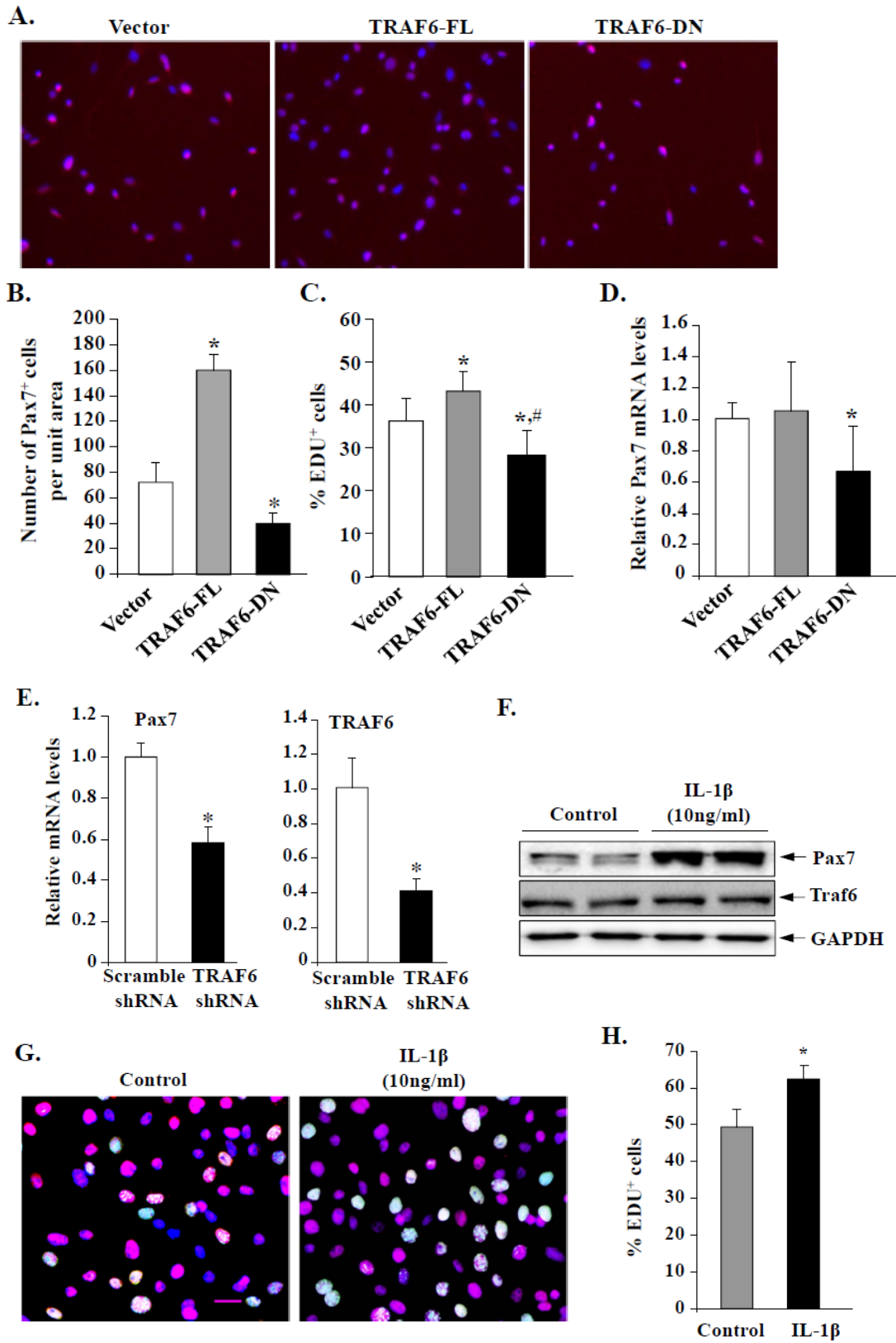


**FIGURE 4.10. TRAF6 axis is required for regulating Pax7 function in satellite cells.**

Primary myoblasts were transfected with vector alone (pcDNA3) or plasmids containing full length TRAF6 (TRAF6-FL) or dominant negative TRAF6 (TRAF6-DN) cDNA. Following 72h, cells were pulsed with EdU for 90 minutes after which cells were fixed and Pax7<sup>+</sup> cells were analyzed for EdU incorporation. **(A)** Representative photomicrograph of transfected primary myoblasts labeled with Pax7 anti body and DAPI. Quantification indicates **(B)** number of Pax7<sup>+</sup> cells and **(C)** percentage of EDU<sup>+</sup> cells to total nuclei. Error bars represent S.D. \* p < 0.05 vs. pcDNA3 transfected cells. #p<0.05 vs. Wt-TRAF6 transfected cells. **(D)** In a separate experiment, cells were collected and processed for qRT-PCR. Relative levels of Pax7 mRNA were quantified **(E)** Primary WT myoblasts were transfected with scramble shRNA or TRAF6 shRNA and Pax7 transcription levels were measured \* p < 0.05 vs. scramble shRNA transfected cells. To elucidate the role of TRAF6-mediated IL-1 $\beta$  pathway, primary myoblasts were treated with 10 ng/ml recombinant IL-1 $\beta$  protein and after 24h cells were processed for biochemical analysis. **(F)** Representative immunoblot labeled with Pax7 and TRAF6 antibodies. **(G)** In a separate experiment cells treated with IL-1 $\beta$  were pulsed with EdU for 90 minutes and EdU incorporation in Pax7<sup>+</sup> cells was analyzed. **(H)** Quantification of percentage of EdU<sup>+</sup> cells per number of nuclei is presented. Error bars represent S.D. \* p < 0.05 vs. vehicle treated myoblasts.

**FIGURE 4.11.**

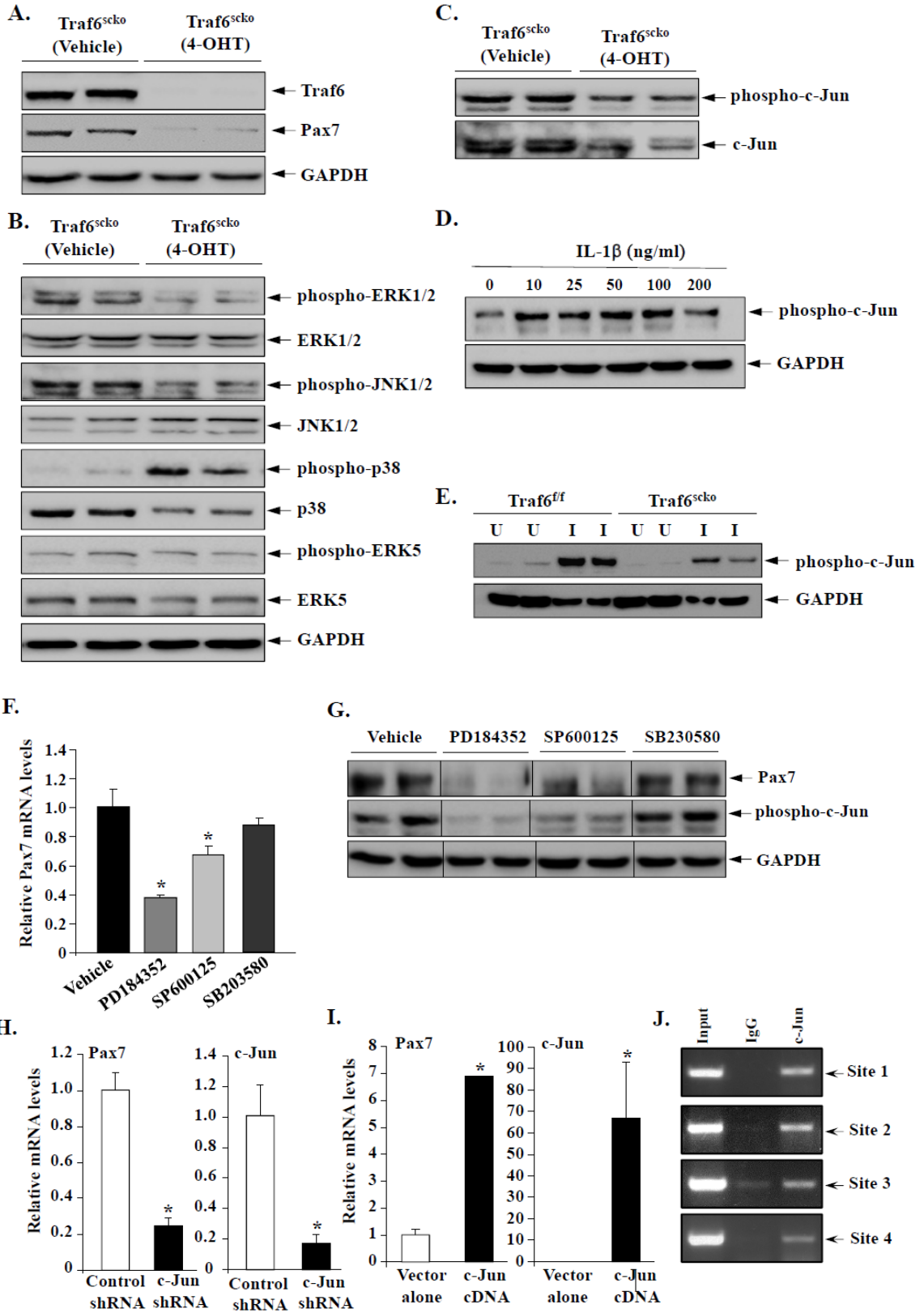




**FIGURE 4.11. TRAF6 regulates Pax7 function in satellite cells potentially through MAPK signaling.** Primary myoblasts isolated from lower limb muscle of TRAF6<sup>sko</sup> mice were treated with 4-OHT or vehicle. After 10 days in culture cells were collected and processed for western blotting. Representative immunoblots demonstrating (A) TRAF6 and Pax7 levels following Cre-recombination, (B) Levels of phosphorylated and total MAPK family signaling proteins, (C) Levels of phosphorylated and total c-Jun. (D) Protein extracts were prepared from WT primary myoblasts treated with IL-1 $\beta$  at different concentrations for 24h. Representative immunoblot of phosphorylated c-Jun is presented here. (E) Representative immunoblot displaying phosphorylated c-Jun protein levels in injured and non-injured TA muscle of TRAF6<sup>ff</sup> and TRAF6<sup>sko</sup> mice. To understand the role of MAPK signaling in regulating Pax7 expression, WT primary myoblasts were treated with various MAPK-signaling inhibitors for 48h after which cells were processed for biochemical analysis. Illustration of (F) Pax7 protein and (G) Pax7 mRNA levels are presented here. In a separate experiment, primary myoblasts were transfected with control vector, c-Jun shRNA or c-Jun cDNA for 72hours and Pax7 mRNA levels were measured as shown in (H) and (I) respectively. (J) Enrichment of c-Jun at four putative sites in Pax7 promoter was confirmed through ChIP assay. Error bars represent S.D. \*, p < 0.05, values significantly different from corresponding controls.

**FIGURE 4.12.**

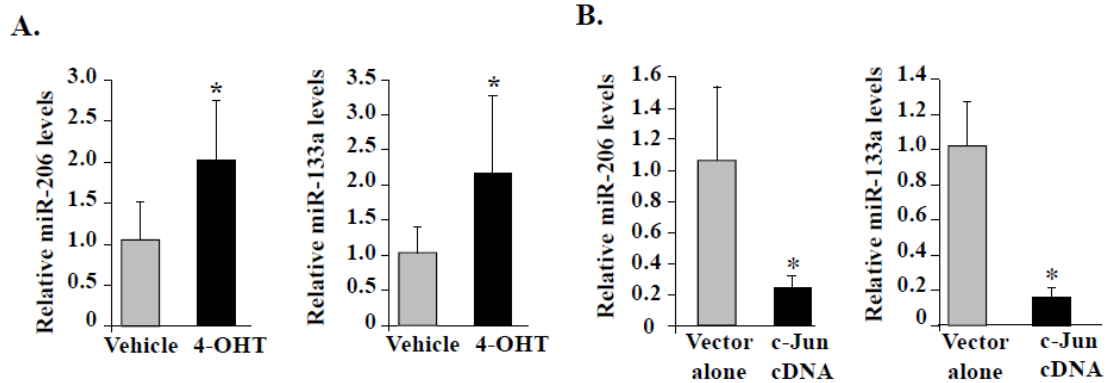


**FIGURE 4.12. TRAF6 deletion augments the levels of muscle-specific microRNAs**

**(MyomiRs) in satellite cells.** Primary myoblasts isolated from lower limb muscle of non-

tamoxifen treated TRAF6<sup>scko</sup> mice were treated with 4-OHT or vehicle. After 10 days in

culture cells were processed for miRNA analysis. (A) Representative bar diagrams

illustrating expression levels of miR-1, miR-206 and miR-133a in 4-OHT and vehicle

treated TRAF6<sup>scko</sup> myoblasts. (B) WT primary myoblasts were transfected with vector alone

(pcDNA3) or c-Jun cDNA and 72h later expression levels of miR-206 and miR-206 were

quantified. \*p < 0.05, values significantly different from corresponding controls.

**FIGURE 4.13.**

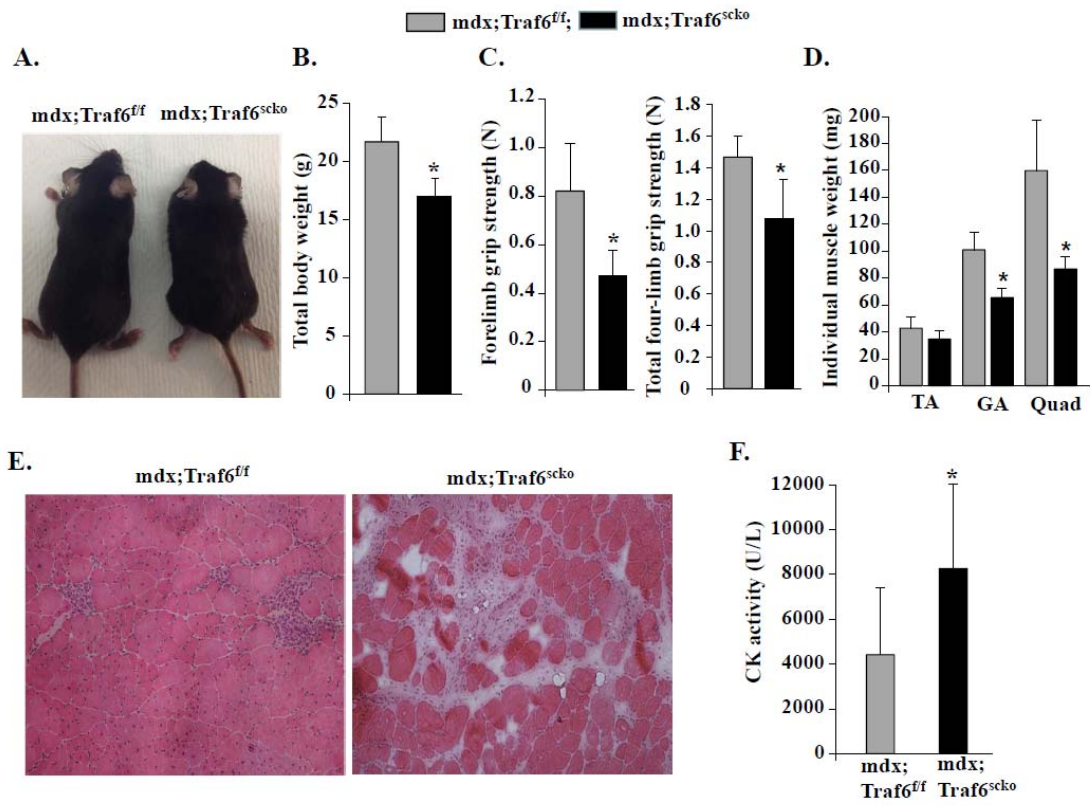


**FIGURE 4.13. Depletion of TRAF6 in satellite cells exacerbates myopathy in mdx mice.** TRAF6<sup>scko</sup> mice were crossed with mdx mice and progression of dystrophinopathy was analyzed at the age of 8 weeks. **(A)** Body size and **(B)** weight of mdx;TRAF6<sup>scko</sup> and TRAF6<sup>f/f</sup> mice are presented here. **(C)** Functional output was evaluated in mdx;TRAF6<sup>scko</sup> by performing four-limb grip strength and total-limb grip strength tests. **(D)** Bar diagrams representing wet weight of TA, GA, and quadriceps muscle of TRAF6<sup>f/f</sup> and TRAF6<sup>scko</sup> mice. **(E)** Representative photomicrograph of H&E-stained GA muscle of 8-week old TRAF6<sup>f/f</sup> and TRAF6<sup>scko</sup> mice are presented here. **(F)** Relative fold change in CK activity in serum of 8-week old TRAF6<sup>f/f</sup> and TRAF6<sup>scko</sup> mice. Error bars represent S.D. N=4 in each group. \*, p < 0.05, values significantly different from TRAF6<sup>f/f</sup> mice.

## CHAPTER 5

### CONCLUSIONS AND FUTURE WORK

This chapter summarizes the work presented in this dissertation and discusses its implications in understanding adult skeletal muscle regeneration. It also highlights the significance of the findings obtained throughout this dissertation while acknowledging the limitations in implementing such findings in future research.

#### **5.1 Review of dissertation**

Skeletal muscle constitutes a greatly adaptable cellular system. Such pliant capacity is acquired by a regulated signaling network that emanates from the differentiated muscle fibers, the mitotic satellite cells, and the resident and infiltrating immune cells that populate the muscle microenvironment. Through systematic examination of upstream signaling regulator TRAF6, the findings of this dissertation accentuate the complexity of the molecular events that take place in restoration of muscle homeostasis. Our investigations revealed that TRAF6 mediates diverse functional outcomes at various stages of postnatal myogenesis.

As discussed in Chapter 2, deletion of TRAF6 in differentiated muscle (TRAF6<sup>mk0</sup>) enhanced muscle regeneration following acute injury through modulating the inflammatory profile of the injured muscle microenvironment. Lack of TRAF6 signaling emitting from muscle fibers attenuated the activation of NF- $\kappa$ B pathway and promoted the induction of pro-regenerative molecules (i.e. IGF-1 and IL-4) which neutralized the effect of various inflammatory cytokines such as TNF- $\alpha$  and IL-1 $\beta$ . Our findings revealed that the mitigated inflammatory response brought about by deletion of TRAF6 augmented the conversion of pro-inflammatory M1-macrophages into pro-regenerative M2-macrophages leading to accelerated regeneration. Our findings further revealed that TRAF6 signal from differentiated muscle antagonizes Notch signaling in satellite cells in a non-cell autonomous manner as regenerating muscle of TRAF6<sup>mk0</sup> mice displayed heightened activation of Notch signaling which enhanced the myogenic potential of satellite cells in driving the regeneration program.

The findings in Chapter 2 portrayed TRAF6 signaling as a promising molecular target in combating various acquired and genetic myopathies. Along those lines, we contemplated in Chapter 3 that abrogation of TRAF6 signaling from differentiated myofibers in dystrophic muscle of mdx (model for Duchene muscular dystrophy) mice would similarly pacify the inflammatory environment and improve muscle regeneration. Indeed, signs of dystrophinopathy were greatly diminished in 8-week old mdx mice upon deletion of TRAF6. mdx;TRAF6<sup>mk0</sup> mice preserved muscle integrity evident by decreased CK activity in blood serum and enhanced muscle regeneration on histological analysis. However, examination in 9-month old mdx; TRAF6<sup>mk0</sup> mice revealed exacerbated symptoms of mdx

pathology manifested by increased muscle necrosis and inflammatory infiltration accompanied by fibrotic tissue accumulation. Our investigations showed that exaggerated myopathy in muscle of mdx;TRAF6<sup>mk0</sup> mice is potentially due to reduced autophagy which is known to be downstream of TRAF6 signaling. Impaired autophagic flux responsible for clearing out cellular debris is associated with progression of dystrophinopathy and was shown by our results to be further impaired as a result of deletion of TRAF6.

The focus of Chapter 4 was to understand the role of TRAF6 signaling in satellite cells of adult skeletal muscle. Conditional deletion of TRAF6 under a tamoxifen-induced Pax7 promoter (TRAF6<sup>sck0</sup>) led to deleterious muscle regeneration defects following induced and myopathic muscle injury due to loss of satellite cell myogenic potential. The findings in this chapter identified TRAF6 as a regulator of Pax7 function in satellite cells. TRAF6 was shown to regulate Pax7 expression via downstream activation of ERK1/2 and JNK-MAPK signaling pathways. Our findings further revealed that conditional MAPK regulation of Pax7 is a result of a direct binding of AP-1 transcription factor to the Pax7 promoter. In addition, the study suggests a potential post-transcriptional role of AP-1 in regulating Pax7 expression through modulating the levels of Pax7-targeting myomiRs.

Collectively, the results of this dissertation illustrate a multi-valent role of TRAF6 in mediating the events of regenerative myogenesis. While deletion of TRAF6 in differentiated muscle fibers enhanced muscle regeneration following acute injury, continued inhibition of TRAF6 signaling was shown to be detrimental as evident by our investigations at the later

stages of mdx pathology. Our findings further revealed an absolute requirement of TRAF6 in maintaining satellite cell function in adult skeletal muscle.

## **5.2 Contribution of dissertation and future implementations**

Although the work presented in this dissertation underlines the role of a single signaling transducer amongst a plethora of molecules that mediate the events of adult skeletal muscle regeneration, the findings obtained serve broader implications. It has been clearly evident that progression of myopathy is associated with aberrant activation of multiple signaling cascades and modulation of such pathways has been perused as means of treatment.

However research strategies have been restricted to modulating single molecular axes, which limited therapeutic potential. TRAF6 stands at a hierarchical advantage of several signaling cascades which mediate deleterious outcomes. Thus, modulation of TRAF6 represents a promising strategy for collective modification of anomalous signaling, and as result maximize alleviation. Our findings in the TRAF6<sup>mko</sup> mouse are testament for such inference. Conversely, our findings in old mdx;TRAF6<sup>mko</sup> mice refute the same inference. The results in Chapters 2 and 3 give rise to an intriguing line of pending examinations.

Exacerbated myopathy at the later stages of dystrophinopathy in mdx;TRAF6<sup>mko</sup> mice was suggested to be a result of defective autophagy. Therefore, it would be of great interest to delineate whether deletion of TRAF6 in differentiated myofibers combined with forced activation of autophagy through a low protein diet would extend the beneficiary effects of ablated TRAF6 signaling. Such therapeutic strategies might prove beneficial in treating various acquired and genetic muscle disorders.



On contrary lines, sustained TRAF6 signaling was shown to have a positive role in satellite cells. Satellite cell myogenic potential is greatly compromised in many disease states including DMD and is a major cause of failed regeneration. Strategies aimed at improving endogenous satellite cell function as well as donor cells' myogenicity are center of tremendous investigations. Enhanced TRAF6 signaling in resident and donor satellite cells represents a potential means for prolonging/restoring myogenic potential.

This work has unveiled the downstream outcomes of TRAF6 signaling in the skeletal muscle cellular system. However, it remains unclear whether the expression of TRAF6 in differentiated myofibers versus satellite cells is driven by common molecular regulators or is mediated through distinct signaling events. Precise delineation of such mechanisms represents an area of forthcoming investigations.

### **5.3 Limitations of future implications**

The dissertation concludes in identifying distinct roles of TRAF6 signaling at various stages of muscle formation. In addition to the role of TRAF6 in mediating destructive molecular outcomes, TRAF6 signaling is essential for maintaining normal biological functions required for skeletal muscle homeostasis. While genetic engineering techniques have allowed for conditional deletion or overexpression of molecules in lab mouse models, such discriminatory modification is not yet attainable upon consideration for translational research. Therefore pharmacological inhibition of TRAF6 might ultimately lead to detrimental effects due to compromising its physiological role in skeletal muscle and other cellular systems. This warrants caution on developing various target-based therapies. Thus, pursuing

a means of selective modulation represents yet another challenging but crucial upcoming endeavor. Addressing the matters at mention would elevate the significance of the findings acquired throughout this dissertation.

## REFERENCES

1. Charge, S. B., and Rudnicki, M. A. (2004) Cellular and molecular regulation of muscle regeneration. *Physiol Rev* **84**, 209-238
2. Kuang, S., Gillespie, M. A., and Rudnicki, M. A. (2008) Niche regulation of muscle satellite cell self-renewal and differentiation. *Cell stem cell* **2**, 22-31
3. Kuang, S., and Rudnicki, M. A. (2008) The emerging biology of satellite cells and their therapeutic potential. *Trends Mol Med* **14**, 82-91
4. Le Grand, F., and Rudnicki, M. A. (2007) Skeletal muscle satellite cells and adult myogenesis. *Curr Opin Cell Biol* **19**, 628-633
5. Emery, A. E. (2002) The muscular dystrophies. *Lancet* **359**, 687-695
6. Blake, D. J., Weir, A., Newey, S. E., and Davies, K. E. (2002) Function and genetics of dystrophin and dystrophin-related proteins in muscle. *Physiol Rev* **82**, 291-329
7. Campbell, K. P. (1995) Three muscular dystrophies: loss of cytoskeleton-extracellular matrix linkage. *Cell* **80**, 675-679
8. Hoffman, E. P., Brown, R. H., Jr., and Kunkel, L. M. (1987) Dystrophin: the protein product of the Duchenne muscular dystrophy locus. *Cell* **51**, 919-928
9. Prins, K. W., Humston, J. L., Mehta, A., Tate, V., Ralston, E., and Ervasti, J. M. (2009) Dystrophin is a microtubule-associated protein. *J Cell Biol* **186**, 363-369

10. Rando, T. A. (2001) The dystrophin-glycoprotein complex, cellular signaling, and the regulation of cell survival in the muscular dystrophies. *Muscle Nerve* **24**, 1575-1594
11. Petrof, B. J., Shrager, J. B., Stedman, H. H., Kelly, A. M., and Sweeney, H. L. (1993) Dystrophin protects the sarcolemma from stresses developed during muscle contraction. *Proc Natl Acad Sci U S A* **90**, 3710-3714
12. Engvall, E., and Wewer, U. M. (2003) The new frontier in muscular dystrophy research: booster genes. *FASEB J* **17**, 1579-1584
13. Khurana, T. S., and Davies, K. E. (2003) Pharmacological strategies for muscular dystrophy. *Nat Rev Drug Discov* **2**, 379-390
14. Chakkalakal, J. V., Thompson, J., Parks, R. J., and Jasmin, B. J. (2005) Molecular, cellular, and pharmacological therapies for Duchenne/Becker muscular dystrophies. *FASEB J* **19**, 880-891
15. Spencer, M. J., and Tidball, J. G. (2001) Do immune cells promote the pathology of dystrophin-deficient myopathies? *Neuromuscul Disord* **11**, 556-564
16. Acharyya, S., Villalta, S. A., Bakkar, N., Bupha-Intr, T., Janssen, P. M., Carathers, M., Li, Z. W., Beg, A. A., Ghosh, S., Sahenk, Z., Weinstein, M., Gardner, K. L., Rafael-Fortney, J. A., Karin, M., Tidball, J. G., Baldwin, A. S., and Guttridge, D. C. (2007) Interplay of IKK/NF-kappaB signaling in macrophages and myofibers promotes muscle degeneration in Duchenne muscular dystrophy. *J Clin Invest* **117**, 889-901

17. Bhatnagar, S., and Kumar, A. (2010) Therapeutic targeting of signaling pathways in muscular dystrophy. *J Mol Med* **88**, 155-166
18. Dogra, C., Changotra, H., Wergedal, J. E., and Kumar, A. (2006) Regulation of phosphatidylinositol 3-kinase (PI3K)/Akt and nuclear factor-kappa B signaling pathways in dystrophin-deficient skeletal muscle in response to mechanical stretch. *J Cell Physiol* **208**, 575-585
19. Dogra, C., Srivastava, D. S., and Kumar, A. (2008) Protein-DNA array-based identification of transcription factor activities differentially regulated in skeletal muscle of normal and dystrophin-deficient mdx mice. *Mol Cell Biochem* **312**, 17-24
20. Kumar, A., and Boriek, A. M. (2003) Mechanical stress activates the nuclear factor-kappaB pathway in skeletal muscle fibers: a possible role in Duchenne muscular dystrophy. *FASEB J* **17**, 386-396
21. Kumar, A., Khandelwal, N., Malya, R., Reid, M. B., and Boriek, A. M. (2004) Loss of dystrophin causes aberrant mechanotransduction in skeletal muscle fibers. *FASEB J* **18**, 102-113
22. Shin, J., Tajrishi, M. M., Ogura, Y., and Kumar, A. (2013) Wasting mechanisms in muscular dystrophy. *The international journal of biochemistry & cell biology* **45**, 2266-2279
23. Yamauchi, J., Kumar, A., Duarte, L., Mehuron, T., and Girgenrath, M. (2013) Triggering regeneration and tackling apoptosis: a combinatorial approach to treating congenital muscular dystrophy type 1 A. *Human molecular genetics* **22**, 4306-4317

24. Guibinga, G. H., Lochmuller, H., Massie, B., Nalbantoglu, J., Karpati, G., and Petrof, B. J. (1998) Combinatorial blockade of calcineurin and CD28 signaling facilitates primary and secondary therapeutic gene transfer by adenovirus vectors in dystrophic (mdx) mouse muscles. *Journal of virology* **72**, 4601-4609
25. Bradley, J. R., and Pober, J. S. (2001) Tumor necrosis factor receptor-associated factors (TRAFs). *Oncogene* **20**, 6482-6491
26. Lee, N. K., and Lee, S. Y. (2002) Modulation of life and death by the tumor necrosis factor receptor-associated factors (TRAFs). *Journal of biochemistry and molecular biology* **35**, 61-66
27. Chung, J. Y., Lu, M., Yin, Q., Lin, S. C., and Wu, H. (2007) Molecular basis for the unique specificity of TRAF6. *Adv Exp Med Biol* **597**, 122-130
28. Deng, L., Wang, C., Spencer, E., Yang, L., Braun, A., You, J., Slaughter, C., Pickart, C., and Chen, Z. J. (2000) Activation of the IkappaB kinase complex by TRAF6 requires a dimeric ubiquitin-conjugating enzyme complex and a unique polyubiquitin chain. *Cell* **103**, 351-361
29. Chen, Z. J. (2005) Ubiquitin signalling in the NF-kappaB pathway. *Nat Cell Biol* **7**, 758-765
30. Mukhopadhyay, D., and Riezman, H. (2007) Proteasome-independent functions of ubiquitin in endocytosis and signaling. *Science* **315**, 201-205

31. Pickart, C. M. (2001) Mechanisms underlying ubiquitination. *Annu Rev Biochem* **70**, 503-533
32. Baba, S. P., Barski, O. A., Ahmed, Y., O'Toole, T. E., Conklin, D. J., Bhatnagar, A., and Srivastava, S. (2009) Reductive metabolism of AGE precursors: a metabolic route for preventing AGE accumulation in cardiovascular tissue. *Diabetes* **58**, 2486-2497
33. Lamothe, B., Besse, A., Campos, A. D., Webster, W. K., Wu, H., and Darnay, B. G. (2007) Site-specific Lys-63-linked tumor necrosis factor receptor-associated factor 6 auto-ubiquitination is a critical determinant of I kappa B kinase activation. *J Biol Chem* **282**, 4102-4112
34. Lamothe, B., Webster, W. K., Gopinathan, A., Besse, A., Campos, A. D., and Darnay, B. G. (2007) TRAF6 ubiquitin ligase is essential for RANKL signaling and osteoclast differentiation. *Biochem Biophys Res Commun* **359**, 1044-1049
35. Yamashita, M., Fatyol, K., Jin, C., Wang, X., Liu, Z., and Zhang, Y. E. (2008) TRAF6 mediates Smad-independent activation of JNK and p38 by TGF-beta. *Mol Cell* **31**, 918-924
36. Yang, W. L., Wang, J., Chan, C. H., Lee, S. W., Campos, A. D., Lamothe, B., Hur, L., Grabiner, B. C., Lin, X., Darnay, B. G., and Lin, H. K. (2009) The E3 ligase TRAF6 regulates Akt ubiquitination and activation. *Science* **325**, 1134-1138
37. Moscat, J., Diaz-Meco, M. T., and Wooten, M. W. (2007) Signal integration and diversification through the p62 scaffold protein. *Trends Biochem Sci* **32**, 95-100

38. Nakamura, K., Kimple, A. J., Siderovski, D. P., and Johnson, G. L. (2010) PB1 domain interaction of p62/sequestosome 1 and MEKK3 regulates NF-kappaB activation. *J Biol Chem* **285**, 2077-2089
39. Seibenhener, M. L., Babu, J. R., Geetha, T., Wong, H. C., Krishna, N. R., and Wooten, M. W. (2004) Sequestosome 1/p62 is a polyubiquitin chain binding protein involved in ubiquitin proteasome degradation. *Mol Cell Biol* **24**, 8055-8068
40. Wooten, M. W., Geetha, T., Seibenhener, M. L., Babu, J. R., Diaz-Meco, M. T., and Moscat, J. (2005) The p62 scaffold regulates nerve growth factor-induced NF-kappaB activation by influencing TRAF6 polyubiquitination. *J Biol Chem* **280**, 35625-35629
41. Paul, P. K., Gupta, S. K., Bhatnagar, S., Panguluri, S. K., Darnay, B. G., Choi, Y., and Kumar, A. (2010) Targeted ablation of TRAF6 inhibits skeletal muscle wasting in mice. *J Cell Biol* **191**, 1395-1411
42. Mueck, T., Berger, F., Buechsler, I., Valchanova, R. S., Landuzzi, L., Lollini, P. L., Klingel, K., and Munz, B. (2011) TRAF6 regulates proliferation and differentiation of skeletal myoblasts. *Differentiation* **81**, 99-106
43. Paul, P. K., Bhatnagar, S., Mishra, V., Srivastava, S., Darnay, B. G., Choi, Y., and Kumar, A. (2012) The E3 ubiquitin ligase TRAF6 intercedes in starvation-induced skeletal muscle atrophy through multiple mechanisms. *Mol Cell Biol* **32**, 1248-1259
44. Naito, A., Azuma, S., Tanaka, S., Miyazaki, T., Takaki, S., Takatsu, K., Nakao, K., Nakamura, K., Katsuki, M., Yamamoto, T., and Inoue, J. (1999) Severe



- osteopetrosis, defective interleukin-1 signalling and lymph node organogenesis in TRAF6-deficient mice. *Genes Cells* **4**, 353-362
45. Lomaga, M. A., Yeh, W. C., Sarosi, I., Duncan, G. S., Furlonger, C., Ho, A., Morony, S., Capparelli, C., Van, G., Kaufman, S., van der Heiden, A., Itie, A., Wakeham, A., Khoo, W., Sasaki, T., Cao, Z., Penninger, J. M., Paige, C. J., Lacey, D. L., Dunstan, C. R., Boyle, W. J., Goeddel, D. V., and Mak, T. W. (1999) TRAF6 deficiency results in osteopetrosis and defective interleukin-1, CD40, and LPS signaling. *Genes Dev* **13**, 1015-1024
46. Shi, C. S., and Kehrl, J. H. (2010) TRAF6 and A20 regulate lysine 63-linked ubiquitination of Beclin-1 to control TLR4-induced autophagy. *Sci Signal* **3**, ra42
47. Argiles, J. M., Busquets, S., Toledo, M., and Lopez-Soriano, F. J. (2009) The role of cytokines in cancer cachexia. *Curr Opin Support Palliat Care* **3**, 263-268
48. Chung, J. Y., Park, Y. C., Ye, H., and Wu, H. (2002) All TRAFs are not created equal: common and distinct molecular mechanisms of TRAF-mediated signal transduction. *J Cell Sci* **115**, 679-688
49. Zapata, J. M., Lefebvre, S., and Reed, J. C. (2007) Targeting TRAFs for therapeutic intervention. *Adv Exp Med Biol* **597**, 188-201
50. Mittal, A., Bhatnagar, S., Kumar, A., Lach-Trifilieff, E., Wauters, S., Li, H., Makonchuk, D. Y., Glass, D. J., and Kumar, A. (2010) The TWEAK–Fn14 system is a critical regulator of denervation-induced skeletal muscle atrophy in mice. *J Cell Biol* **188**, 833–849

51. Jackman, R. W., and Kandarian, S. C. (2004) The molecular basis of skeletal muscle atrophy. *Am J Physiol Cell Physiol* **287**, C834-843
52. Dhawan, J., and Rando, T. A. (2005) Stem cells in postnatal myogenesis: molecular mechanisms of satellite cell quiescence, activation and replenishment. *Trends Cell Biol* **15**, 666-673
53. Beauchamp, J. R., Heslop, L., Yu, D. S., Tajbakhsh, S., Kelly, R. G., Wernig, A., Buckingham, M. E., Partridge, T. A., and Zammit, P. S. (2000) Expression of CD34 and Myf5 defines the majority of quiescent adult skeletal muscle satellite cells. *J Cell Biol* **151**, 1221-1234
54. Tedesco, F. S., Dellavalle, A., Diaz-Manera, J., Messina, G., and Cossu, G. (2010) Repairing skeletal muscle: regenerative potential of skeletal muscle stem cells. *J Clin Invest* **120**, 11-19
55. Ten Broek, R. W., Grefte, S., and Von den Hoff, J. W. (2010) Regulatory factors and cell populations involved in skeletal muscle regeneration. *J Cell Physiol* **224**, 7-16
56. Buas, M. F., and Kadesch, T. (2010) Regulation of skeletal myogenesis by Notch. *Exp Cell Res* **316**, 3028-3033
57. Conboy, I. M., and Rando, T. A. (2002) The regulation of Notch signaling controls satellite cell activation and cell fate determination in postnatal myogenesis. *Dev Cell* **3**, 397-409

58. Ehebauer, M., Hayward, P., and Arias, A. M. (2006) Notch, a universal arbiter of cell fate decisions. *Science* **314**, 1414-1415
59. Kopan, R., and Ilagan, M. X. (2009) The canonical Notch signaling pathway: unfolding the activation mechanism. *Cell* **137**, 216-233
60. Nakagawa, O., McFadden, D. G., Nakagawa, M., Yanagisawa, H., Hu, T., Srivastava, D., and Olson, E. N. (2000) Members of the HRT family of basic helix-loop-helix proteins act as transcriptional repressors downstream of Notch signaling. *Proc Natl Acad Sci U S A* **97**, 13655-13660
61. Artavanis-Tsakonas, S., Rand, M. D., and Lake, R. J. (1999) Notch signaling: cell fate control and signal integration in development. *Science* **284**, 770-776
62. Iso, T., Kedes, L., and Hamamori, Y. (2003) HES and HERP families: multiple effectors of the Notch signaling pathway. *J Cell Physiol* **194**, 237-255
63. Lamar, E., Deblandre, G., Wettstein, D., Gawantka, V., Pollet, N., Niehrs, C., and Kintner, C. (2001) Nrarp is a novel intracellular component of the Notch signaling pathway. *Genes Dev* **15**, 1885-1899
64. Kuang, S., Kuroda, K., Le Grand, F., and Rudnicki, M. A. (2007) Asymmetric self-renewal and commitment of satellite stem cells in muscle. *Cell* **129**, 999-1010
65. Conboy, I. M., Conboy, M. J., Smythe, G. M., and Rando, T. A. (2003) Notch-mediated restoration of regenerative potential to aged muscle. *Science* **302**, 1575-1577

66. Pisconti, A., Cornelison, D. D., Olguin, H. C., Antwine, T. L., and Olwin, B. B. (2010) Syndecan-3 and Notch cooperate in regulating adult myogenesis. *J Cell Biol* **190**, 427-441
67. Shinin, V., Gayraud-Morel, B., Gomes, D., and Tajbakhsh, S. (2006) Asymmetric division and cosegregation of template DNA strands in adult muscle satellite cells. *Nat Cell Biol* **8**, 677-687
68. Schuster-Gossler, K., Cordes, R., and Gossler, A. (2007) Premature myogenic differentiation and depletion of progenitor cells cause severe muscle hypotrophy in Delta1 mutants. *Proc Natl Acad Sci U S A* **104**, 537-542
69. Vasyutina, E., Lenhard, D. C., Wende, H., Erdmann, B., Epstein, J. A., and Birchmeier, C. (2007) RBP-J (Rbpsiuh) is essential to maintain muscle progenitor cells and to generate satellite cells. *Proc Natl Acad Sci U S A* **104**, 4443-4448
70. Conboy, I. M., Conboy, M. J., Wagers, A. J., Girma, E. R., Weissman, I. L., and Rando, T. A. (2005) Rejuvenation of aged progenitor cells by exposure to a young systemic environment. *Nature* **433**, 760-764
71. Carlson, M. E., Hsu, M., and Conboy, I. M. (2008) Imbalance between pSmad3 and Notch induces CDK inhibitors in old muscle stem cells. *Nature* **454**, 528-532
72. Bjornson, C. R., Cheung, T. H., Liu, L., Tripathi, P. V., Steeper, K. M., and Rando, T. A. (2012) Notch signaling is necessary to maintain quiescence in adult muscle stem cells. *Stem Cells* **30**, 232-242

73. Mourikis, P., Sambasivan, R., Castel, D., Rocheteau, P., Bizzarro, V., and Tajbakhsh, S. (2012) A critical requirement for notch signaling in maintenance of the quiescent skeletal muscle stem cell state. *Stem Cells* **30**, 243-252
74. Fukada, S., Yamaguchi, M., Kokubo, H., Ogawa, R., Uezumi, A., Yoneda, T., Matev, M. M., Motohashi, N., Ito, T., Zolkiewska, A., Johnson, R. L., Saga, Y., Miyagoe-Suzuki, Y., Tsujikawa, K., Takeda, S., and Yamamoto, H. (2011) Hesr1 and Hesr3 are essential to generate undifferentiated quiescent satellite cells and to maintain satellite cell numbers. *Development* **138**, 4609-4619
75. Kitamoto, T., and Hanaoka, K. (2010) Notch3 null mutation in mice causes muscle hyperplasia by repetitive muscle regeneration. *Stem Cells* **28**, 2205-2216
76. Guttridge, D. C., Mayo, M. W., Madrid, L. V., Wang, C. Y., and Baldwin, A. S., Jr. (2000) NF-kappaB-induced loss of MyoD messenger RNA: possible role in muscle decay and cachexia. *Science* **289**, 2363-2366
77. Li, H., Malhotra, S., and Kumar, A. (2008) Nuclear factor-kappa B signaling in skeletal muscle atrophy. *J Mol Med* **86**, 1113-1126
78. Mourkioti, F., Kratsios, P., Luedde, T., Song, Y. H., Delafontaine, P., Adami, R., Parente, V., Bottinelli, R., Pasparakis, M., and Rosenthal, N. (2006) Targeted ablation of IKK2 improves skeletal muscle strength, maintains mass, and promotes regeneration. *J Clin Invest* **116**, 2945-2954

79. Oswald, F., Liptay, S., Adler, G., and Schmid, R. M. (1998) NF-kappaB2 is a putative target gene of activated Notch-1 via RBP-Jkappa. *Mol Cell Biol* **18**, 2077-2088
80. Guan, E., Wang, J., Laborda, J., Norcross, M., Baeuerle, P. A., and Hoffman, T. (1996) T cell leukemia-associated human Notch/translocation-associated Notch homologue has I kappa B-like activity and physically interacts with nuclear factor-kappa B proteins in T cells. *J Exp Med* **183**, 2025-2032
81. Kobayashi, T., Walsh, P. T., Walsh, M. C., Speirs, K. M., Chiffoleau, E., King, C. G., Hancock, W. W., Caamano, J. H., Hunter, C. A., Scott, P., Turka, L. A., and Choi, Y. (2003) TRAF6 is a critical factor for dendritic cell maturation and development. *Immunity* **19**, 353-363
82. Kuang, S., Charge, S. B., Seale, P., Huh, M., and Rudnicki, M. A. (2006) Distinct roles for Pax7 and Pax3 in adult regenerative myogenesis. *J Cell Biol* **172**, 103-113
83. Dahiya, S., Bhatnagar, S., Hindi, S. M., Jiang, C., Paul, P. K., Kuang, S., and Kumar, A. (2011) Elevated levels of active matrix metalloproteinase-9 cause hypertrophy in skeletal muscle of normal and dystrophin-deficient mdx mice. *Hum Mol Genet* **20**, 4345-4359
84. Hindi, S. M., Paul, P. K., Dahiya, S., Mishra, V., Bhatnagar, S., Kuang, S., Choi, Y., and Kumar, A. (2012) Reciprocal interaction between TRAF6 and notch signaling regulates adult myofiber regeneration upon injury. *Mol Cell Biol* **32**, 4833-4845

85. Yablonka-Reuveni, Z., and Rivera, A. J. (1994) Temporal expression of regulatory and structural muscle proteins during myogenesis of satellite cells on isolated adult rat fibers. *Dev Biol* **164**, 588-603
86. Yan, Z., Choi, S., Liu, X., Zhang, M., Schageman, J. J., Lee, S. Y., Hart, R., Lin, L., Thurmond, F. A., and Williams, R. S. (2003) Highly coordinated gene regulation in mouse skeletal muscle regeneration. *J Biol Chem* **278**, 8826-8836
87. Seale, P., Sabourin, L. A., Girgis-Gabardo, A., Mansouri, A., Gruss, P., and Rudnicki, M. A. (2000) Pax7 is required for the specification of myogenic satellite cells. *Cell* **102**, 777-786
88. Burkin, D. J., and Kaufman, S. J. (1999) The alpha7beta1 integrin in muscle development and disease. *Cell Tissue Res* **296**, 183-190
89. Mourkioti, F., and Rosenthal, N. (2005) IGF-1, inflammation and stem cells: interactions during muscle regeneration. *Trends Immunol* **26**, 535-542
90. Pelosi, L., Giacinti, C., Nardis, C., Borsellino, G., Rizzuto, E., Nicoletti, C., Wannenes, F., Battistini, L., Rosenthal, N., Molinaro, M., and Musaro, A. (2007) Local expression of IGF-1 accelerates muscle regeneration by rapidly modulating inflammatory cytokines and chemokines. *FASEB J* **21**, 1393-1402
91. Akira, S., and Takeda, K. (2004) Toll-like receptor signalling. *Nat Rev Immunol* **4**, 499-511

92. Hayden, M. S., and Ghosh, S. (2004) Signaling to NF-kappaB. *Genes Dev* **18**, 2195-2224
93. Espinosa, L., Ingles-Esteve, J., Robert-Moreno, A., and Bigas, A. (2003) IkappaBalpha and p65 regulate the cytoplasmic shuttling of nuclear corepressors: cross-talk between Notch and NFkappaB pathways. *Mol Biol Cell* **14**, 491-502
94. Acharyya, S., Sharma, S. M., Cheng, A. S., Ladner, K. J., He, W., Kline, W., Wang, H., Ostrowski, M. C., Huang, T. H., and Guttridge, D. C. (2010) TNF inhibits Notch-1 in skeletal muscle cells by Ezh2 and DNA methylation mediated repression: implications in duchenne muscular dystrophy. *PLoS One* **5**, e12479
95. Tidball, J. G., and Villalta, S. A. (2010) Regulatory interactions between muscle and the immune system during muscle regeneration. *Am J Physiol Regul Integr Comp Physiol* **298**, R1173-1187
96. Kumar, A., Bhatnagar, S., and Kumar, A. (2010) Matrix metalloproteinase inhibitor batimastat alleviates pathology and improves skeletal muscle function in dystrophin-deficient mdx mice. *Am J Pathol* **177**, 248-260
97. Mittal, A., Bhatnagar, S., Kumar, A., Paul, P. K., and Kuang, S. (2010) Genetic ablation of TWEAK augments regeneration and post-injury growth of skeletal muscle in mice. *Am J Pathol* **177**, 1732-1742
98. Mantovani, A., Sica, A., Sozzani, S., Allavena, P., Vecchi, A., and Locati, M. (2004) The chemokine system in diverse forms of macrophage activation and polarization. *Trends Immunol* **25**, 677-686



99. Villalta, S. A., Nguyen, H. X., Deng, B., Gotoh, T., and Tidball, J. G. (2009) Shifts in macrophage phenotypes and macrophage competition for arginine metabolism affect the severity of muscle pathology in muscular dystrophy. *Hum Mol Genet* **18**, 482-496
100. Villalta, S. A., Rinaldi, C., Deng, B., Liu, G., Fedor, B., and Tidball, J. G. (2011) Interleukin-10 reduces the pathology of mdx muscular dystrophy by deactivating M1 macrophages and modulating macrophage phenotype. *Hum Mol Genet* **20**, 790-805
101. Mason, N. J., Fiore, J., Kobayashi, T., Masek, K. S., Choi, Y., and Hunter, C. A. (2004) TRAF6-dependent mitogen-activated protein kinase activation differentially regulates the production of interleukin-12 by macrophages in response to *Toxoplasma gondii*. *Infect Immun* **72**, 5662-5667
102. Baeza-Raja, B., and Munoz-Canoves, P. (2004) p38 MAPK-induced nuclear factor-kappaB activity is required for skeletal muscle differentiation: role of interleukin-6. *Mol Biol Cell* **15**, 2013-2026
103. Xiao, F., Wang, H., Fu, X., Li, Y., and Wu, Z. (2012) TRAF6 promotes myogenic differentiation via the TAK1/p38 mitogen-activated protein kinase and Akt pathways. *PLoS One* **7**, e34081
104. Koenig, M., Hoffman, E. P., Bertelson, C. J., Monaco, A. P., Feener, C., and Kunkel, L. M. (1987) Complete cloning of the Duchenne muscular dystrophy (DMD) cDNA and preliminary genomic organization of the DMD gene in normal and affected individuals. *Cell* **50**, 509-517

105. Skaug, B., Jiang, X., and Chen, Z. J. (2009) The role of ubiquitin in NF-kappaB regulatory pathways. *Annu Rev Biochem* **78**, 769-796
106. Sandri, M. (2010) Autophagy in skeletal muscle. *FEBS Lett* **584**, 1411-1416
107. Mammucari, C., Milan, G., Romanello, V., Masiero, E., Rudolf, R., Del Piccolo, P., Burden, S. J., Di Lisi, R., Sandri, C., Zhao, J., Goldberg, A. L., Schiaffino, S., and Sandri, M. (2007) FoxO3 controls autophagy in skeletal muscle in vivo. *Cell Metab* **6**, 458-471
108. Masiero, E., Agatea, L., Mammucari, C., Blaauw, B., Loro, E., Komatsu, M., Metzger, D., Reggiani, C., Schiaffino, S., and Sandri, M. (2009) Autophagy is required to maintain muscle mass. *Cell Metab* **10**, 507-515
109. Sandri, M., Sandri, C., Gilbert, A., Skurk, C., Calabria, E., Picard, A., Walsh, K., Schiaffino, S., Lecker, S. H., and Goldberg, A. L. (2004) Foxo transcription factors induce the atrophy-related ubiquitin ligase atrogin-1 and cause skeletal muscle atrophy. *Cell* **117**, 399-412
110. Zhao, J., Brault, J. J., Schild, A., Cao, P., Sandri, M., Schiaffino, S., Lecker, S. H., and Goldberg, A. L. (2007) FoxO3 coordinately activates protein degradation by the autophagic/lysosomal and proteasomal pathways in atrophying muscle cells. *Cell Metab* **6**, 472-483
111. De Palma, C., Morisi, F., Cheli, S., Pambianco, S., Cappello, V., Vezzoli, M., Rovere-Querini, P., Moggio, M., Ripolone, M., Francolini, M., Sandri, M., and

- Clementi, E. (2012) Autophagy as a new therapeutic target in Duchenne muscular dystrophy. *Cell Death Dis* **3**, e418
112. Srivastava, A. K., Qin, X., Wedhas, N., Arnush, M., Linkhart, T. A., Chadwick, R. B., and Kumar, A. (2007) Tumor necrosis factor-alpha augments matrix metalloproteinase-9 production in skeletal muscle cells through the activation of transforming growth factor-beta-activated kinase 1 (TAK1)-dependent signaling pathway. *J Biol Chem* **282**, 35113-35124
113. Dogra, C., Changotra, H., Mohan, S., and Kumar, A. (2006) Tumor necrosis factor-like weak inducer of apoptosis inhibits skeletal myogenesis through sustained activation of nuclear factor-kappaB and degradation of MyoD protein. *J Biol Chem* **281**, 10327-10336
114. Bulfield, G., Siller, W. G., Wight, P. A., and Moore, K. J. (1984) X chromosome-linked muscular dystrophy (mdx) in the mouse. *Proc Natl Acad Sci U S A* **81**, 1189-1192
115. Stedman, H. H., Sweeney, H. L., Shrager, J. B., Maguire, H. C., Panettieri, R. A., Petrof, B., Narusawa, M., Leferovich, J. M., Sladky, J. T., and Kelly, A. M. (1991) The mdx mouse diaphragm reproduces the degenerative changes of Duchenne muscular dystrophy. *Nature* **352**, 536-539
116. Dangain, J., and Vrbova, G. (1984) Muscle development in mdx mutant mice. *Muscle Nerve* **7**, 700-704

117. DiMario, J. X., Uzman, A., and Strohman, R. C. (1991) Fiber regeneration is not persistent in dystrophic (MDX) mouse skeletal muscle. *Dev Biol* **148**, 314-321
118. Tidball, J. G., and Wehling-Henricks, M. (2005) Damage and inflammation in muscular dystrophy: potential implications and relationships with autoimmune myositis. *Curr Opin Rheumatol* **17**, 707-713
119. Engvall, E., and Wewer, U. M. (2003) The new frontier in muscular dystrophy research: booster genes. *FASEB J* **17**, 1579-1584
120. Khurana, T. S., and Davies, K. E. (2003) Pharmacological strategies for muscular dystrophy. **2**, 379-390
121. Kumar, A., Takada, Y., Boriek, A. M., and Aggarwal, B. B. (2004) Nuclear factor-kappaB: its role in health and disease. *J Mol Med* **82**, 434-448
122. Peterson, J. M., Bakkar, N., and Guttridge, D. C. (2011) NF-kappaB signaling in skeletal muscle health and disease. *Curr Top Dev Biol* **96**, 85-119
123. Lu, A., Proto, J. D., Guo, L., Tang, Y., Lavasani, M., Tilstra, J. S., Niedernhofer, L. J., Wang, B., Guttridge, D. C., Robbins, P. D., and Huard, J. (2012) NF-kappaB negatively impacts the myogenic potential of muscle-derived stem cells. *Mol Ther* **20**, 661-668
124. Mann, C. J., Perdiguero, E., Kharraz, Y., Aguilar, S., Pessina, P., Serrano, A. L., and Munoz-Canoves, P. (2011) Aberrant repair and fibrosis development in skeletal muscle. *Skelet Muscle* **1**, 21

125. Bernasconi, P., Torchiana, E., Confalonieri, P., Brugnoli, R., Barresi, R., Mora, M., Cornelio, F., Morandi, L., and Mantegazza, R. (1995) Expression of transforming growth factor-beta 1 in dystrophic patient muscles correlates with fibrosis. Pathogenetic role of a fibrogenic cytokine. *J Clin Invest* **96**, 1137-1144
126. Peter, A. K., and Crosbie, R. H. (2006) Hypertrophic response of Duchenne and limb-girdle muscular dystrophies is associated with activation of Akt pathway. *Exp Cell Res* **312**, 2580-2591
127. Shin, J., Tajrishi, M. M., Ogura, Y., and Kumar, A. (2013) Wasting mechanisms in muscular dystrophy. *Int J Biochem Cell Biol*
128. Langen, R. C., Schols, A. M., Kelders, M. C., Wouters, E. F., and Janssen-Heininger, Y. M. (2001) Inflammatory cytokines inhibit myogenic differentiation through activation of nuclear factor-kappaB. *FASEB J* **15**, 1169-1180
129. Langen, R. C., Van Der Velden, J. L., Schols, A. M., Kelders, M. C., Wouters, E. F., and Janssen-Heininger, Y. M. (2004) Tumor necrosis factor-alpha inhibits myogenic differentiation through MyoD protein destabilization. *FASEB J* **18**, 227-237
130. Peterson, J. M., and Guttridge, D. C. (2008) Skeletal muscle diseases, inflammation, and NF-kappaB signaling: insights and opportunities for therapeutic intervention. *Int Rev Immunol* **27**, 375-387
131. Bonaldo, P., and Sandri, M. (2013) Cellular and molecular mechanisms of muscle atrophy. *Dis Model Mech* **6**, 25-39

132. Pauly, M., Daussin, F., Burelle, Y., Li, T., Godin, R., Fauconnier, J., Koechlin-Ramonatxo, C., Hugon, G., Lacampagne, A., Coisy-Quivy, M., Liang, F., Hussain, S., Matecki, S., and Petrof, B. J. (2012) AMPK activation stimulates autophagy and ameliorates muscular dystrophy in the mdx mouse diaphragm. *Am J Pathol* **181**, 583-592
133. Manning, B. D., and Cantley, L. C. (2007) AKT/PKB signaling: navigating downstream. *Cell* **129**, 1261-1274
134. Kim, M. H., Kay, D. I., Rudra, R. T., Chen, B. M., Hsu, N., Izumiya, Y., Martinez, L., Spencer, M. J., Walsh, K., Grinnell, A. D., and Crosbie, R. H. (2011) Myogenic Akt signaling attenuates muscular degeneration, promotes myofiber regeneration and improves muscle function in dystrophin-deficient mdx mice. *Hum Mol Genet* **20**, 1324-1338
135. Yamauchi, J., Kumar, A., Duarte, L., Mehuron, T., and Girgenrath, M. (2013) Triggering regeneration and tackling apoptosis: a combinatorial approach to treating congenital muscular dystrophy type 1 A. *Hum Mol Genet*
136. Mauro, A. (1961) Satellite cell of skeletal muscle fibers. *J Biophys Biochem Cytol* **9**, 493-495
137. Relaix, F., and Marcelle, C. (2009) Muscle stem cells. *Curr Opin Cell Biol* **21**, 748-753
138. Relaix, F., and Zammit, P. S. (2012) Satellite cells are essential for skeletal muscle regeneration: the cell on the edge returns centre stage. *Development* **139**, 2845-2856

139. Yin, H., Price, F., and Rudnicki, M. A. (2013) Satellite cells and the muscle stem cell niche. *Physiol Rev* **93**, 23-67
140. Zammit, P. S., Golding, J. P., Nagata, Y., Hudon, V., Partridge, T. A., and Beauchamp, J. R. (2004) Muscle satellite cells adopt divergent fates: a mechanism for self-renewal? *J Cell Biol* **166**, 347-357
141. Olguin, H. C., and Olwin, B. B. (2004) Pax-7 up-regulation inhibits myogenesis and cell cycle progression in satellite cells: a potential mechanism for self-renewal. *Dev Biol* **275**, 375-388
142. Oustanina, S., Hause, G., and Braun, T. (2004) Pax7 directs postnatal renewal and propagation of myogenic satellite cells but not their specification. *EMBO J* **23**, 3430-3439
143. Sambasivan, R., Yao, R., Kissenpfennig, A., Van Wittenberghe, L., Paldi, A., Gayraud-Morel, B., Guenou, H., Malissen, B., Tajbakhsh, S., and Galy, A. (2011) Pax7-expressing satellite cells are indispensable for adult skeletal muscle regeneration. *Development* **138**, 3647-3656
144. von Maltzahn, J., Jones, A. E., Parks, R. J., and Rudnicki, M. A. (2013) Pax7 is critical for the normal function of satellite cells in adult skeletal muscle. *Proc Natl Acad Sci U S A* **110**, 16474-16479
145. Kawabe, Y., Wang, Y. X., McKinnell, I. W., Bedford, M. T., and Rudnicki, M. A. (2012) Carm1 regulates Pax7 transcriptional activity through MLL1/2 recruitment during asymmetric satellite stem cell divisions. *Cell stem cell* **11**, 333-345

146. McKinnell, I. W., Ishibashi, J., Le Grand, F., Punch, V. G., Addicks, G. C., Greenblatt, J. F., Dilworth, F. J., and Rudnicki, M. A. (2008) Pax7 activates myogenic genes by recruitment of a histone methyltransferase complex. *Nature cell biology* **10**, 77-84
147. Juan, A. H., Derfoul, A., Feng, X., Ryall, J. G., Dell'Orso, S., Pasut, A., Zare, H., Simone, J. M., Rudnicki, M. A., and Sartorelli, V. (2011) Polycomb EZH2 controls self-renewal and safeguards the transcriptional identity of skeletal muscle stem cells. *Genes & development* **25**, 789-794
148. Chen, J. F., Tao, Y., Li, J., Deng, Z., Yan, Z., Xiao, X., and Wang, D. Z. (2010) microRNA-1 and microRNA-206 regulate skeletal muscle satellite cell proliferation and differentiation by repressing Pax7. *J Cell Biol* **190**, 867-879
149. Wen, Y., Bi, P., Liu, W., Asakura, A., Keller, C., and Kuang, S. (2012) Constitutive Notch activation upregulates Pax7 and promotes the self-renewal of skeletal muscle satellite cells. *Mol Cell Biol* **32**, 2300-2311
150. Kuroda, K., Tani, S., Tamura, K., Minoguchi, S., Kurooka, H., and Honjo, T. (1999) Delta-induced Notch signaling mediated by RBP-J inhibits MyoD expression and myogenesis. *J Biol Chem* **274**, 7238-7244
151. Le Grand, F., Jones, A. E., Seale, V., Scime, A., and Rudnicki, M. A. (2009) Wnt7a activates the planar cell polarity pathway to drive the symmetric expansion of satellite stem cells. *Cell stem cell* **4**, 535-547



152. Abou-Khalil, R., Le Grand, F., Pallafacchina, G., Valable, S., Authier, F. J., Rudnicki, M. A., Gherardi, R. K., Germain, S., Chretien, F., Sotiropoulos, A., Lafuste, P., Montarras, D., and Chazaud, B. (2009) Autocrine and paracrine angiopoietin 1/Tie-2 signaling promotes muscle satellite cell self-renewal. *Cell stem cell* **5**, 298-309
153. Inoue, J., Gohda, J., and Akiyama, T. (2007) Characteristics and biological functions of TRAF6. *Advances in experimental medicine and biology* **597**, 72-79
154. Chiffoleau, E., Kobayashi, T., Walsh, M. C., King, C. G., Walsh, P. T., Hancock, W. W., Choi, Y., and Turka, L. A. (2003) TNF receptor-associated factor 6 deficiency during hemopoiesis induces Th2-polarized inflammatory disease. *Journal of immunology* **171**, 5751-5759
155. Seale, P., Ishibashi, J., Holterman, C., and Rudnicki, M. A. (2004) Muscle satellite cell-specific genes identified by genetic profiling of MyoD-deficient myogenic cell. *Dev Biol* **275**, 287-300
156. Jones, N. C., Tyner, K. J., Nibarger, L., Stanley, H. M., Cornelison, D. D., Fedorov, Y. V., and Olwin, B. B. (2005) The p38alpha/beta MAPK functions as a molecular switch to activate the quiescent satellite cell. *J Cell Biol* **169**, 105-116
157. Feng, Y., Niu, L. L., Wei, W., Zhang, W. Y., Li, X. Y., Cao, J. H., and Zhao, S. H. (2013) A feedback circuit between miR-133 and the ERK1/2 pathway involving an exquisite mechanism for regulating myoblast proliferation and differentiation. *Cell Death Dis* **4**, e934

158. Li, X., Wang, X., Zhang, P., Zhu, L., Zhao, T., Liu, S., Wu, Y., Chen, X., and Fan, M. (2012) Extracellular signal-regulated kinase 1/2 mitogen-activated protein kinase pathway is involved in inhibition of myogenic differentiation of myoblasts by hypoxia. *Exp Physiol* **97**, 257-264
159. Troy, A., Cadwallader, A. B., Fedorov, Y., Tyner, K., Tanaka, K. K., and Olwin, B. B. (2012) Coordination of satellite cell activation and self-renewal by Par-complex-dependent asymmetric activation of p38alpha/beta MAPK. *Cell stem cell* **11**, 541-553
160. Derijard, B., Hibi, M., Wu, I. H., Barrett, T., Su, B., Deng, T., Karin, M., and Davis, R. J. (1994) JNK1: a protein kinase stimulated by UV light and Ha-Ras that binds and phosphorylates the c-Jun activation domain. *Cell* **76**, 1025-1037
161. Halazonetis, T. D., Georgopoulos, K., Greenberg, M. E., and Leder, P. (1988) c-Jun dimerizes with itself and with c-Fos, forming complexes of different DNA binding affinities. *Cell* **55**, 917-924
162. Fabian, M. R., Sonenberg, N., and Filipowicz, W. (2010) Regulation of mRNA translation and stability by microRNAs. *Annu Rev Biochem* **79**, 351-379
163. Naguibneva, I., Ameyar-Zazoua, M., Polesskaya, A., Ait-Si-Ali, S., Groisman, R., Souidi, M., Cuvellier, S., and Harel-Bellan, A. (2006) The microRNA miR-181 targets the homeobox protein Hox-A11 during mammalian myoblast differentiation. *Nature cell biology* **8**, 278-284

164. McCarthy, J. J., Esser, K. A., Peterson, C. A., and Dupont-Versteegden, E. E. (2009) Evidence of MyomiR network regulation of beta-myosin heavy chain gene expression during skeletal muscle atrophy. *Physiol Genomics* **39**, 219-226
165. Chen, J. F., Mandel, E. M., Thomson, J. M., Wu, Q., Callis, T. E., Hammond, S. M., Conlon, F. L., and Wang, D. Z. (2006) The role of microRNA-1 and microRNA-133 in skeletal muscle proliferation and differentiation. *Nat Genet* **38**, 228-233
166. Bernet, J. D., Doles, J. D., Hall, J. K., Kelly Tanaka, K., Carter, T. A., and Olwin, B. B. (2014) p38 MAPK signaling underlies a cell-autonomous loss of stem cell self-renewal in skeletal muscle of aged mice. *Nat Med* **20**, 265-271

## APPENDICES

### APPENDIX-1

Sequence of the primers used in QRT-PCR assay.

<b>Gene name</b>	<b>Forward primer (5'-3')</b>	<b>Reverse primer (5'-3')</b>
TRAF6	GCAGTGAAAGATGACAGCGTGA	TCCCGTAAAGCCATCAAGCA
Myh4	CGGCAATGAGTACGTCACCAAA	TCAAAGCCAGCGATGTCCAA
Notch1	CAGGAAAGAGGGCATCAG	AGCGTTAGGCAGAGCAAG
Notch2	GCAGGAGCAGGAGGTGATAG	GCGTTTCTTGGACTCTCCAG
Notch3	GTCCAGAGGCCAAGAGACTG	CAGAAGGAGGCCAGCATAAG
Dll1	ACTGTACTCACCATAAGCCGTGCA	TCAGCTCACAGACCTTGCCATAGA
Dll4	CACTTGCCACGATCTGGAGAAT	TGCCCAAAGCCATAAGGA
Jagged1	AACAAAGCTATCTGCCGACAGG	GGCTGATGAGTCCCACAGTAATTC
Jagged2	TTGGTGGCAAGAAGTCTCAGT	GCTGTCACAGATGCAGGAGAAGTT
Hes1	GCACAGAAAGTCATCAAAGCC	TTGATCTGGGTCTATGCAGTTG
Hes6	GCCGGATTTGGTGTCTACAT	TCCTGAGCTGTCTCCACCTT
Hey1	TGAATCCAGATGACCAGCTACTGT	TACTTTCAGACTCCGATCGCTTAC
HeyL	CAGATGCAAGCCCAGGAAGAA	ACCAGAGGCATGGAGCATCT
Nrarp	TGGTGAAGCTGTTGGTCAAG	CTTGGCCTTGGTGTGATGAGAT
Myh3	ACATCTCTATGCCACCTTCGCTAC	GGGTCTTGGTTTCGTTGGGTAT
Myogenin	CATCCAGTACATTGAGCGCCTA	GAGCAAATGATCTCCTGGGTTG
Igf1	CTCAGACAGGCATTGTGGATGAGT	GGTCTTGTTTCCTGCACTTCCTCT
TNF- $\alpha$	GCATGATCCGCGACGTGGAA	AGATCCATGCCGTTGGCCAG
IL-1 $\beta$	CTCCATGAGCTTTGTACAAGG	TGCTGATGTACCAGTTGGGG
IL-4	GGATGTGCCAAACGTCCTC	GAGTCTTCTTCAAGCATGGAG
IL-10	CAAGGAGCATTGGAATTCCC	GGCCTGTAGACACCTTGGTC
Pax7	CAGTGTGCCATCTACCCATGCTTA	GGTGCTTGGTTCAAATTGAGCC
$\beta$ -actin	CAGGCATTGCTGACAGGATG	TGCTGATCCACATCTGCTGG

## APPENDIX-2

### LIST OF ABBREVIATIONS

ALS.....	autophagy lysosome system
cDNA.....	complimentary deoxyribonucleic acid
CK.....	creatine kinase
CTX.....	cardiotoxin
Cre.....	cyclase recombinase
CSA.....	cross sectional area
DAPT.....	<i>N</i> -[2 <i>S</i> -(3, 5-difluorophenyl)acetyl]-L-alanyl-2-phenyl-1,1-dimethylethyl ester-glycine
DGC.....	dystrophin-glycoprotein complex
DM.....	differentiations medium
DMEM.....	Dulbecco's modified eagle medium
EMSA.....	electrophoretic mobility shift assay
MyHC.....	myosin heavy chain
eMyHC.....	embryonic myosin heavy chain
MAPK.....	mitogen associated protein kinase
ERK.....	extracellular signal-regulated kinase
FGF.....	fibroblast growth factor
GA.....	gastrocnemius
GM.....	growth medium
H&E.....	hematoxylin and eosin

IGF.....	insulin like growth factor
IgG.....	immunoglobulin G
IFN $\gamma$ .....	interferon gamma
IL.....	interleukin
JNK.....	c-Jun N-terminal kinase
LC3.....	microtubule-associated
mko.....	muscle specific knock out
scko.....	satellite cell-specific knock out
mTOR.....	mammalian target of rapamycin
MMP.....	matrix metalloproteinase
mRNA.....	messenger RNA
MuRF1.....	muscle Ring-finger protein
NF- $\kappa$ B.....	nuclear factor kappa-B
NICD.....	notch intracellular domain
Pax7.....	paired box protein 7
PCR.....	polymerase chain reaction
QRT-PCR.....	quantitative real-time polymerase chain reaction
SD.....	standard deviation
shRNA.....	short hairpin RNA
TA.....	tibial anterior
TGF.....	transforming growth factor
TNF.....	tumor necrosis factor
TNFR.....	tumor necrosis factor receptor

TRAF.....TNFR associated factor

Ub.....ubiquitin

UPS.....ubiquitin-proteasome system

## CURRICULUM VITAE

### **Sajedah M. Hindi, M.S.**

8412 Running Spring Drive

Louisville, KY 40241

Email: [smhind01@louisville.edu](mailto:smhind01@louisville.edu)

Phone: 502-852-8594 (Laboratory)

502-468-1358 (Mobile)

**Date of Birth:** September 6, 1986

**Residency Status:** US Citizen

### **A. EDUCATION & TRAINING:**

(Month/Year)

06/2008: B.S. in Physical Therapy

University of Jordan, Amman, Jordan.

09/2012 M.S. in Anatomical Sciences and Neurobiology

University of Louisville, Louisville, KY

12/2014 Ph.D. in Anatomical Sciences and Neurobiology

(Expected) Specialization: Skeletal muscle biology and Muscular Dystrophy

University of Louisville, Louisville, KY

### **B. PROFESSIONAL EXPERIENCE:**

#### **Graduate Research Assistant**

Department of Anatomical Sciences and Neurobiology

University of Louisville, Louisville, KY 40202

2010-2014

#### **Teaching Assistant**

Department of Anatomical Sciences and Neurobiology

University of Louisville, Louisville, KY 40202

2012-2013

### **C. AWARDS AND HONORS:**

- Graduate Fellowship Awarded, University of Louisville, Aug 2011-2013



- First place award in poster presentation, Master-Graduate Category, at “Research Louisville-2012” symposium.
- Awarded **Ruth L. Kirschstein National Research Service Award (NRSA)** F31 application, from National Institute of Health (NIH). 2014-onward
- **John M Huchens Prize for outstanding dissertation** for Fall 2014 graduation at the University of Louisville.

**D. PARTICIPATED IN REVIEWING MANUSCRIPTS FOR THE FOLLOWING JOURNALS:**

- Science Signaling
- Nature Communications
- Science Translational Medicine
- FASEB Journal
- Scientific Reports: Nature Publishing Group
- American Journal of Physiology-Cell Physiology
- PLOS One
- American Journal of Pathology
- Frontiers in Physiology

**E. RESEARCH SUPPORT**

**Title:** TRAF6 signaling in skeletal muscle regeneration during aging (F31AG046950)

**Source:** National Institute of Health (NIH)

**Support period:** 07/01/2014-06/30/2017

**Role in project:** PI

**Goal:** The major goal of this study is to understand the role of TRAF6 in skeletal muscle regeneration during aging.

**F. PEER-REVIEWED PUBLICATIONS (\*Editorial and/or highlighted in news):**

**1).** Dahiya S, Bhatnagar S, **Hindi SM**, Jiang C, Paul PK, Kuang S, and Kumar A (2011) Elevated levels of active matrix metalloproteinase-9 cause hypertrophy in skeletal muscle of normal and dystrophin-deficient mdx mice. *Human Molecular Genetics*, 20: 4345-4359.

**2).** **Hindi SM**, Paul PK, Dahiya S, Bhatnagar S, Mishra V, Choi Y, and Kumar A (2012). Reciprocal interaction between TRAF6 and Notch Signaling regulates regeneration of adult myofibers upon injury. *Molecular and Cellular Biology* 32:4833-4845.

**\*3).** **Hindi SM**, Tajrishi M, and Kumar A (2013). Signaling mechanisms in mammalian myoblast fusion. *Science Signaling*, 6, re2 (1-9pp). (**Previewed on the cover of the journal**).

- 4). Hindi SM**, Shin J, Ogura Y, Li H, and Kumar A (2013). Matrix metalloproteinase-9 inhibition improves proliferation and engraftment of myogenic cells in dystrophic muscle of mdx mice. *PLoS One* 8: e72121 (1-11pp).
- 5).** Ogura Y, Mishra V, **Hindi SM**, Kuang S, Kumar A (2013). Proinflammatory cytokine tumor necrosis factor (TNF)-like weak inducer of apoptosis (TWEAK) suppresses satellite cell self-renewal through inversely modulating Notch and NF- $\kappa$ B signaling pathways. *Journal of Biological Chemistry*, 288: 35159-35169.
- 6).** **Hindi SM**, Sato S, Choi Y, and **Kumar A** (2014) Distinct roles of TRAF6 at early and late stages of muscle pathology in the mdx model of Duchenne muscular dystrophy. *Human Molecular Genetics*, 23:1492-1505.
- 7).** **Hindi SM**, Mishra V, Bhatnagar S, Tajrishi MM, Ogura Y, Yan Z, Burkly LC, and Zheng TS, and Kumar A (2014). Regulatory circuitry of TWEAK-Fn14 system and PGC-1 $\alpha$  in skeletal muscle atrophy program. *FASEB Journal*, 28: 1398-1411.
- 8).** Ogura Y, Tajrishi MM, Sato S, **Hindi SM**, and Kumar A (2014). Therapeutic potential of matrix metalloproteinases in muscular dystrophy. *Frontiers in Cell and Developmental Biology*, 2:11 (1-11pp).

#### **G. POSTER PRESENTATION IN SCIENTIFIC CONFERENCES:**

- 2012 Specific inhibition of TRAF6 accelerates skeletal muscle regeneration. **Hindi, Sajedah**; Paul, Pradyut; Kumar, Ashok. Presented at “Development, Function and Repair of the muscle cell” meeting in June, 2012, New York, NY
- 2012 Signaling mechanisms in cancer cachexia: Role of TRAF6. Kumar, Ashok; Paul, Pradyut; **Hindi, Sajedah**. Presented at the “Cancer Cachexia: Molecular Mechanisms and Therapeutic Approaches” Meeting. September 21-23, 2012. In Boston, MA)
- 2012 Reciprocal Interaction between TRAF6 and Notch signaling regulates adult myofibers regeneration upon injury. **Hindi, Sajedah**; Paul, Pradyut; Kumar, Ashok. Presented at Research Louisville on 19<sup>th</sup> September, 2012.
- 2013 Distinct roles of TRAF6 at early and late stages of disease progression in the mdx model of Duchenne muscular dystrophy. **Hindi, Sajedah**, Sato S, and Kumar A. Presented at the Cardiovascular Forum, Louisville on August 16, 2013.
- 2013 Reciprocal interaction between TWEAK-Fn14 system and PGC-1 $\alpha$  regulates skeletal muscle atrophy program. **Hindi, Sajedah**, Sato S, Tajrishi MM, Mishra V, Ogura Y, and Kumar. Presented at EMBO Workshop - Molecular Mechanisms of muscle growth and wasting in health and disease in Ascona, Switzerland on September 17, 2013.

- 2013 Distinct roles of TRAF6 at early and late stages of disease progression in the mdx model of Duchenne muscular dystrophy. **Hindi, Sajedah**, Sato S, and Kumar A. Presented at the Research Louisville from September 24 - 27, 2013.
- 2014 TRAF6 is critical for satellite cell function and skeletal muscle regeneration upon injury. **Hindi, Sajedah** and Ashok Kumar. Experimental Biology, April 26-30, 2014 in San Diego, California.
- 2014 TRAF6 is critical for satellite cell function and skeletal muscle regeneration upon injury. **Hindi, Sajedah** and Ashok Kumar. Presented at “The Muscle Microenvironment: A niche for the next generation of biomedical scientists” on May 12, 2014 at Ohio State University, Columbus.
- 2014 TRAF6 is critical for satellite cell function and skeletal muscle regeneration upon injury. **Hindi, Sajedah** and Ashok Kumar. Presented at “Research!Louisville” on 16<sup>th</sup> September, 2014.